ROLE OF VON WILLEBRAND FACTOR IN SHEAR INDUCED PLATELET ACCUMULATION IN A MICROFLUIDIC DEVICE

A Dissertation
Presented to
The Academic Faculty

By

Lauren Danielle Couch Casa

In Partial Fulfillment
Of the Requirements for the Degree
Doctor of Philosophy in Mechanical Engineering

Georgia Institute of Technology

May 2015

Copyright © Lauren D. C. Casa 2015

ROLE OF VON WILLEBRAND FACTOR IN SHEAR INDUCED PLATELET ACCUMULATION IN A MICROFLUIDIC DEVICE

Approved by:

Dr. David N. Ku, Advisor
George W. Woodruff School of Mechanical Engineering
Georgia Institute of Technology

Dr. Craig R. Forest
George W. Woodruff School of Mechanical Engineering
Georgia Institute of Technology

Dr. Cheng Zhu
Wallace H. Coulter Department of Biomedical Engineering
Georgia Institute of Technology

Dr. Wilbur A. Lam
Wallace H. Coulter Department of Biomedical Engineering
Georgia Institute of Technology

Dr. Shannon L. Meeks
Department of Pediatrics
Emory University School of Medicine

Date Approved: March 6, 2015

ACKNOWLEDGEMENTS

This dissertation reflects the contributions of so many in my academic and personal life, and I am faced with the challenge of condensing the ever-growing list to only a few. Indeed, without the support and encouragement of so many family members, friends, educators, and colleagues, I would never have undertaken, much less completed, a PhD dissertation.

Thanks first to Dr. David Ku, my PhD advisor, for his scientific insight in guiding my research. Every meeting with him left me with more questions to ponder and investigations to pursue. Thanks also to my committee member, Dr. Shannon Meeks, for her clinical insight into experimental and device design, as well as for her enthusiasm in recruiting subjects for my studies. Thanks also to her research team, particularly David Hellwege, for coordinating the logistics of recruitment. Thanks to my committee members Dr. Craig Forest for providing very helpful device design insight and Dr. Wilbur Lam and his lab for providing valuable guidance in platelet isolation techniques. Thanks also to my committee member, Dr. Cheng Zhu, for honing my research proposal and reviewing my final dissertation. The help I received from all my committee was invaluable in improving the work.

Thanks also goes to Dr. Rhett Mayor and his students for their manufacturing insight and for fabricating molds for my microfluidic device. Additional machining support was provided by Steven Sheffield and the Mechanical Engineering machine shop. Special thanks to all my blood donors. The staff of the Stamps Student Health Center lab provided phlebotomy services for studies conducted at Georgia Tech. Scott Gillespie and Dr. Traci Leong provided valuable assistance with statistical analyses.

Thanks to the members of the Ku lab and IBB Wing 2A for both scientific and social conversations when the research was slow. In particular: Marmar Mehrabadi, Susan Hastings, Sumit Khetarpal, Kathleen Bernhard, Max Jordan Nguemeni, Joav Birjiniuk, and Renee Bonagura.

Funding for my research was provided by the National Defense Science and Engineering Graduate Fellowship, the AHA Predoctoral Fellowship, and the Center for Pediatric Innovation. Additional support was provided by the Georgia Tech President's Fellowship, the George W. Woodruff School of Mechanical Engineering, and the ARCS Scholars Award.

Portions of this dissertation have been published in peer-reviewed academic journals. CHAPTER 2 was published in *Cardiovascular Engineering and Technology* in 2014, Volume 5, Issue 2. Section 3.2 was published in *Biomedical Microdevices* in 2014, Volume 16, Issue 1.

Special thanks is due to my family. First, thanks to my parents, Brad and Annette Couch, for their unwavering support of me during the pursuit of my education, starting even before kindergarten, through all of the ups and downs. My brother, Jared Couch, has always been there to laugh and complain with me through all my studies. I couldn't have asked for a better family. Finally, my unending love and thanks to my best friend and husband, Sean Casa. Sean, you have selflessly supported and encouraged (and even married) me while I pursued my PhD. I am so excited to begin the next chapter of our lives together.

TABLE OF CONTENTS

LIST OF TABLES

LIST OF FIGURES

NOMENCLATURE

Latin Symbols

a	Area occupied by platelet
A, A_C, A_R, A_B	Area of functionalized surface, area in circular cross sections, area in rectangular cross sections, area in rectangular cross sections with only the bottom surface functionalized
ADAMTS13	A disintegrin and metalloproteinase with a thrombospondin type 1 motif, member 13
b	Test section half-width
c	Test section half-height
CFD	Computational fluid dynamics
D	Test section diameter
d, d_{eff}, d_{sf}	Mass diffusivity, effective diffusivity, static diffusivity
D_1, D_2	Upstream, stenosis diameter
D_o, D_i	Nonstenotic, nonstenotic diameter
dV/dt	Thrombus growth rate
GPIb	Glycoprotein Ib
h	Test section height
Δh	Height between fluid inlet and outlet
J	Normalized thrombus growth rate
L	Length scale
LTA	Light transmission aggregometry
m	Thrombus thickness
MI	Myocardial infarction
N_p	Number of platelet-bound platelets

N_s	Number of surface-bound platelets
N_{tot}	Number of platelets
P	Percent platelet-platelet interactions
p	Percent of thrombus composed of platelets
Δp	Pressure drop
P_1, P_2	Upstream, downstream pressure
PDMS	Polydimethylsiloxane
Pe	Peclet number
Q	Volumetric flow rate
r	Radius
R	Ratio of platelet-platelet to platelet-surface interactions
Re	Reynolds number
R_h	Hydraulic resistance
RPA	Rapid platelet accumulation
Sc	Schmidt number
t	Time
t_g	Rapid growth time
t_{lag}	Lag time
t_{occ}	Occlusion time
ULVWF	Ultra-large von Willebrand Factor
U_{mean}	Velocity scale
u_x	Velocity in the axial direction
v	Platelet volume
V, V_C, V_R	Thrombus volume, thrombus volume in circular cross sections, thrombus volume in rectangular cross sections

VWD	von Willebrand disease
vWF	von Willebrand Factor
VWF:RCo	Ristocetin cofactor assay
w	Test section width
x,y,z	Cartesian coordinates

Greek Symbols

α	Aspect ratio
$\alpha_{IIb}\beta_3$	Integrin αIIbβ3
γ, $\dot{\gamma}$	Wall shear rate
μ	Dynamics viscosity
ρ	Density
τ	Wall shear stress

SUMMARY

Thrombus formation under high fluid shear rates at the site of atherosclerotic plaque rupture leads to myocardial infarction and stroke. At high shear rates, thrombus is formed by platelets adhering via the glycoprotein von Willebrand factor (vWF). To investigate the relative contributions of vWF and platelets in high shear thrombosis, the present work developed a microfluidic thrombosis assay to meet low blood volume requirements and fluid shear conditions (3500-6000 s^{-1}). Microfluidic conditions were selected to mimic the high shear environment of a diseased coronary artery, with the long-term objective of developing a clinically relevant assay for the assessment of thrombosis risk and treatment efficacy. The microfluidic design also addressed the requirement for volumetric thrombus formation rather than only surface platelet adhesion. As part of the design of the microfluidic assay, the effect of flow pulsatility on high shear thrombosis was investigated. It was found that steady wall shear rate matched to the mean pulsatile wall shear rate reproduced bulk thrombus formation characteristics of occlusion time, lag time, and thrombus growth rate, allowing subsequent experiments and future device design to utilize steady flow. The microfluidic assay was implemented to study the roles of vWF and platelets to thrombus formation using blood analogs produced from whole human blood diluted with normal saline at 90% and 99%. Hematocrit was restored to normal in all cases with the addition of red blood cells, and vWF and platelets were selectively restored to normal levels. Results showed that 90% dilutions with only vWF restored to normal levels occluded in 6/7 subject tested. The addition of platelets accelerated thrombus formation, but blood analogs with only platelets restored to normal levels occluded in only 2/5

subjects, indicating that vWF is more contributory in high shear occlusive thrombosis. At 99% dilutions, large thrombus formed with the addition of both platelets and vWF but was unstable and did not fully occlude the channel, indicating the possible requirement of an additional stabilizing factor(s) in occlusive thrombosis. Results of this study may lead to the development of improved anti-thrombotic treatments and improve patient care by providing a potential assay to evaluate treatment effectiveness and predict thrombosis risk.

CHAPTER 1: INTRODUCTION

1.1 The Clinical Problem of Thrombosis

Thrombosis is the pathological clotting of blood within a vessel. Thrombosis can lead to vessel occlusion, ischemia, and death. Biological mechanisms, namely the coagulation cascade and platelet aggregation, normally act in concert to prevent excessive bleeding in a process called hemostasis. However, the same mechanisms under pathological conditions result in thrombosis. In general, thrombosis results from the combination of 1) a thrombogenic surface, 2) abnormal fluid mechanic conditions, and 3) pro-thrombotic blood chemistry (Chung & Lip, 2003; Lowe, 2003). Often, a thrombogenic surface results from the disruption of the endothelial cells lining a blood vessel, but foreign surfaces, such as those of vascular grafts or prosthetic heart valves, may also initiate thrombosis. Pathologically elevated fluid shear rates result in thrombi composed primarily of platelets, known as "white clots." In addition to platelets, plasma proteins, including coagulation factors, thrombin, fibrinogen, and von Willebrand factor (vWF) are critical for thrombosis, and their relative contributions depend on shear rate (Jackson, 2007).

Platelet thrombus formation in the coronary arteries leading to myocardial infarction (MI) occurs under very high shear rates (Davies, Thomas, McMichael, & Richardson, 1981; Davies & Thomas, 1985; Falk, 1983; Friedman & van den Bovenkam, 1966; Friedman, 1971). Occlusive thrombus formation can lead sudden cardiac ischemic death in less than an hour (Davies & Thomas, 1984). Given the substantial public health burden associated with MI, the study of thrombus formation at high shear rates, and in particular platelet adhesion, aggregation, and accumulation, is an important field of study.

1.2 Characteristics of High Shear Thrombosis

Fluid mechanic conditions determine the formation pathway and composition of thrombi. Wall shear rate has been identified as a critical fluid dynamic metric governing thrombus formation (Jackson, 2007; Maxwell et al., 2007). Wall shear rate, $\dot{\gamma}$, is defined as the velocity gradient at the vessel wall, and for Poiseuille flow in a round, rigid tube is calculated as

$$\dot{\gamma} = \frac{4Q}{\pi r^3} \tag{1-1}$$

where Q is the volumetric flow rate and r is the tube radius. Shear rate, τ, is related to fluid shear stress through the fluid's kinematic viscosity, μ, by

$$\tau = \mu\dot{\gamma}\,. \tag{1-2}$$

At low shear rates (<500 s^{-1}), thrombus formation is dominated by coagulation, leading to erythrocyte- and fibrin-rich thrombi or "red clots." The medical condition of deep vein thrombosis exemplifies this process. Coagulation is the process by which the plasma protein fibrinogen is cleaved by thrombin to form fibrin, an insoluble protein that results in the formation of a gel-like structure. Thrombin formation is critical for coagulation and is generated via a cascade of coagulation factor interactions initiated by tissue factor, which is found in the extracellular matrix of blood vessels and is exposed by vessel injury.

Conversely, thrombus formation at high shear rates (>3500 s^{-1}) is dominated by platelet aggregation, leading to "white clots." MI is precipitated by platelet-rich thrombus formation at the site of atherosclerotic plaque rupture (Davies, Fulton, & Robertson, 1979; Davies & Thomas, 1984, 1985; Davies, 1994) under high shear rates (Bark & Ku, 2010).

The rapid time scales of occlusion combined with the observation of reocclusion despite full heparinization (Gold et al., 1986), indicate that platelet adhesion and aggregation, rather than coagulation, is the primary pathway of arterial thrombus formation. Additionally, a limited number of pathological specimens show platelet-rich thrombus formation at or near the sites of atherosclerotic coronary stenosis (Davies et al., 1981; Davies & Thomas, 1985; Falk, 1983; Friedman & van den Bovenkam, 1966; Friedman, 1971), and platelet-rich emboli have been identified distal of atherosclerotic lesions (Falk, 1985). These observations have led to a consensus that arterial thrombi associated with MI can be characterized at platelet-rich "white clots," distinct from erythrocyte-rich "red clots" that occur in veins (Lippi, Franchini, & Targher, 2011; Lowe, 2003; Mackman, 2008; Rumbaut & Thiagarajan, 2010).

Occlusive platelet thrombosis has been studied *in vitro* by perfusing whole blood or platelet rich plasma through a test section at high shear rate. Studies have used cylindrical and parallel platelet perfusion chambers both with (Badimon, Badimon, Galvez, Chesebro, & Fuster, 1986; Barstad, Roald, Cui, Turitto, & Sakariassen, 1994; Ku & Flannery, 2007; Li, Ku, & Forest, 2012) and without a stenosis (Gutierrez et al., 2008; Hosokawa et al., 2011; Maloney, Brass, & Diamond, 2010; Neeves et al., 2008; Sixma, de Groot, van Zanten, & Ijsseldijk, 1998). Using whole blood perfusion through a cylindrical, stenotic test section that closely mimics coronary artery geometry, Ku and colleagues have demonstrated that *in vitro* high-shear, platelet-rich thrombus formation is characterized by three phases (Wootton, Markou, Hanson, & Ku, 2001): Phase I, an initial deposition phase with limited thrombus growth, Phase II, rapid platelet accumulation (RPA), and finally Phase III, lumen occlusion (Ku & Flannery, 2007; Para, Bark, Lin, & Ku, 2011)

(Figure 1-1 and Figure 1-2). Thrombi formed in this system using lightly heparinized porcine blood were shown to be composed of approximately 80% platelets (Ku & Flannery, 2007).

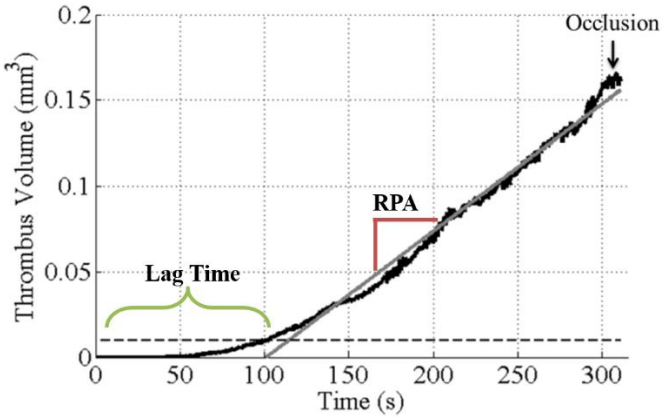

Figure 1-1: Characteristic thrombus volume growth under high shear rate, including initial lag time followed by rapid platelet accumulation (RPA) and subsequent occlusion.

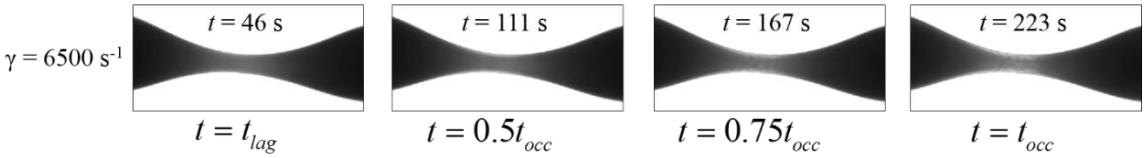

Figure 1-2: *In vitro* thrombus formation in a stenotic glass capillary at an initial wall shear rate of 6500 s^{-1}. The thrombus initially appears as a faint haze at the tube wall and grows to fully occlude flow.

The phases of occlusive thrombus formation may be quantified by initial deposition rate and/or lag time, RPA rate, and occlusion time. To describe Phase I of occlusive thrombosis, lag time has previously been defined as the time for the thrombus thickness to reach 10 μm (Bark, Para, & Ku, 2012), though any definition of the transition from

Phase I to Phase II is somewhat arbitrary. Lag time has been shown to range from 175 to 300 s for initial shear rates of 500-5000 s^{-1} (Bark et al., 2012), with initial deposition rates measures to be approximately 3×10^{-6} cm^3/min at shear rates of 25,000 s^{-1} (Para et al., 2011). Lag time and slower initial platelet deposition rates are thought to represent the time necessary for plasma proteins, such as von Willebrand factor (see Section 1.5 for a detailed discussion), to be absorbed onto the collagen surface to support platelet adhesion (Neeves et al., 2013). Neeves et al. (2013) report a lag time (time for 1% surface coverage) of approximately 150 s^{-1} at a shear rate of 1500 s^{-1}, and lag time is weakly correlated with vWF levels. Lag time and initial deposition rate may also reflect the time necessary for adherent platelets to activate, initiating a positive feedback for further platelet thrombus growth (Bark et al., 2012). Interestingly, lag time decreases with increasing shear rate (Bark et al., 2012), reflecting that protein absorption onto collagen (Schneider et al., 2007) and/or platelet activation (Holme et al., 1997; Ramstack, Zuckerman, & Mockros, 1979) is enhanced by shear rate.

Following initial deposition, Phase II of occlusive thrombus formation is characterized by rapid thrombus growth rates, quantified as RPA rate. For experiments with initial shear rates of approximately 25,000 s^{-1}, RPA rates average 20×10^{-6} cm^3/min, more than 6 times the rate of initial platelet deposition (Para et al., 2011). Phase II growth rates increase with increasing shear rates up to approximately 6000 s^{-1}, with maximum growth rates at 6000-10 000 s^{-1}, an order of magnitude greater than growth rates at physiological shear rates of 500-1500 s^{-1}. Above 6000 s^{-1}, thrombus growth rates more gradually decrease up to 100 000 s^{-1}. Thrombus formation during RPA may be uneven, with "fingers" of thrombus protruding into the lumen.

The growing thrombus ultimately leads to Phase III, the full occlusion of the test section and cessation of blood flow. Occlusion times of approximately 12-17 minutes have been measured in 70-83% stenoses of 1.5 mm test sections (Bark et al., 2012; Para et al., 2011). Though occlusion time provides a bulk measurement occlusive thrombus formation, combining metrics representative of all three phases of platelet thrombus growth provide a more comprehensive description of occlusive thrombus formation relevant to MI that may ultimately prove useful for patient-specific measurement of high shear thrombotic potential.

1.3 Fluid Mechanics of Healthy and Stenotic Arteries

Blood flow in arteries is pulsatile, a consequence of cyclic cardiac pumping, with secondary flows developing at branches and curves. The coronary and carotid arteries are among the arteries most prone to disease, which leads directly to myocardial infarction and stroke, so we will focus the present discussion on flow features at these locations. The carotid arteries, which supply blood to the brain and face, have a unique bifurcation geometry with an expansion, or sinus, at the origin of the internal carotid. In combination with pulsatile flow, this geometry results in reversing velocity profiles along the outer wall and transient flow separation along the posterior wall (Ku, Giddens, Phillips, & Strandness Jr, 1985). The left coronary bifurcation is also characterized by complex, three-dimensional, tortuous geometry that result in reversing and secondary flows (He & Ku, 1996).

In both the coronary and carotid arteries, flow reversal and secondary flows result in low mean wall shear stress and wall shear oscillations. This type of flow regime has been

shown to induce atherosclerotic intimal thickening in a canine model (Salam, Lumsden, Suggs, & Ku, 1996). In contrast, most regions of the arterial tree maintain a wall shear stress of around 15 dyne/sm^2 (Glagov, Zarins, Giddons, & Ku, 1988), or a wall shear rate of between 500 and 1500 s^{-1}. As atherosclerotic lesions grow, the diameter of effected artery is reduced over a short distance, forming a stenosis. Clinically, percent stenosis is defined by percent reduction in diameter:

$$\%\ \text{stenosis} = \frac{D1-D2}{D1} \times 100\% \qquad (1\text{-}3)$$

where D1 is the upstream diameter and D2 is the minimum diameter at the stenosis. As disease progresses, the minimum diameter decreases (percent stenosis increases). Fluid mechanically, the increase in percent stenosis results in higher wall shear rates (Bark & Ku, 2010) in accordance with eq. (1-1), which are present at the time of atherosclerotic plaque rupture and thrombosis.

Arterial flows are inherently pulsatile, but little work has been done to quantify the effect of flow pulsatility on thrombus formation, particularly at very high shear rates associated with arterial stenosis. One previous study (van Breugel, Sixma, & Heethaar, 1988) showed no difference in platelet adhesion under steady flow conditions at shear rates from 0 to 1800 s^{-1} and non-reversing pulsatile with the same mean shear rate and increased platelet deposition with increasing amplitude for a mean shear rate of 0 s^{-1} (reversing flow). However, the shear rates investigated were much lower than expected in stenotic arteries, and reversing flow with non-zero mean shear rate was not considered, so platelet adhesion results may not be relevant to arterial thrombosis in stenotic arteries. Platelet adhesion under pulsatile flow at low shear rates (300-1300 s^{-1}) was also studied by Zhao et al. (2008) at a frequency of 0.067 Hz, much lower than the frequency of arterial pulsatility. Thus,

thrombus formation under high shear ($\dot{\gamma}$ > 3000 s^{-1}), pulsatile flow (frequency > 1 Hz), similar to that found in stenotic arteries, should be investigated to ensure that *in vitro* conditions mimic pathological conditions relevant to MI. Alternatively, if flow pulsatility is found to have no effect compared to steady flow on the thrombus formation parameters of interest, studies may be performed under steady flow conditions, which are simpler to experimentally design and implement.

1.4 Platelet Adhesion, Aggregation, and Accumulation

Historically, platelet adhesion and aggregation were thought to be initiated by platelet adhesion to exposed collagen via integrin $\alpha_{IIb}\beta_3$ (Jackson, 2007). In this model, collagen-bound platelets are activated by soluble agonists, such as ADP, thrombin generated by simultaneous blood coagulation, and thromboxane A_2. Platelet activation induces shape change and the release of α- and dense-granule contents, including vWF, ADP, calcium ions, coagulation factors, and inflammatory factors, which in turn act to recruit and activate circulating platelets (Davi & Patrono, 2007). Activated platelets adhere to each other via $\alpha_{IIb}\beta_3$ binding to fibrinogen. This process is exemplified by light transmission aggregometry, a platelet function test in which platelet rich plasma is stirred in the presence of a platelet agonist, and the formation of platelet aggregates alters the transmissivity of the suspension (Rechner, 2011). Though additional complexities, particularly with respect to the types of adhesive proteins involved, this model remains a accepted framework for platelet aggregation under low flow/low shear (<500 s^{-1}) conditions.

Studies over the last 30 years have illustrated that platelet adhesion and aggregation under physiological shear rates (500-1500 s^{-1}) are more complicated processes involving

1) additional adhesive proteins, particularly von Willebrand factor, 2) multiple stages of binding, and 3) an altered understanding of the role of platelet activation. Sakariassen et al. (1979) showed that the amount of vWF bound to extracellular matrix increased with plasma vWF concentration, and the number of adherent platelets also increased with the amount of bound vWF. However, that study utilized an average shear rate of only 805 s^{-1} and investigated platelet-surface adhesion and not large-scale platelet aggregation and accumulation (many more platelet-platelet adhesion events than platelet-surface adhesion events leading to thrombus growth beyond surface coverage).

A series of later studies indicate a two-stage model of high shear platelet adhesion in which platelets become tethered to extracellular matrix via vWF-GPIb bonds, reducing translocation speed and allowing firm adhesion via $\alpha_{IIb}\beta_3$. Savage et al. (1996) showed that the number of platelets adhering to fibrinogen decreased with increasing shear rate, whereas the number of platelet adhering to vWF increased over the range of 50-1500 s^{-1}. Platelets adhering to vWF tended to translocate in the direction of flow before firmly adhering, whereas platelets adhering to fibrinogen did not translocate. These results indicate that only vWF-GPIb binding has a sufficiently fast on-rate to initiate platelet tethering at shear rates greater than 1000 s^{-1} (Ruggeri, 2007). A subsequent study (Savage, Almus-Jacobs, & Ruggeri, 1998) in which blood was perfused over Type I collagen showed synergistic behavior of platelet adhesive substrates and receptors. Maxwell et al. (2007) demonstrated a similar two-stage process of platelet aggregation by perfusing whole blood over platelet monolayers in capillary tubes at 1800 s^{-1}. To extend these studies to platelet adhesion to atheromatous plaque, Reininger et al. (2010) perfused whole blood over human plaque material at 1500 s^{-1}. Results also indicate a two-stage thrombus

formation process, though with initial adhesion mediated by GPVI binding to collagen and stabilization via tissue factor mediated coagulation.

Several developments in the understanding of platelet activation have also increased the complexity of platelet aggregation under flow. In addition to soluble agonists, platelets have been shown to be activated by fluid shear stress (Holme et al., 1997; Jesty, Yin, Perrotta, & Bluestein, 2003; Ramstack et al., 1979). Additionally, Ruggeri et al. (2006) showed that at shear rates greater than 10 000 s^{-1}, non-activated platelet form aggregates on immobilized vWF in the presence of plasma vWF. Recently, vWF was shown to be essential for platelet aggregation *in vitro* (Westein et al., 2013).

Taking the results for platelet aggregation under flow collectively, distinct high-shear mechanisms are apparent, particularly above a shear rate of 10 000 s^{-1}. Under these conditions, platelets become initially tethered to collagen via platelet glycoprotein Ib (GPIb) binding to immobilized vWF (Bergmeier, Chauhan, & Wagner, 2008; Yago et al., 2008). Subsequently, rolling aggregates of non-activated platelets and vWF form (Jackson, 2007; Ruggeri et al., 2006). However, non-activated aggregates are not capable of forming large-scale stable thrombus, and activation of $\alpha_{IIb}\beta_3$ appears to be necessary for occlusive thrombosis (Para, 2012). VWF-tethered platelets are then activated by shear rate, vWF binding, soluble agonists, or some combination of factors to initiate firm adhesion via $\alpha_{IIb}\beta_3$. Studies also indicate that the growing thrombus under high shear may be stabilized by fibrinogen (Maxwell et al., 2007; Savage et al., 1998). Between 1000 and 10 000 s^{-1} exists an intermediate range of platelet aggregation that involved platelet tethering via vWF and aggregate stabilization via fibrinogen and/or fibronectin to greater

or lesser extents (Jackson, 2007), though the relative contributions vWF, platelets, and fibrinogen are as yet unclear.

1.5 Von Willebrand Factor in High Shear Thrombosis

The studies outlined in the previous section indicate that vWF is essential for high shear thrombus formation. VWF undergoes a conformational change at shear rates >5000 s^{-1} that is thought to expose additional collagen- and platelet-binding sites. Plasma vWF concentration and activity have also been shown to be significantly higher in subjects with recurrent MI and first-ever ischemic stroke compared to control subjects (Bongers et al., 2006; Jansson, Kilsson, & Johnson, 1991). Together, these data indicate that vWF may play critical role in thrombus formation related to MI and stroke.

Von Willebrand factor (vWF) is a multimeric glycoprotein essential in hemostasis and implicated in atherothrombosis. VWF is found in blood plasma, platelet α-granules, and the extracellular matrix of blood vessels. The fundamental subunit of vWF multimers is a dimer, each component of which is composed of 14 domains: D1-D2-D'-D3-A1-A2-A3-B1-B2-B3-C1-C2-CK. Dimers are assembled tail-to-tail at the CK domain, and the vWF multimers are subsequently assembled head-to-head at the D1 domain to form "ultra-large" long chain molecules (Sadler, 1998) of lengths between 100 and 1000 μm (Springer, 2011). Ultra-large vWF is subsequently cleaved at the A2 domain by ADAMTS13 to about 15 μm in the normal circulation (Schneider et al., 2007). VWF binds to collagen via the A3 domain, platelet receptor GPIb via the A1 domain, and platelet integrin $\alpha_{IIb}\beta_3$ at the C1 domain.

VWF has been shown to undergo a conformational change modulated by shear (Siedlecki et al., 1996). Under low shear, vWF assumes a globular form and at high shear is elongated. Recently, Colace and Diamond (2013) showed formation of long fibers or nets of vWF in whole flowing blood at shear rates >25 000 s^{-1}. In addition to modeling shear unfolding of vWF, Schneider et al. (2007) showed that vWF adsorption onto collagen is enhanced at high shear rates (>5000 s^{-1}). These results indicate that vWF unfolding exposes binding sites that are important for platelet adhesion. Additionally, vWF elongation exposes sites for multimer cleavage by protease ADAMTS13 (Dong, 2005).

Quantitative or qualitative defects in vWF or its protease, ADAMTS13, result in bleeding and thrombotic disorders. Von Willebrand disease (VWD) is defined as a quantitative deficiency of vWF (Type 1 and Type 3) or by qualitative abnormalities in vWF structure and function (Type 2) resulting in a decreased capability to form hemostatic platelet plugs. Von Willebrand Disease (VWD) is the most common inherited bleeding disorder in children (Rodeghiero, Castaman, & Dini, 1987). The symptoms of VWD include nose bleeding, skin bruises and hematomas, prolonged bleeding from trivial wounds, oral cavity bleeding, and excessive menstrual bleeding (Sadler et al., 2000). ADAMTS13 deficiency has been linked to thrombotic thrombocytopenia purpura (TTP), a disorder characterized by decreased platelet count, platelet thrombosis of the microvasculature, and skin rash due to bleeding under the skin (Bianchi, Robles, Alberio, Furlan, & Lämmle, 2002; Furlan et al., 1997). ADAMTS13 deficiency results in higher than normal concentrations of circulating ultra-large vWF (ULVWF) multimers. ULVWF has a higher affinity for platelet binding, and thus platelets are scavenged from circulation and form micro-thrombi, resulting in the symptoms of TTP.

As discussed above, vWF is thought to be the primary protein responsible for high shear platelet binding. Wellings and Ku (2012) modeled platelet capture via vWF under very high shear (10 000 to 500 000 s^{-1}) assuming that only A1 domains on the outside of globular vWF were available to bind platelets, with more A1 domains exposed as vWF elongates under shear. Given the high shear conditions leading to large drag forces on adhering platelets and short exposure times of platelet GPIb to vWF-A1, the authors conclude the following conditions necessary for platelet capture at shear rates greater than 50 000 s^{-1}: multiple GPIb-vWF bonds, vWF unfolding, formation of concave vWF nets, and GPIb-(vWF-A1) on-rates greater than 10^8 $M^{-1}s^{-1}$. All but the final conclusion require vWF unfolding for high shear platelet capture and indicate that vWF-A1 availability is the critical factor in high shear platelet capture and thrombus growth. Additionally, modeling showed that local vWF concentration must be elevated by the vWF release from platelets.

1.6 Summary of High Shear Thrombus Formation

Taking the information presented in the preceding sections together leads to a model of high shear thrombosis outlined in Table 1-1 and Figure 1-3. First, atherosclerotic plaques form stenotic regions that induce high fluid shear rates (Figure 1-3A). Plaque cap rupture exposes a thrombogenic surface supporting thrombus initiation. The high shear region caused by the stenosis induces vWF unfolding (Figure 1-3B). Elongated vWF nets are adsorbed onto the surface and form nets (Figure 1-3C). Enhanced platelet diffusivity and margination act to move platelets to the vessel wall (Figure 1-3D) where they reversible bind to surface-bound vWF (Figure 1-3E). After adhesion, platelets activate, likely by a combination of binding, soluble agonists, and high shear. Activation leads to irreversible

binding via $\alpha_{IIb}\beta_3$ and release of platelet granule contents, including vWF, which locally increases the vWF concentration at the site of thrombosis (Figure 1-3F). This process initiates a positive-feedback system that results in billions of platelets rapidly binding and activating, leading to very rapid thrombus growth (Figure 1-3G to J). However, it is unclear what the relative contributions of vWF and platelets are to the process of high shear thrombosis or what the minimum necessary concentrations are. Furthermore, the roles of plasma vWF and platelet vWF remain to be determined (Jackson, 2007). A better understanding of the contributions of vWF and platelets in high shear thrombus formation may lead to better therapeutic targets to prevent arterial thrombosis.

Table 1-1: Process of High Shear Thrombus Formation

1	Regions of stenosis induce high wall shear rates.
2	vWF unfolds in high shear regions.
3	Unfolded vWF is adsorbed onto non-endothelialized surfaces.
4	Shear enhanced diffusivity induces platelet margination and transports platelets to the exposed surface.
5	Non-activated platelets bind to surface-bound vWF.
6	Activation of adhered platelets by shear and/or soluble agonists releases large amount of vWF locally and activates $\alpha_{IIb}\beta_3$ for firm adhesion.
7	vWF nets form on the growing thrombus as platelets are continually captured and activated.
8	The vWF nets rapidly capture billions of platelets with large thrombus formation, vessel occlusion, or embolization.

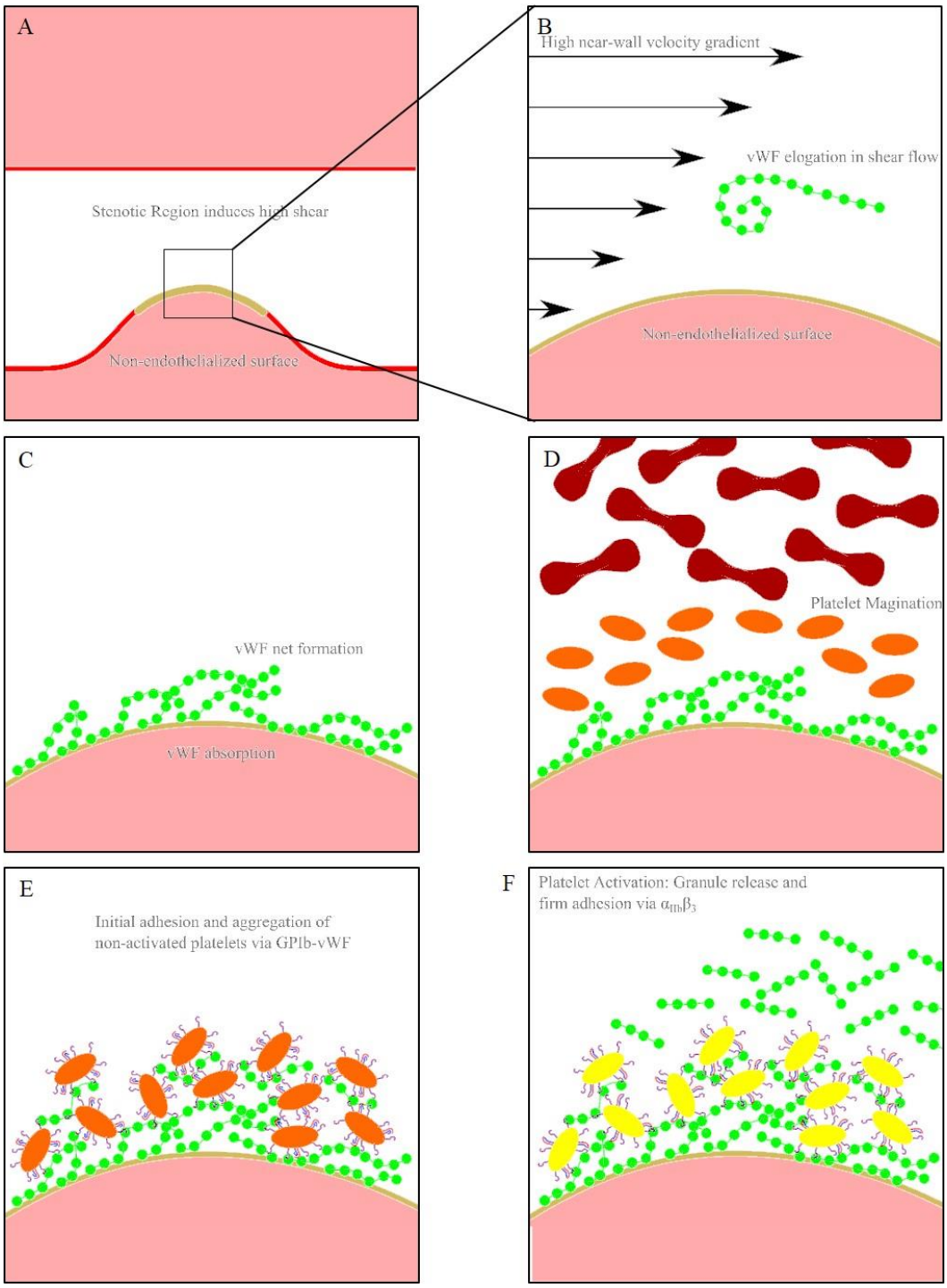

Figure 1-3: Summary of high shear thrombosis. (A) Stenotic regions induce wall high shear rates, (B) high shear conditions result in vWF elongation, (C) vWF is adsorbed to non-endothelialized surfaces, (D) enhanced diffusivity and platelet margination transport platelets to the vessel wall, (E) non-activated platelets bind to vWF, (F) platelet activation releases of granule contents and activates $\alpha_{IIb}\beta_3$, (G-H) vWF is adsorbed to the growing thrombus, and platelets are continually captured and activated, (I) large-scale thrombus formation leads to occlusion or embolization.

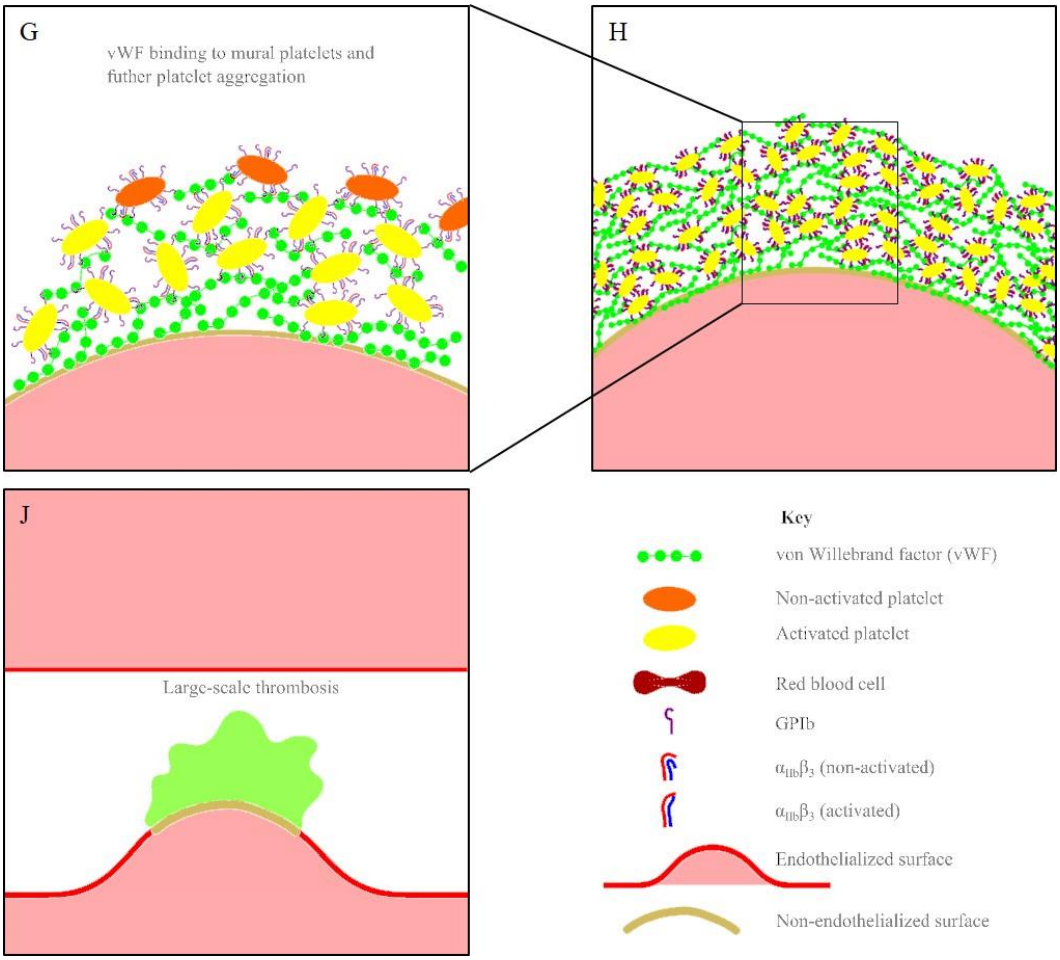

Figure 1-3 cont.: Summary of high shear thrombosis. (A) Stenotic regions induce wall high shear rates, (B) high shear conditions result in vWF elongation, (C) vWF is adsorbed to non-endothelialized surfaces, (D) enhanced diffusivity and platelet margination transport platelets to the vessel wall, (E) non-activated platelets bind to vWF, (F) platelet activation releases of granule contents and activates $\alpha_{IIb}\beta_3$, (G-H) vWF is adsorbed to the growing thrombus, and platelets are continually captured and activated, (I) large-scale thrombus formation leads to occlusion or embolization.

1.7 Predicting and Preventing Thrombosis

Despite the high population rates of MI and stroke, individual prediction remains elusive. Though a number of systemic risk factors have been identified, including age, weight, blood pressure, cholesterol levels, and diabetes, a European Society of Cardiology proposed 10-year risk score gives results between 0% and ~50% (Perk et al., 2012; Smith

et al., 2001). Severe coronary or carotid stenosis are linked to increased risk of stroke (Autret et al., 1987; Ellis et al., 1988), but when specific arterial lesions are assessed, medically treated patients have individually low rates of MI and stroke. One study showed patients with severe stenosis (>50%) of the left anterior descending coronary artery had a three-year risk of anterior MI of 6-11%, and patients with very severe stenosis (>90%) had a 15% risk of anterior MI. Equally noteworthy, patients with less than 50% stenosis had a 2% risk of anterior MI (Ellis et al., 1988). A separate study similarly showed that that two-year risk of ischemic stroke in patients with severe carotid stenosis (>70%) was 10-20%, and patients with mild to moderate stenosis had rates of 5-10% (Rothwell, Gibson, & Warlow, 2000).

Since evidence implicates shear induced platelet accumulation in MI and ischemic stroke, anti-platelet therapies (e.g. aspirin, clopidogrel/Plavix®) to prevent ischemic events (CAPRIE Steering Committee, 1996; Lewis et al., 1983) and platelet function testing to assess efficacy have been developed (Kundu, Heilmann, Sio, Garcia, & Ostgaard, 1996; Lordkipanidze et al., 2007; Rechner, 2011). However, evidence has also emerged that 5 to 25% of patients are not responsive to aspirin therapy (Gum, Kottke-Marchant, Welsh, White, & Topol, 2003; Hovens et al., 2007) based on light transmission aggregometry and point-of-care platelet function tests, including PFA-100® (see Section 1.7.1), and aspirin resistance increases the risk of ischemic events (Krasopoulos, Brister, Beattie, & Buchanan, 2008; Snoep, Hovens, Eikenboom, Van der Bom, & Huisman, 2007; Sofi, Marcucci, Gori, Abbate, & Gensini, 2008), though existing tests give disparate results for patient-specific aspirin resistance (Lordkipanidze et al., 2007). Limited data also suggests that 5-10% of patients are non-responsive to clopidogrel (Michos, Ardehali, Blumenthal,

Lange, & Ardehali, 2006). Thus further methods for patient risk stratification may be useful to guide and assess therapy.

1.7.1 Clinically Available Thrombosis Test Systems

Currently available clinical platelet function tests may not adequately test the platelet accumulation pathways most relevant to MI and stroke. Most assays do not test platelet aggregation under flow, and none provide continuous analysis of thrombus growth. Presently, at least four platelet function tests are marketed for clinical use: light transmission aggregometry (LTA), PFA-100® (Siemens Corp.; Munich, Germany), Chrono-log Whole Blood Aggregometer (Chrono-log Corp.; Haverton, PA), VerifyNow® (Accumetrics, San Diego, CA). LTA, VerifyNow®, and the Chronolog Whole Blood Aggregometer utilize light transmission or impedance to measure platelet aggregation in response to platelet agonists under static flow conditions. LTA requires the use of platelet rich plasma (Rechner, 2011), while VerifyNow® and Chrono-log uses whole blood (Lordkipanidze et al., 2007), but neither system simulates the high shear environment of arterial stenosis and therefore results may not be relevant to arterial thrombosis leading to MI and ischemic stroke.

The PFA-100® system perfuses a whole blood sample through a membrane orifice coated with fibrillar Type I collagen and epinephrine or ADP (Kundu et al., 1995; Kundu et al., 1996). The time to orifice closure is used as the test endpoint. Though this system results in high shear (~6000 s^{-1}) platelet adhesion and aggregation, the fluid mechanics of flow through an orifice, with near zero shear before the orifice and a very short region (150 μm) of elevated shear, are substantially different from flow in a stenotic artery, which

is characterized by a region of normal physiological shear rate (500-1000 s^{-1}) followed by a region of elevated shear rate. Additionally, rather than using only collagen to support platelet adhesion and activation, the membrane is also coated with potent platelet agonists that affect individual activation pathways and may cause the results to differ from *in vivo*. The PFA-100® also does not allow the quantification of thrombus growth during the test. Thus, none of the currently available clinical methods for platelet function analysis utilize test conditions relevant to high shear occlusive thrombus formation and simulate arterial fluid mechanics, especially shear rate, or give insight into how high shear thrombus forms in real time. Furthermore, these tests and others give disparate results when used to assess patient-specific aspirin resistance (Lordkipanidze et al., 2007), and it is unclear which, if any, of the results are most relevant to thrombosis leading to MI and stroke.

VWF mediated platelet aggregation is currently measured using a ristocetin cofactor assay (VWF:RCo). Ristocetin, a now-unused antibiotic, induces vWF-mediated platelet agglutination via a presently unknown mechanism (NHLBI von Willebrand Disease Expert Panel, 2007), though results of VWF:RCo have been shown to correlate with shear dependent platelet-vWF interactions (Dong, 2001). In addition to not simulating physiological platelet-vWF binding, VWF:RCo exhibits very high variability (coefficient of variation $\geq$ 30%). Thus improved platelet function tests for vWF mediated platelet aggregation may be useful in clinical practice.

Based on the recommendations of a report (Zwaginga et al., 2006) from the International Society of Thrombosis and Haemostasis (ISTH), a more robust platelet function test relevant to arterial thrombosis at the site of stenosis should meet the following criteria: 1) limited blood volume, 2) a non-invasive method with bed-side/point-of-care

readouts for broad applicability in a clinical setting, 3) real-time monitoring of thrombus formation, 4) quantification of embolization, 5) use of a reproducible thrombogenic surface, 6) use of controlled shear rates applicable to arterial thrombosis, 7) sensitivity to thrombotic disorders and anti-thrombotic drugs and drug efficacy, 8) capability to monitor platelet inflammatory signatures. In addition to these requirements, we also suggest that an appropriately sized test section should be used to ensure many more platelet-platelet adhesion events than platelet-surface adhesion events. For the monitoring of platelet function associated with MI and stroke, since platelet accumulation appears to depend strongly on shear rate, the non-stenotic and stenotic shear rates in the microfluidic test section were designed to fall in the range of normal arteries (500-1000 s^{-1}) and in the range of coronary and carotid stenosis (5000-10 000 s^{-1}). Since experimental evidence suggests that maximum platelet deposition rates occur at approximately 6000 s^{-1}, this shear range was targeted as an advantageous test shear rate to simulate worst-case thrombus formation. To simulate atherosclerotic plaque cap rupture, we use collagen Type I without additional agonists or coagulation factors as the prothrombotic surface. No presently marketed platelet function test meets all of these test requirements. Only the PFA-100® employs arterial shear rates; LTA, VerifyNow®, and the Chronolog whole blood analyzer all assess platelet function only in static blood. However, PFA-100® does not allow for real-time thrombus monitoring or embolus detection, and the shear rates are not well controlled due to its use of flow through an orifice. The present study endeavored to develop the test section of a robust laboratory high shear platelet function test that better meets these requirements by providing for well-controlled shear rates throughout the test section and a non-contact thrombus detection method that provides information about thrombus growth

and embolization for future development into a clinical assay for routine platelet function analysis.

1.7.2 Microfluidic Thrombosis Assays in the Research Laboratory

Microfluidic test sections are a rapidly emerging design for high shear platelet testing. Microfluidic test sections are a rapidly emerging design for high shear platelet testing. Microfluidic test sections have the advantage of requiring lower flow rates to produce the same wall shear rates as larger devices, thus requiring smaller overall blood volumes. This is particularly attractive for small animal studies, high throughput studies with human blood, and clinical testing of high shear platelet function and thrombus formation. Most microfluidic systems use rectangular cross sections (Colace, Muthard, & Diamond, 2012; Gutierrez et al., 2008; Hosokawa et al., 2011; Hosokawa et al., 2012; Maloney et al., 2010; Neeves et al., 2008), which apply only a single shear rate over their whole length, and fail to simulate the shear experienced by a platelet flowing in a normal arterial section and entering and exiting a stenotic, atherosclerotic section. Recently, a multipath microfluidic test device with a stenotic test section was developed by Li, Ku, and Forest (2012). This design meets many of the physiological/pathological design elements noted above, but it is relatively large for a microfluidic device (test section $w \times h = 750 \times 250$ μm) and requires 4-6 mL of blood for occlusion at shear rates of 7000-10 000 s^{-1}, which is large compared to a standard blood draw of 10 mL, particularly if multiple tests are required. Future high-shear thrombosis test devices should aim to reduce the required blood volume and streamline fluid handling to enable routine thrombosis testing. In the present study, a smaller microfluidic test section requiring less than 10 mL of blood for 3 tests was designed

along with a fluid handling system that minimized blood transfers and provides for high throughput. This test bed allowed for the subsequent aims to be performed with a reasonable (<10 mL) amount of human blood and provide the framework for a future commercial device.

1.8 Summary, Hypothesis and Specific Aims

Myocardial infarction (MI) and ischemic stroke result from the formation of occlusive thrombosis at the site of atherosclerotic plaque rupture at very high shear rates (5000 to >10 000 s^{-1}). In general, thrombosis results from the combination of 1) abnormal fluid mechanic conditions, 2) a thrombogenic surface, and 3) pro-thrombotic blood chemistry. In the case of MI and ischemic stroke, plaque formation leads to stenosis, resulting in a region of very high fluid shear rate, which enhances platelet thrombus formation. When plaque rupture exposes the pro-thrombotic collagen, thrombosis may occur. Even in patients with arterial stenosis, prediction of MI and ischemic stroke remains elusive, indicating that pro-thrombotic blood chemistry may be an important risk factor. Still, few studies have endeavored to characterize the effect of plasma protein concentrations on high shear thrombus formation.

Platelet adhesion to collagen via blood glycoprotein von Willebrand Factor (vWF) is important for thrombosis initiation at high shear. VWF is a shear-sensitive multimer that transitions from a globular to elongated conformation under high shear rate, enhancing absorption onto a collagen surface and platelet adhesion. Furthermore, computational modeling of bonding kinetics indicates that vWF unfolding and net formation may be

essential for thrombosis at very high shear rate, indicating that vWF configuration and vWF-A1 availability may be the rate-limiting factors in high shear thrombosis.

The **objective** of the present study was to quantify the role vWF in thrombus formation using a microfluidic test system. The **long term goal** of this project is to assess patient risk of MI and ischemic stroke based on individual blood chemistry and identify potential therapeutic targets. The **hypothesis** of this study is that the rate of shear induced platelet accumulation depends on vWF-A1 availability determined by plasma vWF concentration. To address this hypothesis, the following specific aims were executed:

Specific Aim 1: Assess the effect of flow pulsatility on shear induced platelet accumulation. Flow conditions, particularly shear rate, modulate platelet accumulation, but the effects of arterial pulsatile flow conditions are not well established. In this aim, whole porcine blood was be perfused through collagen-coated stenotic test sections under 1 Hz pulsatile condition generated by a custom pressure driven experimental apparatus corresponding shear-matched steady conditions (~3800, 6500, and ~16 000 s^{-1}). Time to occlusion, lag time, thrombus growth rate were obtained from microscopy images and compared between conditions. Results of this aim provide important design considerations for the high shear occlusive thrombus test described in the following aim.

Specific Aim 2: Develop a high-shear, whole blood device for assessing arterial thrombosis potential. The device should require less than 10 mL of blood and provide high throughput for laboratory personnel. A microfluidic test cartridge was be developed based on the need for an efficient, low volume assay to evaluate patient risk for

thrombotic occlusion based on thrombus growth rate and time to occlusion. Design parameters include shear rate, blood volume, known thrombus growth characteristics, and manufacturing considerations. The test section was characterized by assessing thrombus formation in a normal population, providing a robust microfluidic platform for the subsequent aim.

Specific Aim 3: Demonstrate that thrombus formation at very high shear rates requires a minimum plasma vWF concentration to initiate thrombus growth and vWF release from platelets for large-scale accumulation. Though individual plasma proteins have been implicated in arterial thrombosis, the effects on shear induced platelet accumulation of below-normal plasma vWF concentrations and vWF-deficient platelets have not been previously studied. To show that SIPA is limited by the availability of vWF rather than other blood proteins and constituents, dilutions of whole human blood with normal hematocrit and ranges of platelet counts and vWF concentrations were perfused through the test section developed in Specific Aim 2 at shear rates of 6000 s^{-1}. Microscopy images of thrombus formation were acquired throughout the experiments and time to occlusion was determined by measuring flow rate through the test section. A regression model of thrombotic occlusion was developed over platelet and vWF concentrations assessed.

1.9 References

Autret, A., Saudeau, D., Bertrand, P., Pourcelot, L., Marchal, C., & deBoisvilliers, S. (1987). Stroke risk in patients with carotid stenosis. *The Lancet*.

Badimon, J. J., Badimon, L., Galvez, A., Chesebro, J., & Fuster, V. (1986). Influence of arterial damage and wall shear rate on platelet deposition: Ex vivo study in a swine model. *Arteriosclerosis, Thrombosis, and Vascular Biology, 6*, 312-320.

Bark, D. L., & Ku, D. N. (2010). Wall shear over high degree stenoses pertinent to atherothrombosis. *Journal of Biomechanics, 43*(15), 2970-2977. doi: 10.1016/j.jbiomech.2010.07.011

Bark, D. L., Para, A. N., & Ku, D. N. (2012). Correlation of thrombosis growth rate to pathological wall shear rate during platelet accumulation. *Biotechnology and Bioengineering, 109*(10), 2642-2650.

Barstad, R. M., Roald, H., Cui, Y., Turitto, V., & Sakariassen, K. (1994). A perfusion chamber developed to investigate thombus formation and shear profiles in flowing native human blood at the apex of a well-defined stenosis. *Arteriosclerosis, Thrombosis, and Vascular Biology, 14*, 1984-1991.

Bergmeier, W., Chauhan, A. K., & Wagner, D. D. (2008). Glycoprotein Ibα and von Willebrand factor in primary platelet adhesion and thrombus formation: Lessons from mutant mice. *Thrombosis and Haemostasis*. doi: 10.1160/th07-10-0638

Bianchi, V., Robles, R., Alberio, L., Furlan, M., & Lämmle, B. (2002). Von Willebrand factor–cleaving protease (ADAMTS13) in thrombocytopenic disorders: a severely deficient activity is specific for thrombotic thrombocytopenic purpura. *Blood, 100*(2), 710-713. doi: 10.1182/blood-2002-02-0344

Bongers, T., de Maat, M., van Goor, M., Bhagwanbali, V., van Vliet, H., Gomez Garcia, E., . . . Leebeek, F. W. G. (2006). High von Willebrand factor levels increase the risk of first ischemic stroke: Influence of ADAMTS13, inflammation, and genetic variability. *Stroke, 37*, 2671-2677. doi: 10.1161/01.STR.0000244767.39962.f7

CAPRIE Steering Committee. (1996). A randomised, blinded, trial of clopidogrel versus aspirin in patients at risk of ischeamic events (CAPRIE). *The Lancet, 348*, 1329-1339.

Chung, I., & Lip, G. Y. H. (2003). Virchow's Triad revisited: Blood constituents. *Pathophysiology of Haemostasis and Thrombosis, 33*, 449-454.

Colace, T., Muthard, R., & Diamond, S. L. (2012). Thrombus growth and embolism on tissue factor-bearing collagen surfaces under flow: Role of thrombin with and without fibrin. *Arteriosclerosis, Thrombosis, and Vascular Biology, 32*, 1466-1476. doi: 10.1161/ATVBAHA.112.249789/-/DC1

Colace, T., & Diamond, S. L. (2013). Direct observation of von Willebrand factor elongation and fiber formation on collagen during acute whole blood exposure to pathological flow. *Arteriosclerosis, Thrombosis, and Vascular Biology, 33*, 105-113. doi: 10.1161/ATVBAHA.112.300522/-/DC1
10.1161/ATVBAHA.112.300522>

Davi, G., & Patrono, C. (2007). Platelet activation and atherothrombosis. *New England Journal of Medicine, 357*, 2482-2494.

Davies, M. J., Fulton, W., & Robertson, W. (1979). The relation of coronary thrombosis to ischaemic myocardial necrosis. *Journal of Pathology, 127*, 99-110.

Davies, M. J., Thomas, T., McMichael, J., & Richardson, P. D. (1981). The pathological basis and microanatomy of occlusive thrombus formation in human coronary arteries. *Philosophical Transactions of the Royal Society B: Biological Sciences, 294*(1072), 225-229. doi: 10.1098/rstb.1981.0101

Davies, M. J., & Thomas, A. (1984). Thrombosis and acute coronary-artery lesions in sudden cardiac ischemic death. *New England Journal of Medicine, 310*(18), 1137-1140.

Davies, M. J., & Thomas, A. (1985). Plaque fissuring: The cause of acute myocardial infarction, sudden ischaemic death, and crescendo angina. *British Heart Journal, 53*, 363-373.

Davies, M. J. (1994). Pathology of arterial thrombosis. *British Medical Bulletin, 50*(4), 789-802.

Dong, J.-F. (2005). Cleavage of ultra-large von Willebrand factor by ADAMTS-13 under flow conditions. *Journal of Thrombosis and Haemostasis, 3*, 1710-1716.

Dong, J. F. (2001). Ristocetin-dependent, but not botrocetin-dependent, binding of von Willebrand factor to the platelet glycoprotein Ib-IX-V complex correlates with shear-dependent interactions. *Blood, 97*(1), 162-168. doi: 10.1182/blood.V97.1.162

Ellis, S., Alderman, E., Cain, K., Fisher, L., Sanders, W., & Bourassa, M. (1988). Prediction of risk of anterior myocardial infarction by lesion severity and measurement method of stenoses in the left anterior decendinging coronary distribution: A CASS Registry Study. *Journal of the American College of Cardiology, 11*(5), 908-916.

Falk, E. (1983). Plaque rupture with severe pre-existing stenosis precipitating coronary thrombosis: Characteristics of coronary atherosclerotic plaques underlying fatal occlusive thrombi. *British Heart Journal, 50*, 127-134.

Falk, E. (1985). Unstable angina with fatal outcome: Dynamic coronary thrombosis leading to infarction and/or sudden death. Autopsy evidence of recurrent mural thrombosis

with peripheral embolization culminating in total vascular occlusion. *Circulation, 71*(4), 699-708. doi: 10.1161/01.cir.71.4.699

Friedman, M., & van den Bovenkam, G. (1966). The pathogenesis of a coronary thrombus. *American Journal of Pathology, 48*(1), 19-44.

Friedman, M. (1971). The coronary thrombosis: Its origin and fate. *Human Pathology, 2*(1), 81-128.

Furlan, M., Robles, R., Solenthaler, M., Wassmer, M., Sandoz, P., & Lämmle, B. (1997). Deficient Activity of von Willebrand Factor–Cleaving Protease in Chronic Relapsing Thrombotic Thrombocytopenic Purpura. *Blood, 89*(9), 3097-3103.

Glagov, S., Zarins, C., Giddons, D. P., & Ku, D. N. (1988). Hemodynamics and atherosclerosis. Insights and perspectives gained from studies of human arteries. *Archives of Clinical and Laboratory Medicine, 112*(10), 1018-1031.

Gold, H. K., Leinbach, R. C., Garabedian, H. D., Yasuda, T., Johns, J. A., Grossbard, E. B., . . . Collen, D. (1986). Acute coronary reocclusion after thrombolysis with recombinant human tissue-type plasminogen activator: Prevention by a maintenance infusion. *Circulation, 73*(2), 347-352. doi: 10.1161/01.cir.73.2.347

Gum, P. A., Kottke-Marchant, K., Welsh, P. A., White, J., & Topol, E. J. (2003). A prospective, blinded determination of the natural history of aspirin resistance among stable patients with cardiovascular disease. *Journal of the American College of Cardiology, 41*(6), 961-965. doi: 10.1016/s0735-1097(02)03014-0

Gutierrez, E., Petrich, B. G., Shattil, S. J., Ginsberg, M. H., Groisman, A., & Kasirer-Friede, A. (2008). Microfluidic devices for studies of shear-dependent platelet adhesion. *Lab on a Chip, 8*(9), 1486-1495. doi: 10.1039/b804795b

He, X., & Ku, D. N. (1996). Pulsatile flow in the human left coronary artery bifurcation: average conditions. *Journal of Biomechanical Engineering, 118*(1), 74-82.

Holme, P. A., Ørvim, U., Hamers, M. J. A. G., Solum, N. O., Brosstad, F. R., Barstad, R. M., & Sakariassen, K. S. (1997). Shear-induced platelet activation and platelet microparticle formation at blood flow conditions as in arteries with a severe stenosis. *Arteriosclerosis, Thrombosis, and Vascular Biology, 17*, 646-653.

Hosokawa, K., Ohnishi, T., Kondo, T., Fukasawa, M., Koide, T., Maruyama, I., & Tanaka, K. A. (2011). A novel automated microchip flow-chamber system to quantitatively evaluate thrombus formation and antithrombotic agents under blood flow conditions. *J Thromb Haemost, 9*(10), 2029-2037. doi: 10.1111/j.1538-7836.2011.04464.x

Hosokawa, K., Ohnishi, T., Fukasawa, M., Kondo, T., Sameshima, H., Koide, T., . . . Maruyama, I. (2012). A microchip flow-chamber system for quantitative

assessment of the platelet thrombus formation process. *Microvascular Research, 83*(2), 154-161. doi: 10.1016/j.mvr.2011.11.007

Hovens, M. M. C., Snoep, J. D., Eikenboom, J. C. J., van der Bom, J. G., Mertens, B. J. A., & Huisman, M. V. (2007). Prevalence of persistent platelet reactivity despite use of aspirin: A systematic review. *American Heart Journal, 153*(2), 175-181. doi: 10.1016/j.ahj.2006.10.040

Jackson, S. P. (2007). The growing complexity of platelet aggregation. *Blood, 109*(12), 5087-5095. doi: 10.1182/blood-2006-12-027698

Jansson, J., Kilsson, T., & Johnson, O. (1991). von Willebrand factor in plasma: A novel risk factor for recurrent myocardial infarction and death. *British Heart Journal, 66*, 351-355.

Jesty, J., Yin, W., Perrotta, P., & Bluestein, D. (2003). Platelet activation in a circulating flow loop: Combined effects of shear stress and exposure time. *Platelets, 14*, 143-149. doi: 10.1080/0953710031000092839

Krasopoulos, G., Brister, S. J., Beattie, W. S., & Buchanan, M. R. (2008). Aspirin "resistance" and risk of cardiovascular morbidity: systematic review and meta-analysis. *BMJ, 336*(7637), 195-198. doi: 10.1136/bmj.39430.529549.BE

Ku, D. N., Giddens, D. P., Phillips, D. J., & Strandness Jr, D. E. (1985). Hemodynamics of the normal human carotid bifurcation: In vitro and in vivo studies. *Ultrasound in Medicine and Biology, 11*(1), 13-26. doi: http://dx.doi.org/10.1016/0301-5629(85)90003-1

Ku, D. N., & Flannery, C. J. (2007). Development of a flow-through system to create occluding thrombus. *Biorheology, 44*, 273-284.

Kundu, S., EJ, H., R, S., Garcia, C., Davidson, R., & Ostgaard, R. (1995). Description of an in vitro platelet function analyzer - PFA-100^{TM}. *Seminars in Thrombosis and Hemostatsis, 21*(Suppl. 2), 106-112.

Kundu, S., Heilmann, E., Sio, R., Garcia, C., & Ostgaard, R. (1996). Characterization of an in vitro platelet function analyzer, PFA-100^{TM}. *Clinical and Applied Thrombosis/Hemostatis, 2*(4), 241-249. doi: 10.1177/107602969600200404

Lewis, H., Davis, J., DArchibald, D., Steinke, W., Smitherman, T., Doherty, J., . . . DeMots, E. (1983). Protective effects of aspirin against acute myocardial infarction and death in men with unstable angina. *New England Journal of Medicine, 309*(7), 396-403.

Li, M., Ku, D., & Forest, C. (2012). Microfluidic system for simultaneous optical measurement of platelet aggregation at multiple shear rates in whole blood. *Lab on a Chip, 12*, 1355-1362.

Lippi, G., Franchini, M., & Targher, G. (2011). Arterial thrombus formation in cardiovascular disease. *Nature Reviews Cardiology, 8*, 502-512. doi: 10.1038/nrcardio.2011.91

Lordkipanidze, M., Pharand, C., Schampaert, E., Turgeon, J., Palisaitis, D. A., & Diodati, J. G. (2007). A comparison of six major platelet function tests to determine the prevalence of aspirin resistance in patients with stable coronary artery disease. *European Heart Journal, 28*, 1702-1708. doi: 10.1093/eurheartj/ehm226
10.1093/eurheartj/ehm232

Lowe, G. D. O. (2003). Virchow's Triad revisited: Abnormal flow. *Pathophysiology of Haemostasis and Thrombosis, 33*, 455-457.

Mackman, N. (2008). Triggers, targets and treatments for thrombosis. *Nature, 451*(7181), 914-918. doi: 10.1038/nature06797

Maloney, S. F., Brass, L., & Diamond, S. L. (2010). P2Y12 or P2Y1 inhibitors reduce platelet deposition in a microfluidic model of thrombosis while apyrase lacks efficacy under flow conditions. *Integrative Biology, 2*(4), 153-220. doi: 10.1039/b919728a
10.1039/B919728A

Maxwell, M. J., Westein, E., Nesbitt, W. S., Giuliano, S., Dopheide, S. M., & Jackson, S. P. (2007). Identification of a 2-stage platelet aggregation process mediating shear-dependent thrombus formation. *Blood, 109*(2), 566-576. doi: 10.1182/blood-2006-07-028282

Michos, E. D., Ardehali, R., Blumenthal, R. S., Lange, R. A., & Ardehali, H. (2006). Aspirin and clopidogrel resistance. *Mayo Clinic Proceedings, 81*(4), 518-526.

Neeves, K. B., Maloney, S. F., Fong, K. P., Schmaier, A. A., Kahn, M. L., Brass, L. F., & Diamond, S. L. (2008). Microfluidic focal thrombosis model for measuring murine platelet deposition and stability: PAR4 signaling enhances shear-resistance of platelet aggregates. *Journal of Thrombosis and Haemostasis, 6*, 2193-2201. doi: 10.1111/j.1538-7836.2008.03188.x

Neeves, K. B., Onasoga, A. A., Hansen, R. R., Lilly, J. S., Venckuaite, D., Sumner, M. B., . . . Di Paolo, J. A. (2013). Sources of Variability in Platelet Accumulation on Type 1 Fibrillar Collagen in Microfluidic Flow Assays. *PLoS One, 8*(1), Epub.

NHLBI von Willebrand Disease Expert Panel. (2007). The Diagnosis, Evaluation and Management of von Willebrand Disease Diagnosis and Evaluation: National Heart, Lung, and Blood Institute.

Para, A. N., Bark, D. L., Lin, A., & Ku, D. N. (2011). Rapid platelet accumulation leading to thrombotic occlusion. *Annals of Biomedical Engineering, 39*(7), 1961-1971. doi: 10.1007/s10439-011-0296-3

Para, A. N. (2012). *Preventing Rapid Platelet Accumulation under Very High Shear Stress.* (PhD), Georgia Institute of Technology, Atlanta, GA.

Perk, J., De Backer, G., Gohlke, H., Graham, I., Reiner, Z., Verschuren, M., . . . Zannad, F. (2012). European guidelines on cardiovascular disease prevention in clinical practice. *European Heart Journal, 33*(13), 1635-1701. doi: 10.1093/eurheartj/ehs092

Ramstack, J., Zuckerman, L., & Mockros, L. (1979). Shear-induced activation of platelets. *Journal of Biomechanics, 12*, 113-125.

Rechner, A. R. (2011). Platelet function testing in clinical diagnostics. *Hamostaseologie, 31*(2), 79-87. doi: 10.5482/ha-1133

Reininger, A. J., Bernlochner, I., Penz, S. M., Ravanat, C., Smethurst, P., Farndale, R. W., . . . Siess, W. (2010). A 2-Step mechanism of arterial thrombus formation induced by human atherosclerotic plaques. *Journal of the American College of Cardiology, 55*(11), 1147-1158. doi: 10.1016/j.jacc.2009.11.051

Rodeghiero, F., Castaman, G., & Dini, E. (1987). Epidemiological investigation of the prevalence of von Willebrand's disease. *Blood, 69*, 454-459.

Rothwell, P. M., Gibson, R., & Warlow, C. P. (2000). Interrelation between plaque surface morphology and degree of stenosis on carotid angiograms and the risk of ischemic stroke in patients with symptomatic carotid stenosis. *Stroke, 31*(3), 615-621. doi: 10.1161/01.str.31.3.615

Ruggeri, Z. M., Orje, J., Haberman, R., Federici, A., & Reininger, A. J. (2006). Activation-independent platelet adhesion and aggregation under elevated shear stress. *Blood, 108*(6), 1903-1910. doi: 10.1182/blood-2006-04-011551

Ruggeri, Z. M. (2007). Von Willebrand factor: Looking back and looking forward. *Thrombosis and Haemostasis*. doi: 10.1160/th07-04-0279

Rumbaut, R., & Thiagarajan, P. (2010). Arterial, venous, and microvascular hemostasis/thrombosis *Platelet-vessel Wall Interactions in Hemostasis and Thrombosis*. San Rafael, CA: Morgan & Claypool Life Sciences.

Sadler, J. (1998). Biochemistry and genetics of von Willebrand factor. *Annual Review of Biochemistry, 67*(395-424), 395.

Sadler, J. E., Mannucci, P., Berntorp, E., Bochkov, N., Boulyjenkov, V., Ginsburg, D., . . . Srivastrava, A. (2000). Impact, Diagnosis and Treatment of von Willebrand Disease. *Thrombosis and Haemostasis, 84*, 160-174.

Sakariassen, K. S., Bolhuis, P. A., & Sixma, J. (1979). Human blood platelet adhesion to artery subendothelium is mediated by factor VIII-von Willebrand factor bound to the subendothelium. *Nature, 279*, 636-638.

Salam, T. A., Lumsden, A. B., Suggs, W. D., & Ku, D. N. (1996). Low shear stress promotes intimal hyperplasia thickening. *Journal of Vascular Investigation, 2*, 12-22.

Savage, B., Saldivar, E., & Ruggeri, Z. M. (1996). Initiation of platelet adhesion by arrest onto fibrinogen or translocation on von Willebrand factor. *Cell, 84*, 289-297.

Savage, B., Almus-Jacobs, F., & Ruggeri, Z. M. (1998). Specific synergy of multiple substrate–receptor interactions in platelet thrombus formation under flow. *Cell, 94*, 657-666.

Schneider, S. W., Nuschele, S., Wixforth, A., Gorzelanny, C., Alexander-Katz, A., Netz, R. R., & Schneider, M. F. (2007). Shear-induced unfolding triggers adhesion of von Willebrand factor fibers. *Proceedings of the National Academy of Sciences, 104*(19), 7899-7903. doi: 10.1073/pnas.0608422104

Siedlecki, C., Lestini, B., Kotte-Marchant, K., Eppell, S., Wilson, D., & Marchant, R. (1996). Shear-depedent change in the three-dimensional structure of human von Willebrand factor. *Blood, 88*, 2939-2950.

Sixma, J., de Groot, P. G., van Zanten, H., & Ijsseldijk, M. (1998). A new perfusion chamber to detect platelet adhesion using a small volume of blood. *Thrombosis Research, 92*, S43-S46.

Smith, S. C., Blair, S. N., Bonow, R. O., Brass, L. M., Cerqueira, M. D., Dracup, K., . . . Taubert, K. A. (2001). AHA/ACC guidelines for preventing heart attack and death in patients with atherosclerotic cardiovascular disease: 2001 Update: A statement for healthcare professionals from the American Heart Association and the American College of Cardiology. *Circulation, 104*(13), 1577-1579. doi: 10.1161/hc3801.097475

Snoep, D., Hovens, M., Eikenboom, J., Van der Bom, J. G., & Huisman, M. V. (2007). Association of laboratory-defined aspirin resistance with a higher risk of recurrent cardiovascular events. *Archieves of Internal Medicine, 167*(15), 1593-1599.

Sofi, F., Marcucci, R., Gori, A. M., Abbate, R., & Gensini, G. F. (2008). Residual platelet reactivity on aspirin therapy and recurrent cardiovascular events — A meta-analysis. *International Journal of Cardiology, 128*(2), 166-171. doi: 10.1016/j.ijcard.2007.12.010

Springer, T. A. (2011). Biology and physics of von Willebrand factor concatamers. *J Thromb Haemost, 9 Suppl 1*, 130-143. doi: 10.1111/j.1538-7836.2011.04320.x

van Breugel, H. H., Sixma, J. J., & Heethaar, R. M. (1988). Effects of flow pulsatility on platelet adhesion to subendothelium. *Arteriosclerosis, Thrombosis, and Vascular Biology, 8*(3), 332-335. doi: 10.1161/01.atv.8.3.332

Wellings, P. J., & Ku, D. N. (2012). Mechanisms of platelet capture under very high shear. *Cardiovascular Engineering and Technology, 3*(2), 161-170. doi: 10.1007/s13239-012-0086-6

Westein, E., van der Meer, A. D., Kuijpers, M. J., Frimat, J. P., van den Berg, A., & Heemskerk, J. W. (2013). Atherosclerotic geometries exacerbate pathological thrombus formation poststenosis in a von Willebrand factor-dependent manner. *Proceedings of the National Academy of Sciences of the United States of America, 110*(4), 1357-1362. doi: 10.1073/pnas.1209905110

Wootton, D., Markou, C., Hanson, S., & Ku, D. (2001). A mechanistic model of acute platelet accumulation in thrombogenic stenosis. *Annals of Biomedical Engineering, 29*, 321-329. doi: 10.1114/1.1359449

Yago, T., Lou, J., Wu, T., Yang, J., Miner, J. J., Coburn, L., . . . Zhu, C. (2008). Platelet glycoprotein Ibα forms catch bonds with human WT vWF but not with type 2B von Willebrand disease vWF. *Journal of Clinical Investigation*. doi: 10.1172/jci35754

Zhao, X. M., Wu, Y. P., Cai, H. X., Wei, R., Lisman, T., Han, J. J., . . . de Groot, P. G. (2008). The influence of the pulsatility of the blood flow on the extent of platelet adhesion. *Thrombosis Research, 121*(6), 821-825. doi: 10.1016/j.thromres.2007.07.013

Zwaginga, J. J., Sakariassen, K. S., Nash, G., King, M. R., Heemskerk, J. W., Frojmovic, M., & Hoylaerts, M. F. (2006). Flow-based assays for global assessment of hemostasis. Part 2: current methods and considerations for the future. *J Thromb Haemost, 4*(12), 2716-2717. doi: 10.1111/j.1538-7836.2006.02178.x

CHAPTER 2: HIGH SHEAR THROMBUS FORMATION UNDER PULSATILE AND STEADY FLOW

2.1 Introduction

Myocardial infarction is precipitated by platelet-rich thrombus formation at the site of atherosclerotic plaque rupture (Davies, Fulton, & Robertson, 1979; Davies & Thomas, 1984, 1985; Davies, 1994) under high shear rates (>3500 s^{-1}) (Bark & Ku, 2010). Thrombus formation can fully occlude the vessel and can lead to sudden cardiac ischemic death in less than an hour (Davies & Thomas, 1984). In pursuit of a greater understanding of thrombus formation mechanisms, many investigators have studied platelet adhesion and aggregation *in vitro* under steady flow conditions (Badimon, Badimon, Galvez, Chesebro, & Fuster, 1986; Badimon & Badimon, 1989; Barstad, Roald, Cui, Turitto, & Sakariassen, 1994; Colace, Jobson, & Diamond, 2011; Gutierrez et al., 2008; Hosokawa et al., 2011; Houdijk, de Groot, Nievelstein, Sakariassen, & Sixma, 1986; Li, Ku, & Forest, 2012; Mailhac et al., 1994; Maloney, Brass, & Diamond, 2010; Neeves et al., 2008; Sakariassen, Aarts, & de Groot, 1983; Sixma, de Groot, van Zanten, & Ijsseldijk, 1998; Zhao et al., 2008).

Platelet deposition under high shear rates is thought to be mediated by platelet glycoprotein Ib (GPIb) binding to immobilized von Willebrand factor (vWF) on a thrombogenic surface, *e. g.* collagen (Ruggeri, 2007; Savage, Saldivar, & Ruggeri, 1996). Subsequent platelet activation results in firm adhesion via integrin $\alpha_{IIb}\beta_3$ (Epstein, Lefkovits, Plow, & Topol, 1995). Platelet deposition has been shown to depend on shear rate. Specifically, platelet adhesion and accumulation rates increase with shear rate up to 1500 and 6000 s^{-1}, respectively (Bark, Para, & Ku, 2012; Savage et al., 1996).

Most previous studies have investigated thrombus formation under flow conditions with shear rates of less than 1500 s^{-1}, and nearly all utilized steady flow. However, flow in arteries is pulsatile with a frequency of approximately 1 Hz, and stenotic geometry induces shear rates of well over 1500 s^{-1} (Bark & Ku, 2010). Since platelet deposition depends on shear rate under steady conditions (Bark et al., 2012), it is reasonable to question whether unsteady time variations in pulsatile shear rate may also affect thrombus growth. A small number of studies have investigated platelet deposition under pulsatile flow. Van Breugel et al. (van Breugel, Sixma, & Heethaar, 1988) investigated platelet adhesion using an annular perfusion chamber under mean shear rates ranging from 0 to 1800 s^{-1}, amplitudes of 75 to 1000 s^{-1}, and frequencies of 0.5 to 2 Hz. Results indicated no significant difference in platelet adhesion per unit area between pulsatile and steady flow for mean shear rates >0 s^{-1}, and results show increased platelet adhesion with increasing amplitude for a mean shear rate of 0 s^{-1}. The flow conditions utilized by Van Breugal and colleagues yield shear rates much lower than those expected in stenotic coronary arteries, and their experimental apparatus did not allow for reversing flow for non-zero mean shear rates (Ku, 1997). The deviation of the experimental shear waveform from expected pathological conditions may lead to platelet adhesion results that are not relevant to coronary thrombosis at the site of atherosclerotic stenosis. In a more recent study, Zhao et al. (Zhao et al., 2008) investigated the effect of pulsatility on platelet adhesion at steady shear rates of 300 s^{-1} and 1300 s^{-1} and under a pulsatile condition which alternated between the two shear rates at a frequency of 0.067 Hz (30 s period). In this case, platelet adhesion was shown to increase at a steady shear rate of 1300 s^{-1} compared to 300 s^{-1}, and pulsatile flow resulted in the highest level of platelet adhesion studied, conflicting with the observations of van Breugel et al. The

relevance of the Zhao results to coronary thrombosis is questionable as the pulse frequency used was considerably less than that of the coronary arteries, and the shear rates were lower than expected in coronary stenosis.

The objective of the present study is to quantify the effect of reversing pulsatile flow relevant to the very high shear conditions present in coronary stenoses on platelet accumulation leading to formation of an occlusive thrombus. A tubular stenotic test section (Ku & Flannery, 2007; Para, Bark, Lin, & Ku, 2011) was adapted for use with a pulsatile flow apparatus. Thrombus growth rate, time to occlusion, and lag time were quantified under a surrogate coronary artery pulsatile shear waveform, and under steady flow conditions corresponding to the mean and maximum pulsatile shear rates. Results of this study may be applied to the design of flow-based thrombosis assays, specifically to assess whether a simpler steady flow system yields comparable results to more complicated pulsatile flow systems.

2.2 Methods

2.2.1 Experimental Apparatus

Whole porcine blood was obtained from a local abattoir (Holifield Farms, Covington, GA) and lightly heparinized at 3.5 USP units/mL, as previously described (Para et al., 2011). Porcine blood has red blood cell count of $5.37 \pm 0.74 \times 10^6$ /μL and platelet count of 407 320 ± 121 240 /uL, on average (Velik-Salchner et al., 2006). A sample from the farm pigs used in this study showed a red blood cell count of 5.9×10^6 /μL and a platelet count 480 000 /μL, both comparable to the literature values. For steady flow experiments, blood was perfused through the experimental apparatus described by Ku and Flannery (Ku & Flannery, 2007) (Figure 2-1a). Briefly, stenotic glass test sections were fabricated by a

professional glass blower, and test sections were selected for 77-79% stenosis by diameter, yielding a minimum throat diameter of 315-345 μm. Test sections were incubated with 0.1% collagen (Chronopar; Chronolog, Inc.; Havertown, PA) for 24 hours before experimentation. After rinsing with PBS, the test section was installed downstream of a fixed pressure head, which was varied to achieve the desired shear rate within the stenotic section.

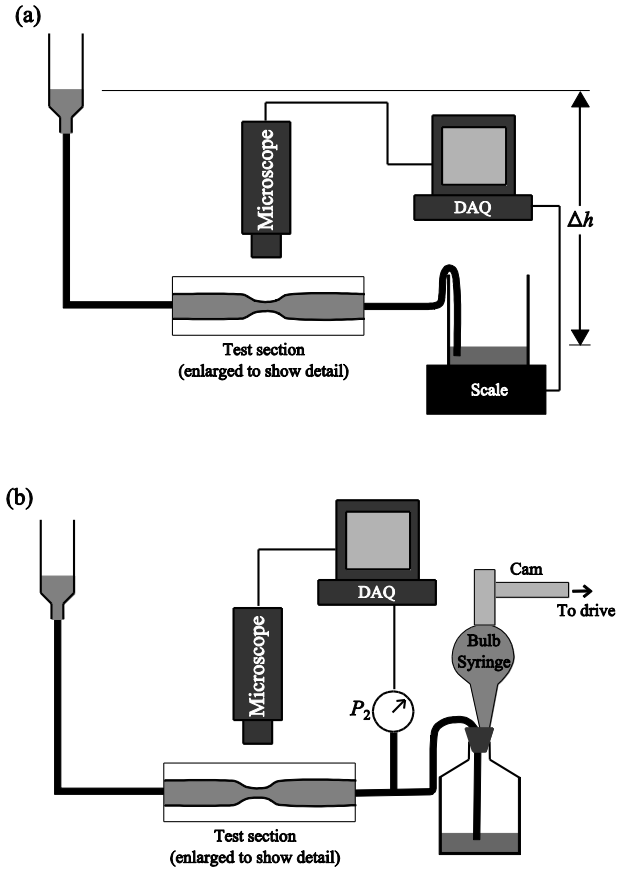

Figure 2-1: Experimental apparatus for (a) steady and (b) pulsatile flow conditions

Steady flow experiments were performed under three shear rates, ~16 000 s^{-1}, ~3800 s^{-1}, and ~6500 s^{-1}, corresponding to the estimated maximum and mean expected

shear rates, as well as an intermediate flow condition, under pulsatile flow conditions. The intermediate flow condition corresponds to a previously measured range of fastest platelet thrombus growth (Bark et al., 2012). For each condition, the nominal shear rate is the initial shear rate at the throat of the stenosis. The shear rate throughout the experiment decreases as the growing thrombus increases the resistance of the test section, resulting in decreased flow rate with the same pressure head, according to Poiseuille's law. Using the calculation of enhanced platelet diffusivity of Zydney and Colton (Zydney & Colton, 1988), the Schmidt numbers under these flow conditions are between 37 and 154, and the Peclet numbers are between 2618 and 2664. See Section 2.6 for more detailed treatment of the calculations for the Reynolds, Peclet, and Schmidt numbers. Blood flow out of the test section was measured using an electronic balance (HCB 302; Adam Equipment Co.; Danbury, CT) and recorded using Labview (National Instruments Corp.; Austin, TX). Time to occlusion, t_{occ}, was defined as the time at which the mass no longer changed for at least 2 minutes.

Pulsatile flow was achieved by having blood flow from a fixed upstream pressure head, through the test section, and into a sealed 250 mL flask (Figure 2-1b). The stopper of the flask was fitted with a 30 mL (1 oz.) bulb syringe, which was compressed using a rotating cam to modulate the downstream pressure. The cam was machined in-house with a circular profile with a diameter of 1.60 in. (40.6 mm) and a shaft offset of 0.20 in. (5.1 mm) to achieve the desired compression of the bulb syringe. The shaft was machined to interface with the drive of a peristaltic pump and controller (Masterflex L/S, model number 77300-40; Cole-Parmer; Vernon Hills, IL). In this way, the pressure difference across the test section was modulated to produce pulsatile flow at 1 Hz. The upstream

reservoir was connected to the test section via 49 cm of 1.6 mm ID Tygon tubing (Masterflex L/S 14; Cole-Parmer; Vernon Hills, IL), and the test section was connected to the flask by 37 mm of the same tubing. The pressure immediately downstream of the test section, p_2 was measured using a pressure transducer (#60-3002; Harvard Apparatus; Holliston, MA) and recorded using Labview. The remaining volume in the upstream reservoir was measured visually and recorded every 30 seconds, and t_{occ} was defined as the time after which the volume no longer changed for at least 2 minutes.

Microscopy images of thrombus formation were recorded during experimentation at 5 Hz using a high resolution CCD (Pixelfly; PCO; Kelheim, Germany) attached to a stereo microscope at 2.5x zoom (Stemi 2000-C; Carl Zeiss; Oberkochen, Germany). Image recording was facilitated by the μManager platform (Edelstein, Amodaj, Hoover, Vale, & Stuurman, 2010). The test section was immersed in a water-glycerol solution with refractive index matched to that of glass to reduce optical distortions, and the microscope was focused at the midline of the test section.

2.2.2 Calculation of Shear Rate

For all calculations, flow within the stenosis throat was approximated as Poiseuille flow, since the Reynolds number was less than 100 and the Womersley number was less than 1. For Poiseuille flow, the wall shear rate, $\dot{\gamma}$, may be calculated as

$$\dot{\gamma}(t) = \frac{4Q(t)}{\pi r^3} \tag{2-1}$$

where Q is the volumetric flow rate and r is the test section radius. Since eq. (2-1) is used principally to assess the initial pulsatile waveform, r is treated as a constant, though r does

decrease as thrombus forms in the test section. Q is related to the pressure drop, Δp, through the hydraulic resistance, R_h, using the equation

$$\Delta p(t) = Q(t) R_h \,. \qquad (2\text{-}2)$$

Prior to experimentation, the total resistance of the test section and connecting tubing was calculated by flowing an approximately 35% by volume glycerol-water mixture with a viscosity of 3.0×10^{-3} Pa-s (comparable to a reference whole blood viscosity of 3.24×10^{-3} Pa-s (Merrill, 1969)) through the system at a range of Δp and measuring the Q. For resistance calculations, a constant blood viscosity was assumed. Though the bulk apparent viscosity decreases with increasing shear rate, the apparent viscosity of whole blood is constant at between 3×10^{-3} Pa-s and 4×10^{-3} Pa-s for shear rates greater than 10 s^{-1} (Replogle, Meiselman, & Merrill, 1967), which includes the full range of the experimental apparatus. The local viscosity immediately adjacent to the wall is likely lower due to the formation of a plasma skimming layer, but since it is difficult to assign a value to the wall viscosity, and since hydraulic resistance is a bulk parameter, the estimation of bulk apparent blood viscosity was used. From the resistance, the required Δp necessary to obtain the desired steady shear rates were calculated. For pulsatile flow, the required increased in upstream pressure to induce pulsatility was calculated to induce the desired pulsatile waveform. Following experimentation, measurements of downstream pressure were used in combination with the known upstream pressure head to calculate the experimental shear waveform from eqs. (2-1) and (2-2).

2.2.3 Automated Image Processing

An automated image processing algorithm, outlined in Figure 2-2, was developed in Matlab (R2012a; The Mathworks, Inc.; Natick, MA) to enhance and accelerate analysis of microscopy images (see APPENDIX A for code). The objective of this analysis was to obtain an estimate of thrombosis volume in each image. For each experimental condition, a 1.5 mm wide region of interest centered at the stenosis throat was selected. Next a reference image was identified in which no visible thrombus was observed. In the reference image, the outer edges of the stenosis within the region of interest were identified using a Laplacian of Gaussian filter (Marr & Hildreth, 1980). Following a global brightness correction to account for variations in illumination intensity, the reference image was subtracted from all subsequent images to highlight regions of thrombus growth. All pixels in the image were then classified as either thrombus or non-thrombus based on a user defined threshold to generated a binary image. For this study, the threshold was selected as 10% of the maximum intensity change from the reference image to the last image in the sequence, acquired approximately 2 minutes after occlusion. From the binary image, the maximum and minimum extents of the thrombus were identified. The thrombus and stenosis edges were then used to calculate the stenosis lumen diameter, D_o, and the thrombus lumen diameter, D_i, at each pixel column. The volume, V, of the growing thrombus in each image was approximated using a semi-axisymmetric assumption (Para et al., 2011), such that

$$V = \sum_{j=1}^{n} \left(\frac{D_{o,j}^2}{4} - \frac{D_{i,j}^2}{4} \right) \pi w \qquad (2\text{-}3)$$

where w is the width of each pixel. All measurements were then converted to μm and μm^3 using the known non-stenotic capillary diameter as a reference. From plots of V versus time, t, thrombosis formation was characterized by computing lag time, t_{lag}, and the rate of thrombus growth, dV/dt. The time to reach an initial deposition volume of 10^6 μm^3 was defined as t_{lag}, and dV/dt was calculated as the slope of a linear fit of all points from t_{lag} to t_{occ}. Metrics were compared between experimental conditions using paired and unpaired t-tests, as appropriate, with statistical significance defined as $p < 0.05$.

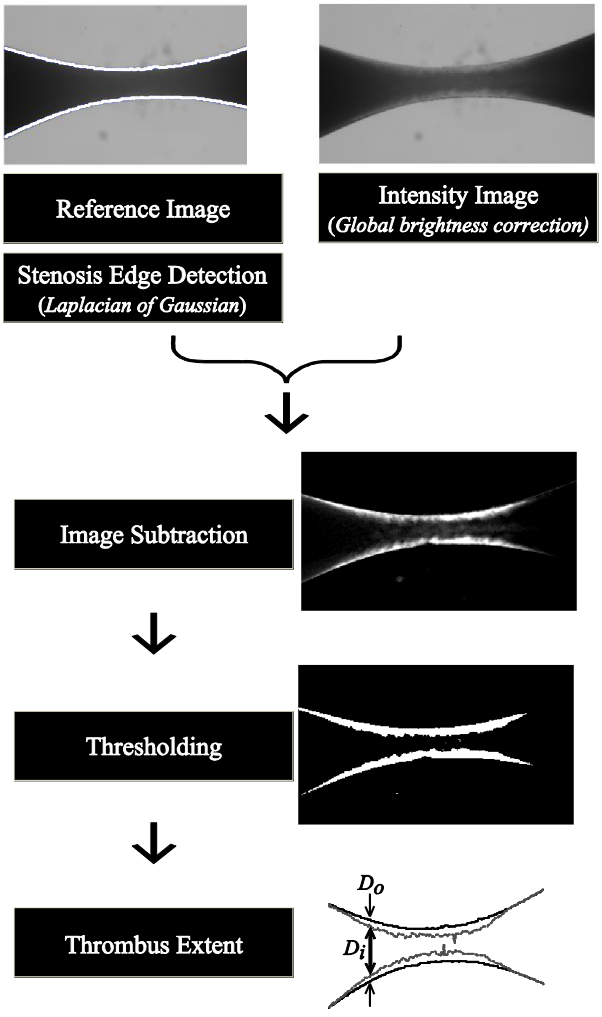

Figure 2-2: Flow chart of automated image processing algorithm

2.3 Results

2.3.1 Pulsatile Flow Characteristics

A characteristic shear rate waveform at the throat of the stenosis is shown in Figure 2-3 both in detail (Figure 2-3a) and over the full experiment (Figure 2-3b). The waveforms show a pulse frequency of approximately 1 Hz with a large amplitude modulation of shear rate, including instances of negative shear rate resulting from backward flow (Figure 2-3a), consistent with coronary flow in a stenosis (Ku, 1997). The waveform across the full experiment (Figure 2-3b) shows shear rates extended from approximately –2500 to 15 000 s^{-1}. The time-averaged mean wall shear rate for the pulsatile flow was calculated to be 3800 s^{-1}. For comparison, the steady shear rates used were approximately 16 000 s^{-1}, 6500 s^{-1}, and 3800 s^{-1}, which fall within the maximum shear envelope measured for the pulsatile flow condition (Bark et al., 2012; Jackson, 2007). Note that the initial shear rates were set for all the experiments but that the subsequent shear rates vary as the thrombus occludes the lumen and the flow rate falls for both the pulsatile and steady flow conditions.

To assess the relevance of the experimental shear rates, the wall shear rates in a coronary artery were calculated assuming a normal physiological (mean) flow rate of 2.2 mL/min (Ku, 1997) for a Reynolds number of 530 and a Womersley number of 2.2. Using Poiseuille flow assumptions, the mean wall shear rate in a 60% coronary stenosis is approximately 5500 s^{-1} and the shear rate ranges from -1700 to 10 000 s^{-1}. The wall shear rate envelope obtained using the present experiment corresponds well to approximated pathological wall shear rates within a coronary stenosis.

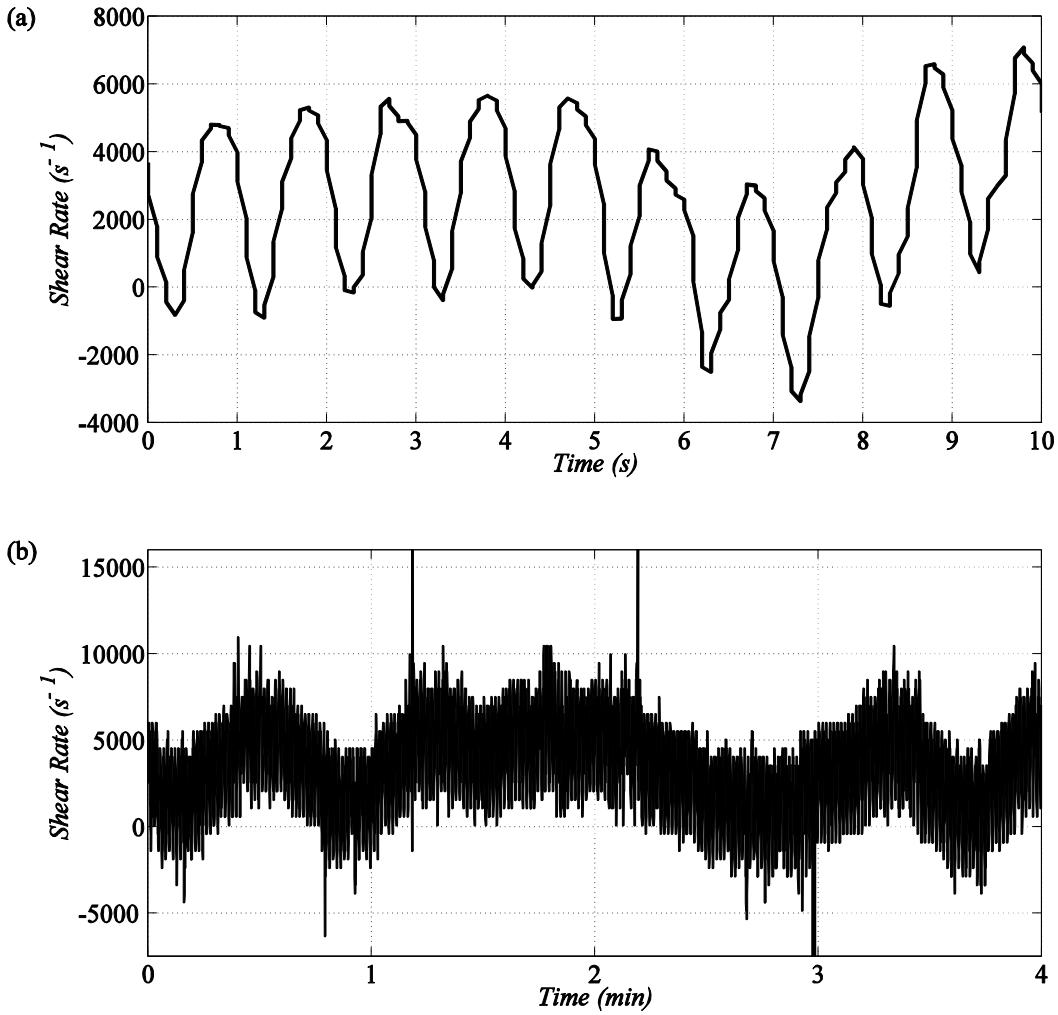

Figure 2-3: Sample experimental shear rate waveform, (a) 10-second detail of shear waveform, filtered using low-pass equiripple filter with bandpass of 3 Hz and bandstop of 5 Hz (Matlab, R2012a; The Mathworks, Inc.; Natick, MA), (b) shear waveform for full experiment time, unfiltered

2.3.2 Thrombus Formation under Steady and Pulsatile Flow Conditions

Figure 2-4 illustrates thrombus formation under pulsatile and steady conditions. Thrombus formation is seen as a brightening caused by the greater transmittance of platelet thrombus compared to whole blood. At t_{lag} (Figure 2-4, first column), thrombus formation is observed as a slight roughness at the edge of the test section. By $t = 0.75t_{occ}$ (third column), thrombus

has progressed well into the test section, and at occlusion (last column), thrombus appears as a blockage at the throat of the stenosis. A qualitative comparison of these images does not reveal substantial differences in thrombus formation characteristics between the four conditions. The average pixel size is 7.5 μm/pixel, and we estimate an uncertainty of ±1 pixel, or ±7.5 μm, in the identification of both the inner and outer edges of the thrombus. Propagating the uncertainty of ±7.5 μm through the subtraction of the two inner and two outer edges to the calculation of D_i and D_o gives an uncertainty of ±15 μm in the diameters. Propagating an uncertainty of ± 7.5 μm through the volume calculation in eq. (2-3) gives an estimated average uncertainty of 8.8×10^6 μm, or less than 5% of the full-scale reported volumes.

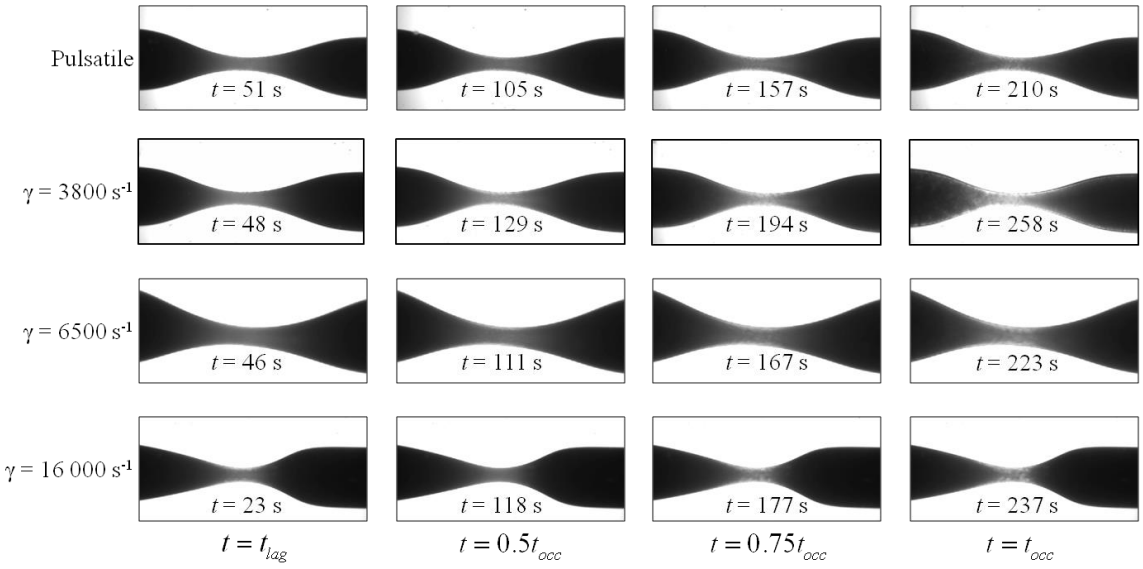

Figure 2-4: Time lapse transmitted intensity images of thrombus formation at lag time, 50% of occlusion time, 75% of occlusion time, and occlusion time; top: pulsatile flow, middle: steady flow at mean shear rate, top: steady flow at maximum shear rate

Characteristic thrombus formation and flow cessation are shown in Figure 2-5. Thrombus volume, *V,* versus *t* is shown in Figure 2-5a, along with linear fits from t_{lag} to t_{occ}. Figure 2-5b shows D_i at the throat of the stenosis versus *t* for each of the experimental conditions, illustrating the closure of the throat of the stenosis. Figure 2-5b shows the discharge mass for steady flow conditions and the decrease in reservoir volume for the pulsatile case, illustrating the cessation of flow in the experimental apparatus. Figure 2-6 and Table 2-1 compare thrombus formation characteristics of occlusion time, lag time, and growth rate (t_{occ}, t_{lag}, and *dV/dt)* under pulsatile and steady flow conditions. No statistical difference was observed for any metric between pulsatile flow and steady flow at mean pulsatile shear rate ($p \approx 0.29$-0.69). However, high shear associated with the maximum of pulsatility was different. The lag time for first appearance of thrombus, t_{lag} is significantly shorter for maximum steady shear compared to pulsatile shear ($p = 0.03$, unpaired t-test). t_{lag} decreases from 42 ± 10 s to 26 ± 9 s (35% and 37%) for maximum shear versus pulsatile conditions. A similar decrease in t_{lag} was seen between maximum steady shear and both mean shear ($p = 0.01$, unpaired t-test) and intermediate shear conditions ($p = 0.02$, paired t-test) (Figure 2-6b). In contrast, t_{occ} for all steady conditions were within about 1 minute (17%) of that for pulsatile flow. Similarly, mean *dV/dt* also varied between conditions by approximately 25%. Most importantly, no endpoint differed between pulsatile to steady, mean shear conditions by more than 25%, and no endpoint showed statistically significant differences between the steady mean shear and pulsatile flow conditions.

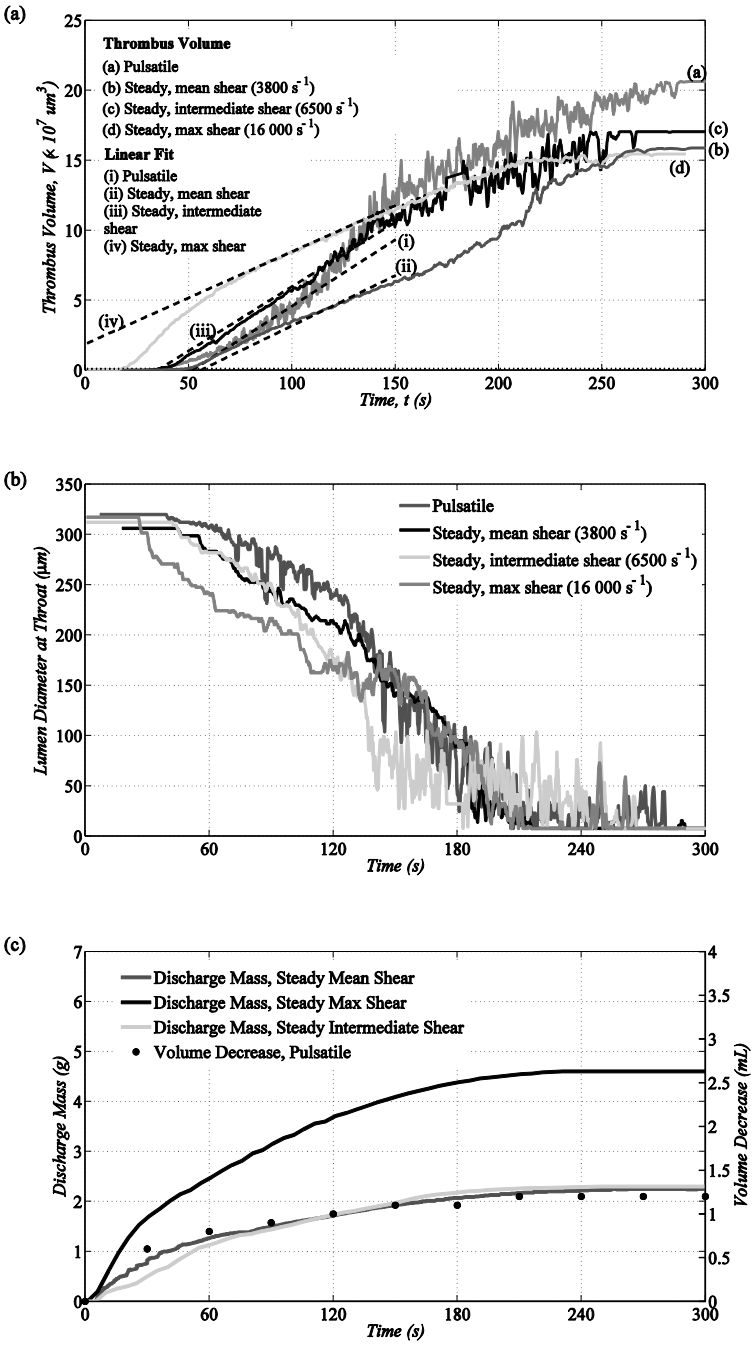

Figure 2-5: Characteristic thrombus formation and flow cessation. a) Thrombus volume versus time. Solid lines show computed thrombus volume, dotted lines show the slope of linear fits used to compute thrombus growth rate (dV/dt), and dashed line shows threshold volume for measurement of lag time (t_{lag}). Linear fits have been translated for clarity. Thrombus volume was processed at 5 Hz and is plotted as a moving average with a period of 1 s. b) Lumen diameter at the throat of the stenosis versus time; c) Mass discharge (steady cases) and reservoir volume decrease (pulsatile) versus time.

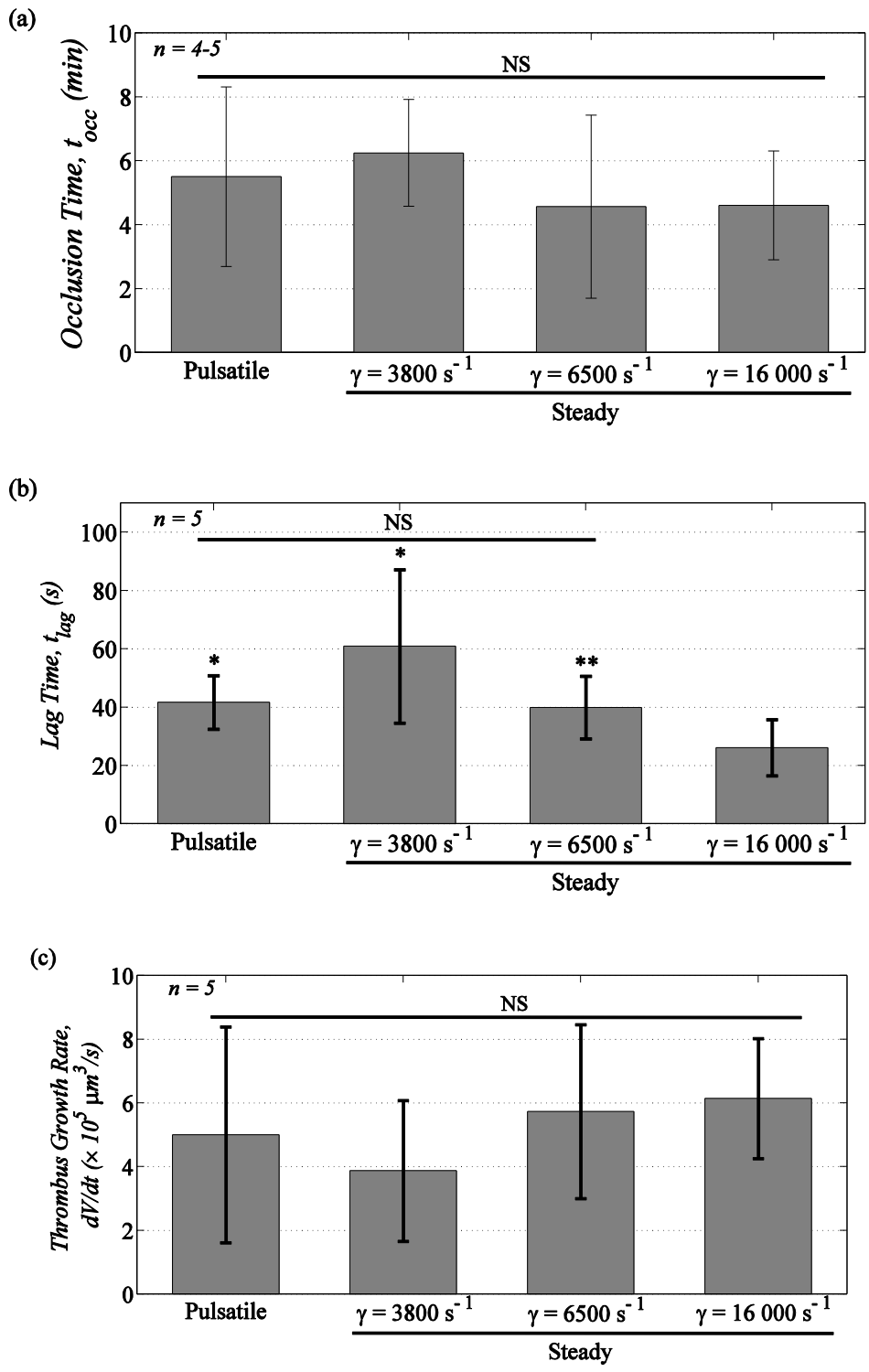

Figure 2-6: Effect of flow pulsatility and shear rate on a) occlusion time, b) lag time, and c) thrombus growth rate, * indicates $p < 0.05$ compared to steady, maximum shear rate condition, unpaired t-test, $n = 5$, and ** indicated $p < 0.05$, paired t-test, $n = 5$

Table 2-1: Summary of Thrombosis Formation Endpoints under Pulsatile and Steady Flow

	Occlusion Time t_{occ} (min)	***p*-value compared to pulsatile**	**Lag Time t_{lag} (sec)**	***p*-value compared to pulsatile**	**Thrombus Growth Rate dV/dt ($\times 10^5$ um^3/s)**	***p*-value compared to pulsatile**
Pulsatile flow	5.5 ± 2.8	-	42 ± 9	-	5.0 ± 3.4	-
Steady flow, γ = 3800 s^{-1}	6.2 ± 1.7	0.63	61 ± 26	0.29	3.9 ± 2.2	0.49
Steady flow, γ = 6500 s^{-1}	4.6 ± 2.7	0.64	40 ± 11	0.66	5.7 ± 2.7	0.23
Steady flow, γ = 16 000 s^{-1}	4.6 ± 1.75	0.57	26 ± 10	0.03	6.1 ± 1.9	0.35

Values are given as mean ± standard deviation, *p*-values were calculated using an unpaired t-test (n = 4-5).

2.4 Discussion

Thrombosis leading to myocardial infarction and stroke forms under high shear rates and pulsatile flow conditions. In the present study, we show that *in vitro* thrombus formation under high shear pulsatile flow can be modeled using steady flow for the bulk thrombosis characteristics of lag time, occlusion time, and thrombus formation rate. We observed no difference in platelet thrombus formation between steady and pulsatile flow with the same mean shear rate, as did van Breugel et al. (van Breugel et al., 1988) for lower shear rates. Our study demonstrates the similarities for higher shear rates and pulsatile waveforms that include both flow reversal and non-zero mean shear. Our endpoints highlighting bulk thrombus formation reflect clinical occlusive thrombosis leading to myocardial infarction, rather than cellular level adhesion.

Our results are contrary to those of Zhao et al. (Zhao et al., 2008), who showed increased platelet deposition with pulsatile flow. Zhao et al. used a pulsatile period of

30 s (0.033 Hz) while the present study used a period of 1 s (1 Hz). Furthermore, the Zhao study employed lower shear rates (300 to 1300 s^{-1}) and investigated surface coverage involving on the order of thousands of platelets and not occlusive thrombus formation involving millions of platelets. The combination of lower periods, non-pathologic low shear rates, and quantification of surface coverage rather than occlusion may explain the difference of our findings. Ultimately, the endpoint used by Zhao et al. may preclude the observation of rapid platelet accumulation described here, since their previous experiments were less than half the time of ours (Bark et al., 2012; Para et al., 2011). Alternatively, slow pulsatility may more strongly affect platelet surface coverage at low shears with adhesion time scales that may be on the order of 30 sec.

Flow pulsatility is unlikely to affect the binding of individual platelets since the platelet binding timescale of microseconds is short compared to an arterial pulsatile period of 1 sec (Wellings & Ku, 2012). Though flow conditions and the presence of red blood cells have been shown to enhance platelet transport to the vessel wall (Aarts et al., 1988; Eckstein, Tilles, & Milero, 1988), a previous study showed no change near-wall platelet concentration as a result of pulsatility (Xu & Wootton, 2004). The present study also supports the results that pulsatility does not have a strong effect on factors like platelet margination that might affect lag time or thrombus growth rate for a matched mean shear rate.

We report a decrease in lag time with increasing mean shear rate from 3800 s^{-1} to 16 000 s^{-1} but no difference in lag time when pulsatility is introduced at the same mean shear rate. Platelet activation time has previously been shown to be inversely proportional to shear rate (Hellums, 1994), which agrees with our observation of a decreased lag time

with increased shear rate. Previous studies have suggested that the lag time phenomenon may be related to the time required for shear activation of an initial layer of collagen-adherent platelets (Bark et al., 2012; Para et al., 2011). The transit time of platelets through the stenosis is on the order of milliseconds, which is likely too short for shear activation prior to adhesion. Ramstack et al. (Ramstack, Zuckerman, & Mockros, 1979) found that shear activation of platelets occurred when the product of shear rate and exposure time exceeded threshold of 10^3. In the present study, exposure times range from 2.31 to 9.72 ms for shear rates from 16 000 s^{-1} to 3800 s^{-1}. For all experimental conditions, the product of shear rate and transit time is only 37, several orders of magnitude less than the threshold for shear activation before platelet adhesion. Thus, evidence suggests non-activated platelets initially adhere to the collagen surface (Ruggeri, Orje, Haberman, Federici, & Reininger, 2006) and are subsequently activated by a combination collagen binding and shear, allowing large scale accumulation of thrombus. At the shear rates studied here, a combination of collagen-induced and shear-induced activation may contribute to platelet activation (Holme et al., 1997). The present study is unable to elucidate the relative contributions of collagen binding and shear to platelet activation, nor were alternative surface functionalization investigated. Rather our results describe the bulk effects of surface and flow conditions that are relevant in arterial thrombosis at the site of atherosclerotic plaque rupture.

The equal lag times between pulsatile and steady flow with matched mean shear rates further suggests that the product of shear rate and time ($\dot{\gamma} \times t$) (Ramstack et al., 1979), rather than maximum shear rate, may be an important determining factor for lag time. The brief excursions to very high shear rates under pulsatile are balanced by phases of lower

shear rate. Thus pulsatile flow imparts a shear history similar to steady flow at a matched mean shear rate, resulting in similar lag times, whereas steady maximum shear flow results in a decrease in lag time.

An alternative or complementary explanation of the decrease lag time with shear rate is an increased rate of plasma protein adsorption, in particular von Willebrand factor (vWF). At high shear rate, vWF is the principle mediator of platelet-collagen bonding (Ruggeri, 2007). High shear rate enhances the diffusion of solutes (Taylor, 1953) and particles in suspension (Leighton & Acrivos, 1987). Thus increasing shear rate increases the diffusivity of vWF and platelets in flowing blood, allowing faster adsorption to the collagen substrate and decreasing lag time (Neeves et al., 2013).

The effects of enhanced shear activation on occlusion time and overall thrombus growth rate at the maximum shear rate may be balanced by increased embolization due to higher drag forces at higher shear rates, yielding minimal differences in growth rate and occlusion time over the duration of the experiment. Furthermore, after initial activation, thrombus growth may no longer be limited by protein transport and absorption as activation of platelets at the surface releases large concentrations of vWF and other factors locally (Ruggeri et al., 2006; Wellings & Ku, 2012). However, the rate-limiting mechanisms of the growth phase remain an unanswered question to be investigated by future studies.

The present study has several limitations. First, only a single pulsatile waveform was analyzed in the present study. The waveform was selected to mimic flow and shear rates within a stenotic coronary artery under resting conditions, including flow reversal and non-zero mean shear rate. Though a relevant physiological waveform was selected, we did not investigate variations in pulse frequency and amplitude. Had the pulsatility created a

significant effect, we would have characterized a frequency response curve. But, since the base frequency did not have a measurable effect, it is unlikely that higher frequency terms will have much effect, either. Our pulse amplitude going from 0 to 16 000 s^{-1} likely exceeds most arterial waveform conditions, so may be considered a worse-case. The experimental apparatus employed rigid walls and thus did not include contributions of arterial wall elasticity to thrombus formation. To routinely obtain blood volumes large enough for the single-pass flow system, porcine rather than human blood was used. Porcine blood has been shown to be similar to human platelet thrombosis in previous studies (Badimon et al., 1986; Bark et al., 2012; Para et al., 2011). Some variations may exist between porcine and human thrombus formation, in particular, lag time is approximately twice as long with human blood compared to porcine blood and the rate of thrombus growth is approximately half as fast (Para & Ku, 2013). To prevent coagulation during transport, blood was lightly anticoagulated with heparin, which may inhibit the contribution of thrombin generation and fibrin formation to thrombus growth.

2.5 Conclusions

Pulsatile and steady flow experiments yielded similar results for the endpoints of thrombus growth rate, lag time and occlusion time when the steady time-averaged mean shear rate at the wall matched that of pulsatile shear rate. Steady shear rates equal to the maximum pulsatile shear, however, exhibited a decreased lag time. The results indicate that hemodynamic assays for platelet thrombosis may use the simpler steady flow arrangement with corresponding clinical relevance to pulsatile arterial conditions with good persistence of the primary endpoints of growth rate, lumen occlusion time, and lag time.

2.6 Appendix

2.6.1 Reynolds Number

The Reynolds number (Re) is the non-dimensional ratio of inertial forces to viscous forces. For this study, Re was defined as

$$\mathrm{Re} = \frac{\rho L U_{mean}}{\mu} \qquad \text{(A1)}$$

where ρ is the fluid density, L is the diameter of the test section, U_{mean} is the mean velocity at the throat, and μ is the fluid viscosity. The density and viscosity of blood were taken as 1050 kg/m^3 and 3.24 × 10^{-3} Pa-s, respectively (Kenner, 1989; Merrill, 1969). Outside the stenosis, the diameter was 1.5 mm and the average velocity ranged from 0.0075 m/s to 0.034 across the three steady flow conditions, yielding a Reynolds number between 3.6 and 16.5. Inside the stenosis throat, an average diameter of 325 μm was used, and the average velocity ranged from 0.16 m/s to 0.687 m/s, yielding a Reynolds number between 17 and 72.

2.6.2 Schmidt Number

The Schmidt number (Sc) is the non-dimensional ratio of momentum diffusivity to mass diffusivity, and is defined as

$$\mathrm{Sc} = \frac{\mu}{\rho d} \qquad \text{(A2)}$$

where d is the diffusivity of platelets. Platelet diffusivity may be considered either as the diffusivity of platelet in plasma, or as the effective diffusivity of platelets in blood under flow. Platelet diffusivity in plasma is 1 × 10^{-13} m^2/s (Jordan, David, Homer-Vanniasinkam, Graham, & Walker, 2004). However, since blood is a dense suspension of cells, effective

platelet diffusivity increases with shear rate. Effective diffusivity (D_{eff}) cab be estimated by (Jordan et al., 2004; Zydney & Colton, 1988)

$$d_{eff} = d_{sf} + 0.8a^2\gamma\phi(1-\phi)^{0.15} \qquad \text{(A3)}$$

where d_{sf} is platelet diffusion in plasma (1×10^{-13} m^2/s), a is the radius of the red blood cells (4.2 μm), γ is the shear rate, and φ is the hematocrit (0.4). Using this equation, the maximum platelet diffusivity using the wall shear rates is 8.3×10^{-8} m^2/s. Substituting the values for diffusivity into eq. (A2) gives a maximum Sc at the throat of the stenosis for the no-shear condition of 3.7×10^6, and effective Sc between 154 for the mean shear condition and 37 for the maximum shear condition. This range of Sc reflects that platelet diffusion is slower than fluid momentum transfer.

2.6.3 Peclet Number

The Peclet number (Pe) is the non-dimensional ratio of advective transport rate to diffusive transport rate. Pe is defined as

$$\mathrm{Pe} = \frac{LU_{mean}}{d} = \mathrm{Re}\,\mathrm{Sc}\,. \qquad \text{(A4)}$$

Multiplying the above values for Re and Sc for the various experimental conditions yields a Pe at the throat of the stenosis of between 6.2×10^7 and 2.6×10^8 for the minimum diffusivity, and between 2618 and 2664 using values for effective diffusivity. Such high Peclet numbers suggest that the platelet mass transport is dominated by the fluid flow and not simple diffusion.

2.7 References

Aarts, P. A., van den Broek, S. A., Prins, G. W., Kuiken, G. D., Sixma, J. J., & Heethaar, R. M. (1988). Blood platelets are concentrated near the wall and red blood cells, in the center in flowing blood. *Arteriosclerosis, Thrombosis, and Vascular Biology, 8*(6), 819-824. doi: 10.1161/01.atv.8.6.819

Badimon, J. J., Badimon, L., Galvez, A., Chesebro, J., & Fuster, V. (1986). Influence of arterial damage and wall shear rate on platelet deposition: Ex vivo study in a swine model. *Arteriosclerosis, Thrombosis, and Vascular Biology, 6*, 312-320.

Badimon, L., & Badimon, J. J. (1989). Mechanisms of arterial thrombosis in nonparallel streamlines: Platelet thrombi grow on the apex of stenotic severely injured vessel wall, experimental study in a pig model. *Journal of Clinical Investigation, 84*, 1134-1144.

Bark, D. L., & Ku, D. N. (2010). Wall shear over high degree stenoses pertinent to atherothrombosis. *Journal of Biomechanics, 43*(15), 2970-2977. doi: 10.1016/j.jbiomech.2010.07.011

Bark, D. L., Para, A. N., & Ku, D. N. (2012). Correlation of thrombosis growth rate to pathological wall shear rate during platelet accumulation. *Biotechnology and Bioengineering, 109*(10), 2642-2650.

Barstad, R. M., Roald, H., Cui, Y., Turitto, V., & Sakariassen, K. (1994). A perfusion chamber developed to investigate thombus formation and shear profiles in flowing native human blood at the apex of a well-defined stenosis. *Arteriosclerosis, Thrombosis, and Vascular Biology, 14*, 1984-1991.

Colace, T., Jobson, J., & Diamond, S. L. (2011). Relipidated tissue factor linked to collagen surfaces potentiates platelet adhesion and fibrin formation in a microfluidic model of vessel injury. *Bioconjugate Chemistry, 22*, 2104-2109. doi: 10.1021/bc200326v

Davies, M. J., Fulton, W., & Robertson, W. (1979). The relation of coronary thrombosis to ischaemic myocardial necrosis. *Journal of Pathology, 127*, 99-110.

Davies, M. J., & Thomas, A. (1984). Thrombosis and acute coronary-artery lesions in sudden cardiac ischemic death. *New England Journal of Medicine, 310*(18), 1137-1140.

Davies, M. J., & Thomas, A. (1985). Plaque fissuring: The cause of acute myocardial infarction, sudden ischaemic death, and crescendo angina. *British Heart Journal, 53*, 363-373.

Davies, M. J. (1994). Pathology of arterial thrombosis. *British Medical Bulletin, 50*(4), 789-802.

Eckstein, E., Tilles, A., & Milero, F. (1988). Conditions for the occurrence of large near-wall excesses of small particles during blood flow. *Microvascular Research, 36*, 31-39.

Edelstein, A., Amodaj, N., Hoover, K., Vale, R., & Stuurman, N. (2010). *Computer Control of Microscopes Using μManager*: John Wiley & Sons, Inc.

Epstein, F. H., Lefkovits, J., Plow, E. F., & Topol, E. J. (1995). Mechanisms of disease: Platelet glycoprotein IIb/IIIa receptors in cardiovascular medicine. *New England Journal of Medicine, 332*(23), 1553-1559.

Gutierrez, E., Petrich, B. G., Shattil, S. J., Ginsberg, M. H., Groisman, A., & Kasirer-Friede, A. (2008). Microfluidic devices for studies of shear-dependent platelet adhesion. *Lab on a Chip, 8*(9), 1486-1495. doi: 10.1039/b804795b

Hellums, J. (1994). 1993 Whitaker Lecture: Biorheology in thrombosis research. *Annals of Biomedical Engineering, 22*, 445-455.

Holme, P. A., Ørvim, U., Hamers, M. J. A. G., Solum, N. O., Brosstad, F. R., Barstad, R. M., & Sakariassen, K. S. (1997). Shear-induced platelet activation and platelet microparticle formation at blood flow conditions as in arteries with a severe stenosis. *Arteriosclerosis, Thrombosis, and Vascular Biology, 17*, 646-653.

Hosokawa, K., Ohnishi, T., Kondo, T., Fukasawa, M., Koide, T., Maruyama, I., & Tanaka, K. A. (2011). A novel automated microchip flow-chamber system to quantitatively evaluate thrombus formation and antithrombotic agents under blood flow conditions. *J Thromb Haemost, 9*(10), 2029-2037. doi: 10.1111/j.1538-7836.2011.04464.x

Houdijk, W. P., de Groot, P. G., Nievelstein, P. F., Sakariassen, K. S., & Sixma, J. J. (1986). Subendothelial proteins and platelet adhesion: von Willebrand factor and fibronectin, not thrombospondin, are involved in platelet adhesion to extracellular matrix of human vascular endothelial cells. *Arteriosclerosis, Thrombosis, and Vascular Biology, 6*(1), 24-33. doi: 10.1161/01.atv.6.1.24

Jackson, S. P. (2007). The growing complexity of platelet aggregation. *Blood, 109*(12), 5087-5095. doi: 10.1182/blood-2006-12-027698

Jordan, A., David, T., Homer-Vanniasinkam, S., Graham, A., & Walker, P. (2004). The effects of margination and red cell augmented platelet diffusivity on platelet adhesion in complex flow. *Biorheology, 41*(641-653), 641.

Kenner, T. (1989). The measurement of blood density and its meaning. *Basic Research in Cardiology, 84*, 111-124.

Ku, D. N. (1997). Blood flow in arteries. *Annual Review of Fluid Mechanics, 29*, 399-434.

Ku, D. N., & Flannery, C. J. (2007). Development of a flow-through system to create occluding thrombus. *Biorheology, 44*, 273-284.

Leighton, D., & Acrivos, A. (1987). The shear-induced migration of particles in concentrated suspension. *Journal of Fluid Mechanics, 181*, 415-439.

Li, M., Ku, D., & Forest, C. (2012). Microfluidic system for simultaneous optical measurement of platelet aggregation at multiple shear rates in whole blood. *Lab on a Chip, 12*, 1355-1362.

Mailhac, A., Badimon, J., Fallon, J., Fernandez-Ortiz, A., Meyer, B., Chesebro, J., . . . Badimon, L. (1994). Effect of an eccentric severe stenosis on fibrin(ogen) deposition on severely damaged vessel wall in arterial thrombosis: Relative contribution of fibrin(ogen) and platelets. *Circulation, 90*, 988-996. doi: 10.1161/01.CIR.90.2.988

Maloney, S. F., Brass, L., & Diamond, S. L. (2010). P2Y12 or P2Y1 inhibitors reduce platelet deposition in a microfluidic model of thrombosis while apyrase lacks efficacy under flow conditions. *Integrative Biology, 2*(4), 153-220. doi: 10.1039/b919728a
10.1039/B919728A

Marr, D., & Hildreth, E. (1980). Theory of edge detection. *Proceedings of the Royal Society B: Biological Sciences, 207*(1167), 187-217. doi: 10.1098/rspb.1980.0020

Merrill, E. W. (1969). Rheology of Blood. *Physiological Reviews, 49*(4), 863-888.

Neeves, K. B., Maloney, S. F., Fong, K. P., Schmaier, A. A., Kahn, M. L., Brass, L. F., & Diamond, S. L. (2008). Microfluidic focal thrombosis model for measuring murine platelet deposition and stability: PAR4 signaling enhances shear-resistance of platelet aggregates. *Journal of Thrombosis and Haemostasis, 6*, 2193-2201. doi: 10.1111/j.1538-7836.2008.03188.x

Neeves, K. B., Onasoga, A. A., Hansen, R. R., Lilly, J. S., Venckuaite, D., Sumner, M. B., . . . Di Paolo, J. A. (2013). Sources of Variability in Platelet Accumulation on Type 1 Fibrillar Collagen in Microfluidic Flow Assays. *PLoS One, 8*(1), Epub.

Para, A. N., Bark, D. L., Lin, A., & Ku, D. N. (2011). Rapid platelet accumulation leading to thrombotic occlusion. *Annals of Biomedical Engineering, 39*(7), 1961-1971. doi: 10.1007/s10439-011-0296-3

Para, A. N., & Ku, D. N. (2013). A low-volume, single pass in-vitro system of high shear thrombosis in a stenosis. *Thrombosis Research, 131*(5), 418-424. doi: http://dx.doi.org/10.1016/j.thromres.2013.02.018

Ramstack, J., Zuckerman, L., & Mockros, L. (1979). Shear-induced activation of platelets. *Journal of Biomechanics, 12*, 113-125.

Replogle, R. L., Meiselman, H. J., & Merrill, E. W. (1967). Clinical Implications of Blood Rheology Studies. *Circulation, 36*, 148-160.

Ruggeri, Z. M., Orje, J., Haberman, R., Federici, A., & Reininger, A. J. (2006). Activation-independent platelet adhesion and aggregation under elevated shear stress. *Blood, 108*(6), 1903-1910. doi: 10.1182/blood-2006-04-011551

Ruggeri, Z. M. (2007). Von Willebrand factor: Looking back and looking forward. *Thrombosis and Haemostasis*. doi: 10.1160/th07-04-0279

Sakariassen, K. S., Aarts, P., & de Groot, P. G. (1983). A perfusion chamber developed to investigate platelet interaction in flowing blood with human vessel wall cells, their extracellular matrix, and purified components. *Journal of Laboratory and Clinical Medicine, 102*(4), 522-535.

Savage, B., Saldivar, E., & Ruggeri, Z. M. (1996). Initiation of platelet adhesion by arrest onto fibrinogen or translocation on von Willebrand factor. *Cell, 84*, 289-297.

Sixma, J., de Groot, P. G., van Zanten, H., & Ijsseldijk, M. (1998). A new perfusion chamber to detect platelet adhesion using a small volume of blood. *Thrombosis Research, 92*, S43-S46.

Taylor, G. (1953). Dispersion of Soluble Matter in Solvent Flowing Slowly through a Tube. *Proceedings of the Royal Society A, 219*, 186-203.

van Breugel, H. H., Sixma, J. J., & Heethaar, R. M. (1988). Effects of flow pulsatility on platelet adhesion to subendothelium. *Arteriosclerosis, Thrombosis, and Vascular Biology, 8*(3), 332-335. doi: 10.1161/01.atv.8.3.332

Velik-Salchner, C., Schnurer, C., Fries, D., Mussigang, P. R., Moser, P. L., Streif, W., . . . Lorenz, I. H. (2006). Normal values for thrombelastography (ROTEM) and selected coagulation parameters in porcine blood. *Thrombosis Research, 117*(5), 597-602. doi: 10.1016/j.thromres.2005.05.015

Wellings, P. J., & Ku, D. N. (2012). Mechanisms of platelet capture under very high shear. *Cardiovascular Engineering and Technology, 3*(2), 161-170. doi: 10.1007/s13239-012-0086-6

Xu, C., & Wootton, D. M. (2004). Platelet near-wall excess in porcine whole blood in artery-sized tubes under steady and pulsatile flow conditions. *Biorheology, 41*, 113-125.

Zhao, X. M., Wu, Y. P., Cai, H. X., Wei, R., Lisman, T., Han, J. J., . . . de Groot, P. G. (2008). The influence of the pulsatility of the blood flow on the extent of platelet adhesion. *Thrombosis Research, 121*(6), 821-825. doi: 10.1016/j.thromres.2007.07.013

Zydney, A., & Colton, C. (1988). Augmented solute transport in the shear flow of a concentrated suspension. *Physiochemical Hydrodynamics, 10*(1), 77-96.

CHAPTER 3: MICROFLUIDIC DEVICE DESIGN

3.1 Design Requirements

For the design of a useful, point-of-care high shear thrombosis assay, several design criteria were identified. Many of the design criteria relate directly to the test section size and shape. The four key requirements, summarized in Table 3-1 are low blood volume, physiological and pathological shear rates, practical total test times, and occlusion dominated by platelet-platelet interactions relevant to large artery occlusive thrombus. The design of each of these criteria is considered in the following sections. In addition to these requirements, several human factors criteria will be targeted, namely, fully disposable test cassettes, the ability to perform multiple tests, and straight-forward endpoints obtained by non-additive, non-contact measurement techniques.

Table 3-1: Test Section Design Criteria

Design Criteria	Design Target
Total Blood Volume	< 10 mL
Shear Rate (in stenosis)	~6000 s^{-1}
Shear Rate (outside stenosis)	~500 s^{-1}
Test time	5-30 min
Platelet Interactions	10x platelet-platelet versus platelet-surface

3.2 Geometric Design of Microfluidic Chambers: Platelet Adhesion versus Accumulation

3.2.1 Introduction

Platelet thrombosis related to myocardial infarction and stroke forms under arterial flow conditions (Cadroy, Horbett, & Hanson, 1989) and is initiated by platelet interactions with extracellular matrix proteins such as collagen or fibrinogen (Savage, Saldivar, & Ruggeri, 1996; Savage, Almus-Jacobs, & Ruggeri, 1998) exposed by atherosclerotic plaque rupture (Falk, 1983). Subsequently platelet-platelet adhesion creates the large volume of thrombus growth (Maxwell et al., 2007) leading to occlusion of flow in atherosclerotic arteries (Davies & Thomas, 1984). Intravascular thrombosis of medium and large arteries is dominated by platelet-platelet interactions due to the large ratio of thrombus volume-to-surface area in the occluded region.

Microfluidic systems are designed to utilize small fluid volumes. However, the quest for miniaturization may skew the study towards platelet-surface adhesion due to the larger surface area relative to thrombus volume. Platelets adhere to extracellular matrix proteins via different molecular mechanisms than platelet-platelet binding (Ruggeri & Mendolicchio, 2007). Thus, test channels that are very small may create platelet surface adhesion, while larger ones can test for platelet-platelet bonding. The question is "How small is small?" To quantify the type of platelet adhesion event within a test channel, we characterize microfluidic assays as dominated by either platelet-surface or platelet-platelet interactions. Multiple investigators have described flow assays to quantify platelet adhesion, summarized in Table 3-2. Some of the studies utilized surface coverage measurement techniques and short test times to isolate platelet-surface interactions. Others created a thrombus that fills a large portion or all of the test section, and it is unclear

whether platelet-platelet or platelet-surface effects were dominant. Though the results of these studies depend on many factors including time, shear rate, and biomolecular interactions, the dominant type of platelet adhesion event, namely platelet-surface or platelet-platelet, depends on size of the test section and final thrombus volume. In future studies, it may be advantageous to design test sections to separate the effects of the different platelet adhesion mechanisms. In particular, it is of interest to determine the minimum allowable size of a microfluidic test section that still permits the observation of large-scale occlusive thrombosis in which many more platelets adhere to each other rather than to the test section walls.

Table 3-2: Summary of Previous Arterial Platelet Adhesion and Aggregation Assays

Test Section Geometry	Test Time	Endpoint	References
Cylindrical (stenosed)			
D = 2 mm D = 1.3 mm D = 0.9 mm D = 4 mm	30 min.	Platelet deposition	(Badimon, Badimon, Galvez, Chesebro, & Fuster, 1986; Badimon & Badimon, 1989; Mailhac et al., 1994)
D = 300 um	20 min.	Thrombus volume	(Bark, Para, & Ku, 2012; Ku & Flannery, 2007; Para, Bark, Lin, & Ku, 2011)
Parallel Plate			
h = 1 mm, w = 10 mm α = 10	5 min.	Surface coverage	(Houdijk, de Groot, Nievelstein, Sakariassen, & Sixma, 1986; Sakariassen, Aarts, & de Groot, 1983)
h = 254 μm, w = 0.22 cm α = 8.7	2 min.	Thrombus volume & height	(Savage et al., 1996; Savage et al., 1998; Savage, Ginsberg, & Ruggeri, 1999; Usami, Chen, Zhao, Chien, & Skalak, 1993)
h = 0.1 mm, w = 5 mm α = 50	5 min.	Surface coverage	(Sixma, de Groot, van Zanten, & Ijsseldijk, 1998)
h = 60 μm, w = 250 μm α = 4.2	7 min. (occlusion)	Fluorescence	(Colace, Muthard, & Diamond, 2012; Maloney, Brass, & Diamond, 2010)

Table 3-2: Summary of Previous Arterial Platelet Adhesion and Aggregation Assays

Test Section Geometry	Test Time	Endpoint	References
h = 80 μm, w = 100 μm α = 1.25	5 min.	Surface coverage	(Neeves et al., 2008)
h = 24 μm, w = 200 μm α = 8.3	1 min.	Fluorescence	(Gutierrez et al., 2008)
h = 80 μm, w = 300 μm α = 3.75	30 min. (occlusion)	Pressure drop	(Hosokawa et al., 2011)
h = w = 40 μm α = 1	10 min (occlusion)	Pressure drop	(Hosokawa et al., 2012)
Parallel Plate (stenosed)			
w = 5 mm h = 0.7 mm, α = 7.1 h = 0.28 mm, α = 17.9 h = 0.14 mm, α = 35.7 h = 0.08 mm, α = 62.5	5 min.	Thrombus volume	(Barstad, Roald, Cui, Turitto, & Sakariassen, 1994; Barstad, Hamers, Stephens, & Sakariassen, 1995; Barstad, Roald, et al., 1995; Bossavy, Sakariassen, Thalamas, Boneu, & Cadroy, 1999; Sakariassen et al., 1990)
h = 250 μm, w = 750 μm α = 3	10 min. (occlusion)	Occlusion time & blood volume	(Li, Ku, & Forest, 2012)

The objective of the present study is to determine the dimensions and conditions for microfluidic assays that favor one type of platelet interaction over another. The ratio of platelet-platelet to platelet-surface interactions, *R*, and the percent of platelet-platelet interactions, *P*, are estimated for circular and rectangular test section geometries. For rectangular test sections, a range of channel aspect ratios were considered: channels with all sides functionalized versus only one side functionalized, where "functionalized" refers to areas of the channel coated with an adhesive protein. The effects of platelet size and

shape were also investigated, and analytical predictions are shown experimentally by comparing a rectangular microfluidic channel to a circular test section that mimics a stenotic coronary artery. Results of this analysis may be useful for the development of micro-scale assays to study either cell-cell or cell-surface bonding. Results may also be extended to characterize micro- and nano-fluidic analyses of leukocyte accumulation, three-dimensional cell culture, and colloidal fouling.

3.2.2 Methods

3.2.2.1 General Analysis

In general, the **ratio**, ***R***, of platelet-platelet to platelet-surface interactions and the **percentage**, ***P***, of platelet-platelet interactions were defined as

$$R = \frac{N_p}{N_s}, \tag{3-1}$$

$$P = \frac{N_p}{N_{tot}} \tag{3-2}$$

where N_{tot} is the total number of adhered platelets, and N_s and N_p are the number of platelets adhered to the surface and to other platelets, respectively. Since in many experimental procedures, the number of platelets is difficult to measure directly, N_{tot} was approximated as

$$N_{tot} = \frac{pV}{v} \tag{3-3}$$

where V is the measured thrombus volume per unit length, p is the fraction of the thrombus composed of platelets, here assumed to be 80% (p = 0.8) (Ku & Flannery, 2007), and v is

the average volume of an individual platelet. The number of surface-adhered platelets, N_s, was approximated as

$$N_s = \frac{A}{a} \tag{3-4}$$

where A is the area of the functionalized surface supporting platelet adhesion per unit length and a is the area occupied by an individual adhered platelet. Finally, the number of platelets adhered to other platelets, N_p, was calculated as

$$N_p = N_{tot} - N_s . \tag{3-5}$$

3.2.2.2 Analysis for Fully Occluded Test Sections

The effect of channel dimensions on R and P were analyzed based on the following. Two common test section geometries, circular and rectangular (Figure 3-1), were considered in the present analysis. Circular cross-sections were quantified by diameter, D, and rectangular test sections were characterized by height, h, and aspect ratio, α, defined as width over height, w/h. For circular test sections, the entire inner surface was considered functionalized to support platelet adhesion. For rectangular test sections, two surface functionalization configurations were considered. First, all interior surfaces were considered functionalized. The analysis was repeated assuming only one surface, either the top or bottom, was functionalized, similar to previous experiments (Barstad et al., 1994; 1995; 1995; Bossavy et al., 1999; Colace, Jobson, & Diamond, 2011; Gutierrez et al., 2008; Hosokawa et al., 2011; 2012; Houdijk et al., 1986; Maloney et al., 2010; Neeves et al., 2008; Sakariassen et al., 1983; Sakariassen et al., 1990; 1996; Savage et al., 1998; 1999; Sixma et al., 1998). For all geometries, the analysis was performed assuming a section of arbitrary length, L, over which the surface is functionalized to support platelet adhesion.

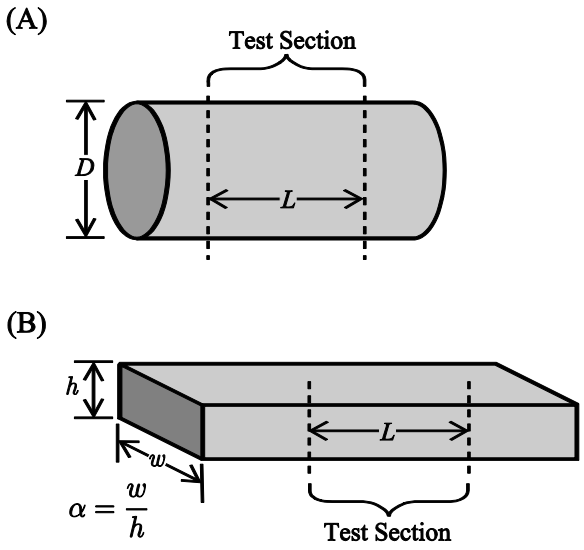

Figure 3-1: Test section geometry, (A) circular, (B) rectangular

For test sections that are fully occluded by thrombus, the thrombus volume per unit length for circular and rectangular test sections, V_C and V_R, respectively, were calculated from geometry as

$$V_C = \frac{\pi D^2}{4}, \tag{3-6}$$

$$V_R = \alpha h^2 \tag{3-7}$$

where α is the aspect ratio of the rectangular channel defined as width divided by height (w/h). For test sections with all surfaces functionalized to support platelet adhesion, the adhesive area per unit length for circular and rectangular test sections, A_C and A_R, respectively, were calculated from geometry as

$$A_C = \pi D, \tag{3-8}$$

$$A_R = 2h(1+\alpha). \tag{3-9}$$

Substituting eqs. (3-6) and (3-8) into eqs. (3-1) to (3-5) and simplifying gave the following for circular test sections.

$$R_C = \frac{Dpa}{4v} - 1 \tag{3-10}$$

$$P_C = 1 - \frac{4v}{Dpa} \tag{3-11}$$

where p is the percentage of the thrombus composed of platelets, v is the volume of an individual platelets, and a is the surface area occupied by an individual platelet. Similarly, substitution yielded the following for rectangular test sections.

$$R_R = \frac{\alpha hpa}{2v(1+\alpha)} - 1 \tag{3-12}$$

$$P_R = 1 - \frac{2v(1+\alpha)}{\alpha hpa} \tag{3-13}$$

In many experimental assays (see Table 3-2), a rectangular test section has been used with only the bottom or top surface functionalized to support platelet adhesion to simulate local atherosclerotic plaque rupture. In this case, the occlusive thrombus volume is identical to that given in eq. (3-7), but the area per unit length, A_B was calculated as

$$A_B = \alpha h . \tag{3-14}$$

Substituting again into eqs. (3-1) to (3-5) gave the following for occlusive thrombus in rectangular test with only the bottom or top surface functionalized

$$R_B = \frac{hpa}{v} - 1 \tag{3-15}$$

$$P_B = 1 - \frac{v}{hpa} . \tag{3-16}$$

For the present analysis, D was varied from 10 μm to 1000 μm for circular test sections, and for rectangular test sections, h was varied from 20 μm to 1000 μm and α from 1 to 70. Dimensions were chosen to correspond with the range of test section dimensions summarized in Table 3-2 as well as to investigate smaller microfluidic test sections. Channel dimensions less than 10 μm were not considered based on observations that average human platelet diameters are approximately 3.6 μm (Frojmovic & Panjwani, 1976), and thus very small dimensions would allow only one or two platelets to fill the cross-section. For the initial analysis, platelets were assumed spherical with v = 6.5 fL (Frojmovic & Panjwani, 1976).

3.2.2.3 Analysis for Partially-Occluded Test Sections

Many of the studies listed in Table 3-2 have short experiment times such that the rectangular test section was only partially occluded. In these cases, only one surface of the test section was functionalized, so eq. (3-14) is valid for the adhesive area per unit length. Either thrombus volume, $V_{R,part}$, or thrombus thickness, m, was measured. In the case where m was measured, $V_{R,part}$ was calculated as

$$V_{R,part} = \alpha h m. \tag{3-17}$$

Substituting into eqs. (3-1) to (3-5) gave the following for partially occlusive thrombus in a rectangular channel.

$$R_{R,part} = \frac{map}{v} - 1 \tag{3-18}$$

$$P_{R,part} = 1 - \frac{v}{map}. \tag{3-19}$$

The partial occlusions mirrors the fully-occluded test sections with only the one surface functionalized, and are not treated separately in the Results section, but were used to analyze the previous results shown in Table 3-2.

Though not applicable to the studies shown in Table 3-2, for completeness, partially occlusive thrombus in a circular channel has an adhesive area per unit length given by eq. (3-8) and a volume per unit length, $V_{C,part}$, given by

$$V_{C,part} = \frac{\pi}{4}\left[D^2 - (D-m)^2\right]. \tag{3-20}$$

Substituting into eqs. (3-1) to (3-5) gave the following for partially occlusive thrombus in a circular channel.

$$R_{C,part} = \frac{pa}{4Dv}\left[D^2 - (D-m)^2\right] - 1 \tag{3-21}$$

$$P_{C,part} = 1 - \frac{4Dv}{pa}\left[D^2 - (D-m)^2\right]^{-1} \tag{3-22}$$

3.2.2.4 Effect of Platelet Shape and Size

Using the analysis above, the effect of platelet size and shape were also analyzed. For spherical platelets, the diameter, d, was calculated from v using

$$d = \left(\frac{6v}{\pi}\right)^{1/3}. \tag{3-23}$$

The area occupied by a surface-adhered platelet was assumed to equal the maximum cross-sectional area, namely $a = \pi d^2/4$.

Discoid platelets were also analyzed, oriented such that they adhered with their major axis parallel to the surface, "flat," or with their major axis perpendicular to the

surface, "upright." Discoid platelet volume and geometry were quantified based on Frojmovic (1982) as

$$v = \frac{\pi}{4} d^2 t + \frac{\pi}{6} t^3 + \frac{\pi^2}{8} dt^2 \tag{3-24}$$

where d is the diameter and t is the thickness of the platelet. An axis ratio of 0.3 was assumed (Frojmovic & Panjwani, 1976), so $t = 0.3d$, and eq. (3-16) was solved for d with $v = 6.5$ fL. For platelets adhered in the flat position, a was assumed equal to the maximum cross sectional area, $a = \pi d^2/4$, and for platelets in the upright position, a was assumed equal to the rectangular projection of the platelet, $a = td$. The effect of platelet size was also analyzed by increasing v from 6.5 to 26 fL, four times the average platelet volume and at the upper range of observed platelet volumes (Paulus, 1975). Figure 3-2 illustrates the analyzed platelet geometries and adhesion orientations.

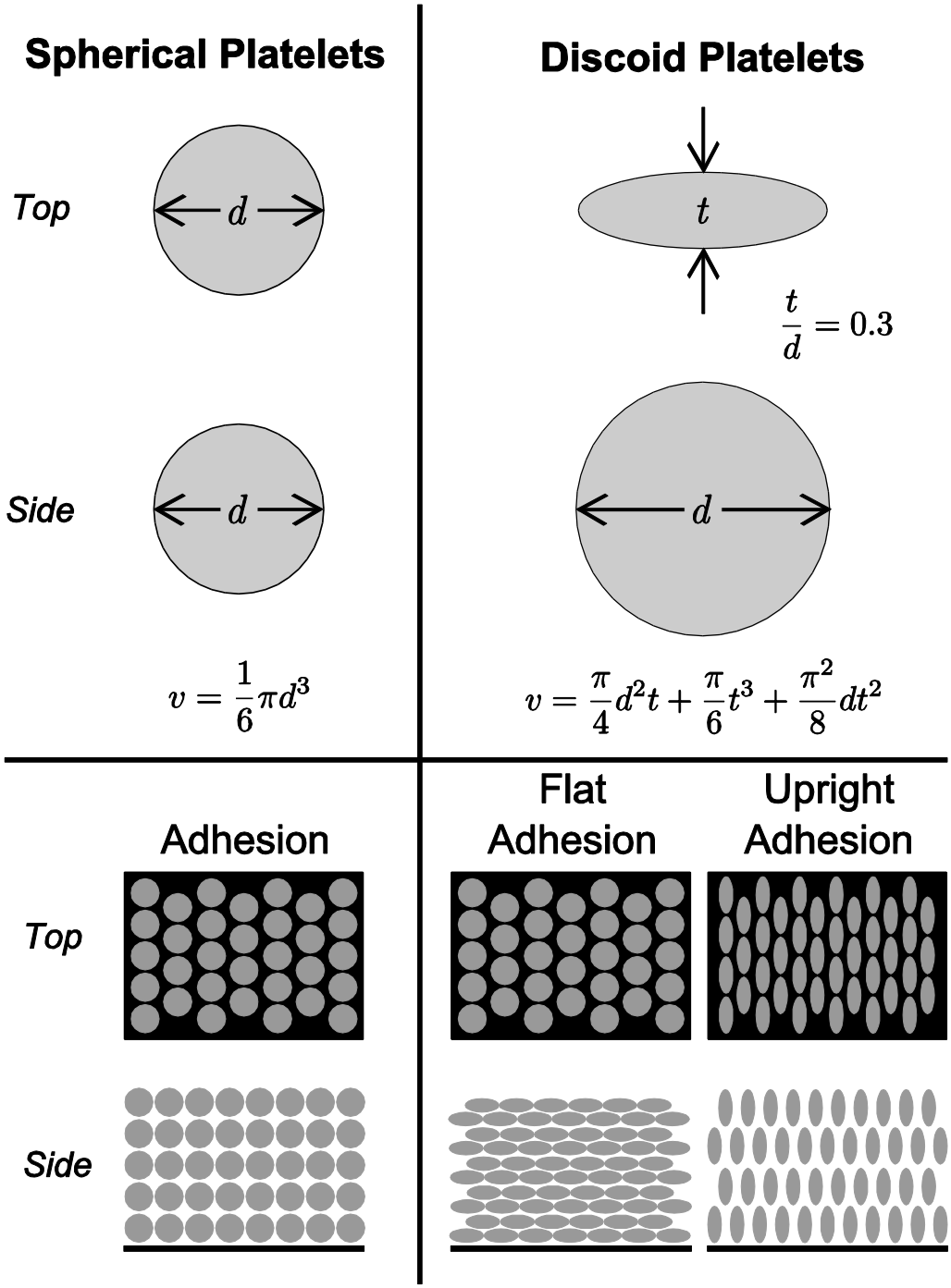

Figure 3-2: Platelet and adhesion geometry. For the initial analysis, all platelets were assumed to have the same volume of 6.5 fL. For spherical platelet (left), the diameter, *d*, was 2.3 μm, and for discoid platelets (right), *d* = 2.6 μm and the thickness, *t*, was 0.8 μm.

3.2.2.5 Particle Size Distribution

In vivo, platelet size varies according to a lognormal distribution with a log-mean of 1.68 fL and a log-standard deviation of 0.61 fL (Paulus, 1975). To model the effect of platelet volume variation, repeated Monte Carlo simulations of platelet adhesion were performed by generating arrays of random platelet sizes according to this distribution. The array represented sequentially bound platelets within the test sections. Stepping through the array, the functionalized surface of the test section was assumed to be coated first by subtracting the calculated area of the platelet from the total functionalized surface area and the volume of the platelet from the total test volume. After full surface coverage, each subsequent adherent platelet volume was subtracted from the total test volume until it was completely filled. The algorithm assigned first all surface-bound and then all platelet-bound platelets. This assignment may not necessarily mimic *in vivo* or *in vitro* thrombosis, but rather was employed as a way to systematically step through the array of platelet sizes. Assigning platelet locations randomly within the test volume and then analyzing the surface- versus platelet-bound platelets does not affect the results. R and P were calculated for each simulation based on the number of platelets adhered to the surface and total number of platelets necessary to fill the test section volume. The simulations were repeated at least 4 times and continued until the standard error of the mean (standard deviation divided by the square root of the number of trials) was less than 1% of the mean for both R and P.

3.2.2.6 Experimental Demonstration of R > 10

To illustrate the applicability of the preceding analysis to experimental systems, a rectangular microfluidic stenotic test section was designed with $R > 10$ yielding cross-sectional dimensions of h = 70 μm and w = 475 μm (α = 6.8). The test section was fabricated from PDMS and plasma-bonded to a glass microscope slide using standard techniques. To support platelet adhesion, the test section was coated with fibrillar collagen Type I (Chronopar; Chronolog, Inc.; Havertown, PA) for 24 hours in a warm, moist environment and rinsed with PBS prior to experimentation. Whole blood was obtained from a healthy donor under an approved IRB protocol. Blood was lightly heparinized at 3.5 USP units/mL (Para et al., 2011). Blood was perfused through the test section as a mean shear rate of 6500 s^{-1} under a constant pressure head.

To compare microfluidic test section performance to a test section that more closely mimics coronary artery geometry, whole blood from the same donor was also perfused through a circular stenotic glass test section ($R > 10$, D = 345 μm, 77% stenosis), as described previously (Ku & Flannery, 2007; Para et al., 2011). The test section was incubated with collagen, and the mean shear rate was matched to that of the microfluidic system. In the circular system, the discharge mass was measured using a scale.

Microscopy images of thrombus formation in each test section were recorded at 2 Hz using a high resolution CCD (Pixelfly; PCO; Kelheim, Germany) attached to a stereo microscope (Leica DM5000b; Leica Microsystems; Wetzlar, Germany and Stemi 2000-C; Carl Zeiss; Oberkochen, Germany). The images were analyzed using an automated image analysis program developed in MATLAB (R2012a; The Mathworks, Inc.; Natick, MA). For both systems, a reference image taken prior to thrombus formation was selected and

subtracted from subsequent images to highlight intensity changes resulting from the thrombus. For the microfluidic system, the total intensity in the region of interest was quantified as a surrogate for thrombus volume, which is not readily obtainable from the *en face* images. In the circular system, thrombus was identified using a user-defined threshold, and the thrombus volume was then estimated using a summation of differential volumes (Para et al., 2011).

Platelet adhesion to the collagen surface is characterized by a lag time before large thrombus formation. In contrast, platelet-platelet volume growth is characterized primarily by the occlusion time. The lag time, t_{lag}, and the occlusion time, t_{occ}, were quantified for both test sections. For the microfluidic system, t_{lag} was identified from the intensity versus time graph as initial non-linear region of thrombus formation, and t_{occ} was determined by identifying the microscopy image in which flow ceased, based on cell motion. For the circular, true-sized system, t_{lag} was defined as when the thrombus volume in the region of interest exceeded 0.001 mm^3, and t_{occ} was defined as when the discharge mass no longer changed.

3.2.3 Results

3.2.3.1 Analytical Results

In circular test sections, R_C increased linearly with D (Figure 3-3a), and P_C asymptotically approached 100% (Figure 3-3b). Similar results were seen for rectangular test sections (Figure 3-4). As α decreased in rectangular channels, the rate of increase of both R_R and P_R decreased, and thus low aspect ratio channels favor platelet-surface interactions. For rectangular channels with only one surface supporting platelet adhesion, α does not affect

R_B or P_B (Figure 3-5) as evident by the absence of α in eqs. (3-15) and (3-16). Rectangular sections with only one surface functionalized had higher R and P and thus favor platelet-platelet interactions, compared to rectangular test sections with all surfaces functionalized.

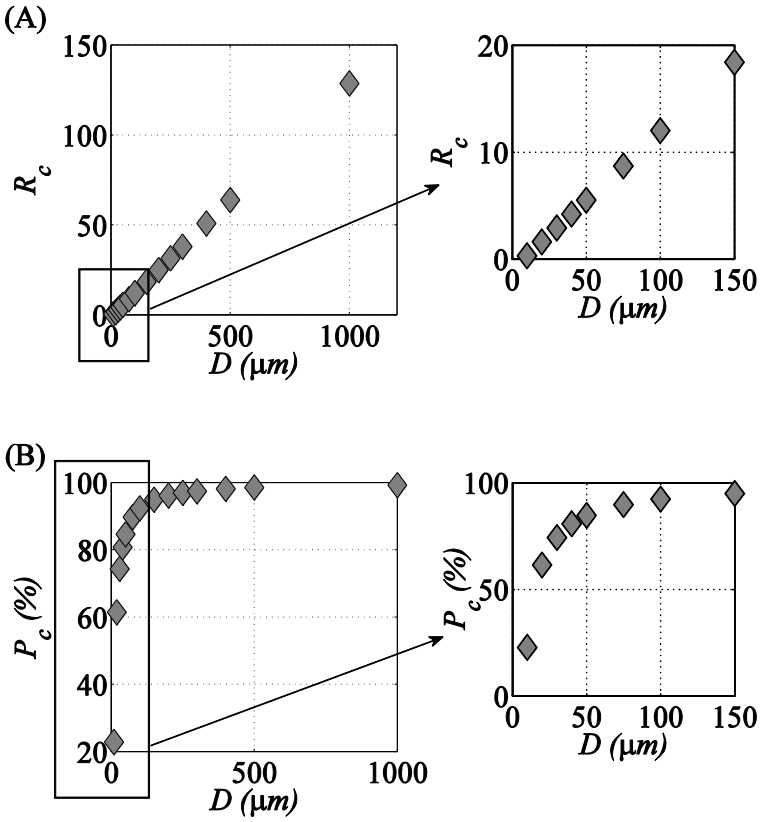

Figure 3-3: Effect of circular test section size on (A) platelet-platelet to platelet-surface interaction ratio, R_C, and (B) percent platelet-platelet interactions, P_C

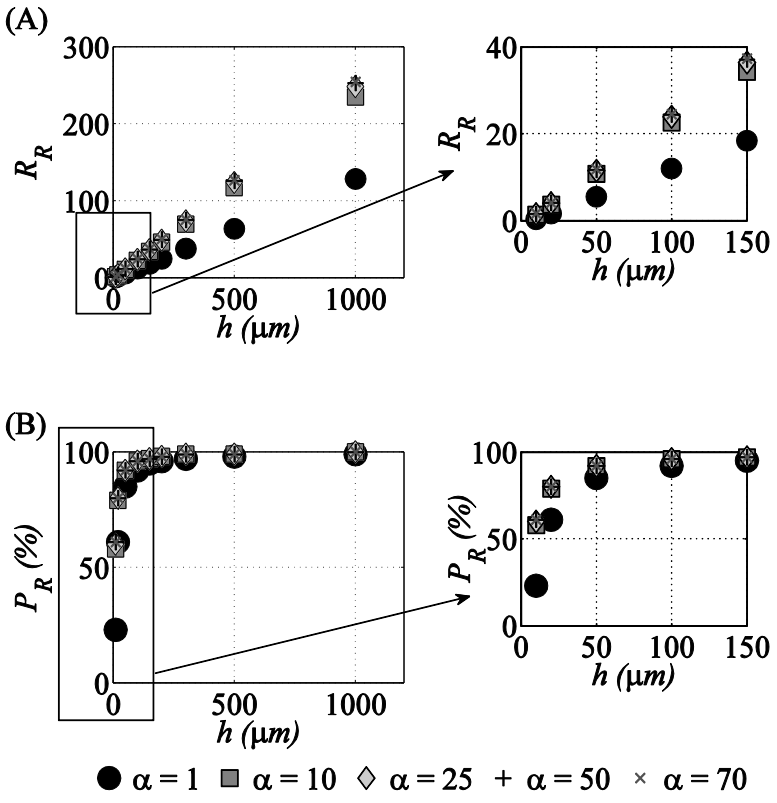

Figure 3-4: Effect of rectangular test section size with all sides functionalized on (A) platelet-platelet to platelet-surface interaction ratio, R_R, and (B) percent platelet-platelet interactions, P_R

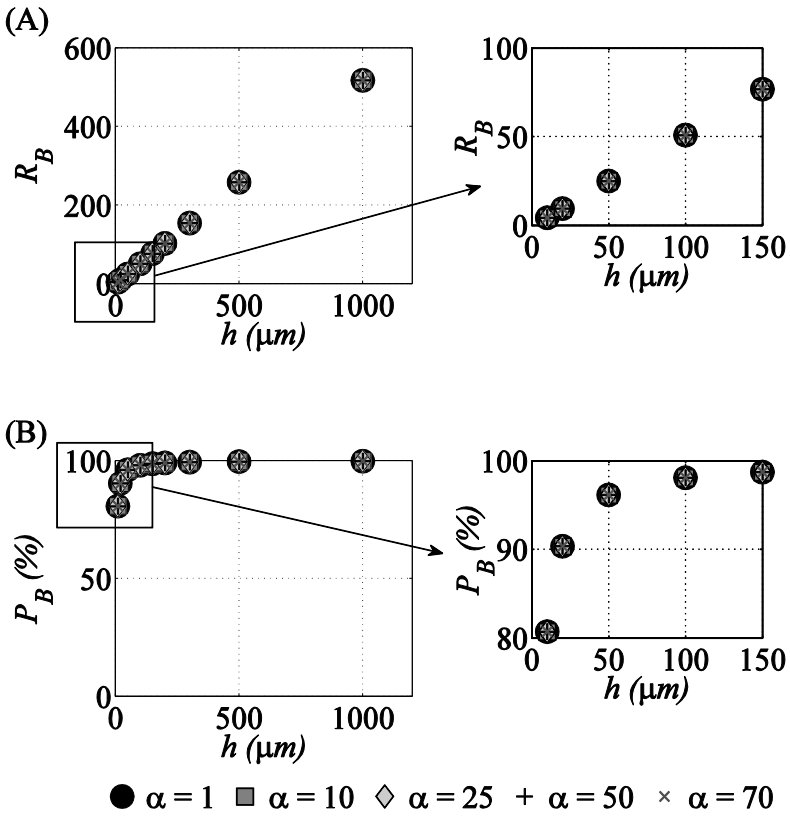

Figure 3-5: Effect of rectangular test section size with single surface functionalization on (A) platelet-platelet to platelet-surface interaction ratio, R_B, and (B) percent platelet-platelet interactions, P_B

Defining $R \geq 10$ (that is, ten times as many platelet-platelet adhesion events at platelet-surface adhesion events) as a threshold for an assay dominated by platelet-platelet interactions, circular test sections meant for full occlusion during experimentation should be manufactured with $D \geq 90$ μm. Rectangular sections with low aspect ratios and all surfaces functionalized should have $h \geq 90$ μm. Rectangular sections with large aspect ratios may be reduced to $h > 50$ μm and still be dominated by platelet-platelet interactions.

In rectangular channels with only one surface functionalized, h should be greater than 20 μm for platelet-platelet interactions to dominate thrombus formation. To isolate

platelet-surface interactions ($P < 50\%$), circular channels with $D < 20$ μm should be used. Alternatively, rectangular channels with only the one surface functionalized may be used to isolated platelet-surface interactions provided that thrombus thickness is limited to less than 10 μm.

Discoid platelets can be oriented flat to the surface or with their major axis perpendicular to the surface (upright). Figure 3-6 shows the effect of platelet shape on *R* and *P* in circular channels. Similar results were obtained for rectangular channels, but are not shown for conciseness. The effect of changing platelet shape from spherical to discoid had a limited effect on *R* and *P* when platelets are oriented flat against the test section wall (Figure 3-6), with discoid platelets slightly increasing *R* and *P* compared to spherical platelets. When platelets are oriented upright against the wall, *R* is substantially decreased compared to spherical platelets, and *P* is substantially decreased at small *D* with less effect as *D* increases. The larger effect of upright platelets compared to spherical platelets is due to an increase in the ratio of platelet volume to occupied surface area, *v/a*, from 1.4 μm for spherical platelets to 2.9 μm for upright platelets. Each surface adherent platelet occupies more volume per unit area in the upright position than in the flat or spherical position. This increases the number of platelets necessary to cover the surface without affecting the total number of platelets in the volume, thus resulting in a larger decrease in both *R* and *P*. In the case of flat platelets, *v/a* is slightly decreased compared to spherical platelets to 1.1 μm, resulting a smaller opposite effect. Given that Maxwell et al. (2006) showed that platelet morphology during translocation varies between discs adhered flat against the wall and spheres depending on shear rate, the case of upright platelet adhesion seems unlikely under high shear. Thus, the results of platelet shape variation suggest that a simplified spherical

geometric assumption yields similar results to flat platelet adhesion and is likely sufficient for design and characterization of microfluidic platelet assays.

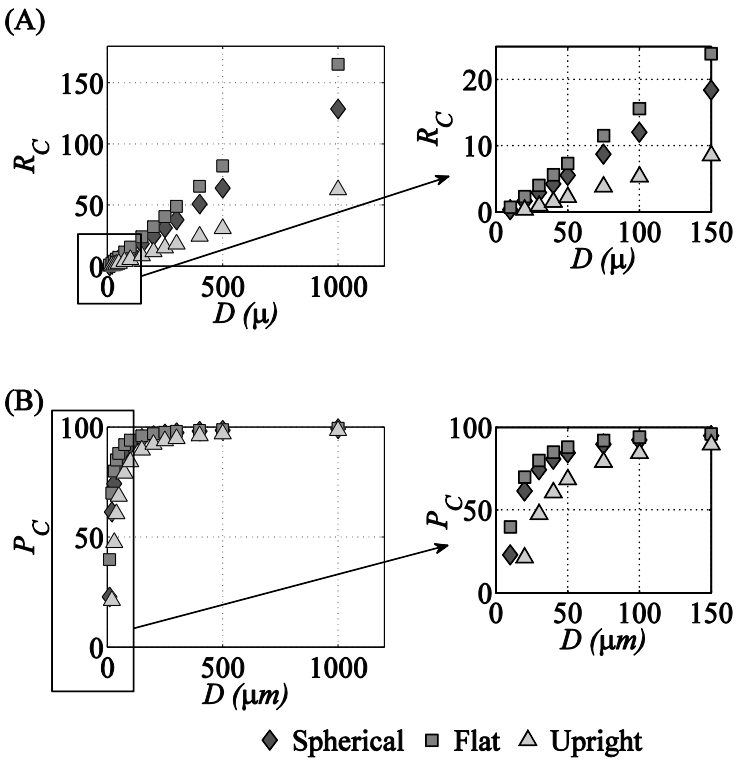

Figure 3-6: Effect of platelet shape on (A) platelet-platelet to platelet-surface interaction ratio, R_C, and (B) percent platelet-platelet interactions, P_C, in circular test sections

Based on the preceding results classifying test section dimensions of <20 μm for predominately platelet-surface interactions, or >90 μm for predominately platelet-platelet interactions, the subsequent analyses were performed for test sections sizes of 20, 100, and 500 μm (α = 10 for rectangular channels). Increasing platelet volume, *v*, from 6.5 to 26 fL had a large effect on *R* for all platelet shapes and test section geometries (Figure 3-7), with *R* decreasing 37-174% depending on the test section geometry and platelet shape. The

percent decrease was greatest in circular channels with D = 20 μm and for platelets in the upright orientation. In rectangular channels, R decreased by 37.1% to 43.6% when discoid platelet volume was increased from 6.5 fL to 26 fL.

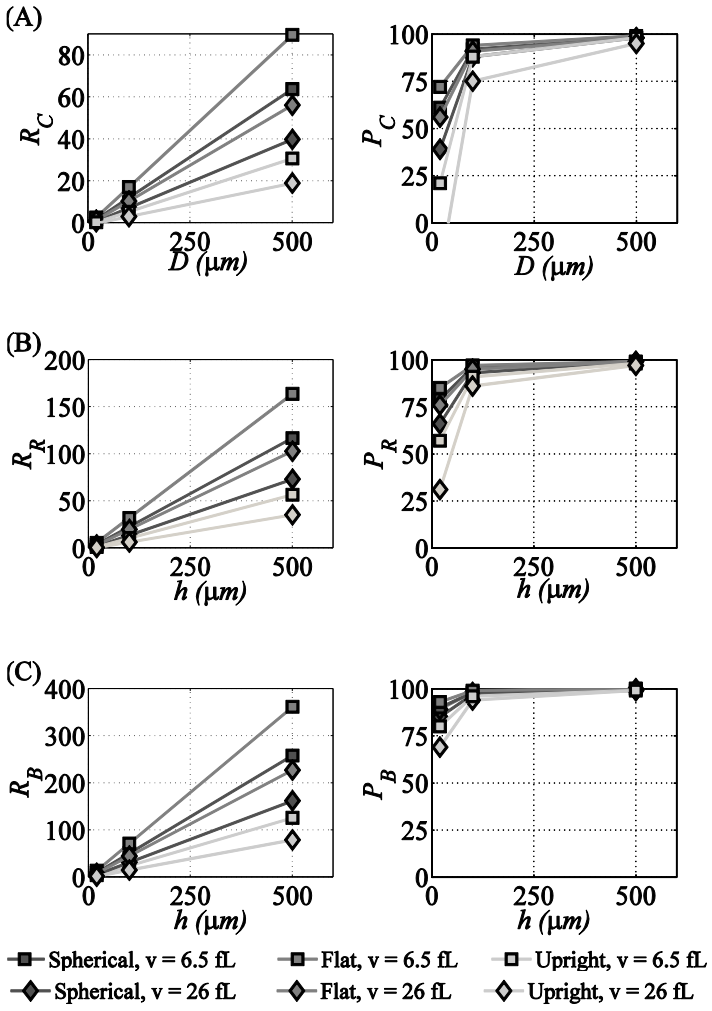

Figure 3-7: Effect of platelet volume on platelet-platelet to platelet-surface interaction ratio, R (left column), and percent platelet-platelet interactions, P (right column) for (A) circular channels and rectangular channels, α = 10, with (B) all surfaces functionalized and (C) only one surface functionalized.

Monte Carlo simulations were performed for spherical platelets in each test section geometry with D or h = 20, 100, and 500 μm and α = 10. The results of the Monte Carlo simulation are compared with the deterministic results in Table 3-3. Results for R differed by less 10% from the deterministic results, and P by less than 1% except in the smallest test sections analyzed. Platelet variability had a greater effect in small test sections because individual platelets with smaller- or larger-than-average volumes result in a greater percent difference in the area and volume occupied compared to the test section dimensions, yielding larger differences in R and P. Still, the small effect of platelet variability on R and P suggests that the deterministic equations derived are likely sufficient for most test section characterization and design.

Table 3-3: Summary of Monte Carlo Simulation Results

Ratio (R)

***D* or *h* (μm)**	**Circular Test Sections**			**Rectangular Test Sections (α = 10)**					
				All Surfaces Functionalized			**Single Surface Functionalized**		
	Eq. (3-1)	Monte Carlo	Percent Differ-ence	Eq. (3-1)	Monte Carlo	Percent Differ-ence	Eq. (3-1)	Monte Carlo	Percent Differ-ence
20	1.6	1.47	-8.26%	3.7	3.54	-4.74%	9.4	8.85	-5.80%
100	12.0	11.34	-5.45%	22.6	21.68	-4.06%	50.8	48.68	-4.42%
500	63.8	61.77	-3.26%	116.8	112.00	-4.27%	258.1	249.20	-3.58%

Percentage (P)

***D* or *h* (μm)**	**Circular Test Sections**			**Rectangular Test Sections (α = 10)**					
				All Surfaces Functionalized			**Single Surface Functionalized**		
	Eq. (3-2)	Monte Carlo	Percent Differ-ence	Eq. (3-2)	Monte Carlo	Percent Differ-ence	Eq. (3-2)	Monte Carlo	Percent Differ-ence
20	61.4%	59.2%	-3.82%	78.8%	78.0%	-1.06%	90.4%	89.8%	-0.58%
100	92.3%	91.9%	-0.44%	95.8%	95.6%	-0.17%	98.1%	98.0%	-0.09%
500	98.5%	98.4%	-0.05%	99.2%	99.1%	-0.04%	99.6%	99.6%	-0.01%

3.2.3.2 Experimental Results

We studied the effect of R and P on observed thrombosis in two test section. Based on the geometric analysis, the circular, true-size test section yielded values of R = 43.7 and P = 97.8%. Assuming all surfaces of the rectangular microfluidic test section absorbed collagen, the lower bounds of R and P were R = 14.8 and P = 93.7%. However, studies have suggested that collagen is absorbed more readily onto glass than PDMS (Li, 2013). Assuming only the bottom glass surface of the channels was coated with collagen, we calculate R = 35.3 and P = 97.2% for our rectangular microfluidic experiments. In both cases, the test sections had the $R \geq 10$ required to observe predominantly platelet-platelet adhesion events and should be comparable.

Thrombus formation in each test section is shown in Figure 3-8. In the circular, true-sized test section, thrombus formation can be seen as a narrowing of the lumen. However, in the microfluidic system, *en face* imaging through the flowing blood shows thrombus as progressively brighter regions. Total intensity in the microfluidic test section and thrombus volume in the true-sized test section are illustrated in Figure 3-9. Curves for each metric appear qualitatively similar, each with a clear initial region of minimal thrombus formation, a region of rapid, nearly linear increase in thrombus, a region of minimal thrombus growth near t_{occ}, and a sharp increase in intensity after occlusion. This final region of intensity build-up after occlusion may be due to thrombus compaction, which increased the image intensity and results in increased thrombus detection. For both test sections, t_{lag} were similar (Figure 3-9a) at 113 s in the microfluidic system and 133 s in the true-sized system, a difference of only 15%. Lag time is thought to occur from the absorption of plasma proteins, such as von Willebrand factor, that support high-shear

platelet adhesion and may also account for initial activation of surface-bound platelets. Lag time may be somewhat shorter in the microfluidic system due to the small surface area onto which proteins and platelet initially adhere. To compare the later stages of thrombus formation, the time after t_{lag}, Δt, was normalized by t_{occ} to account for difference in test section volume that must be fill with thrombus (Figure 3-9b). Under this normalization, the similarities in thrombus formation between the two test sections are striking. The similarities support our analysis that large-scale platelet accumulation can be created in two test sections with very different geometry and size as long as the ratio R is above 10.

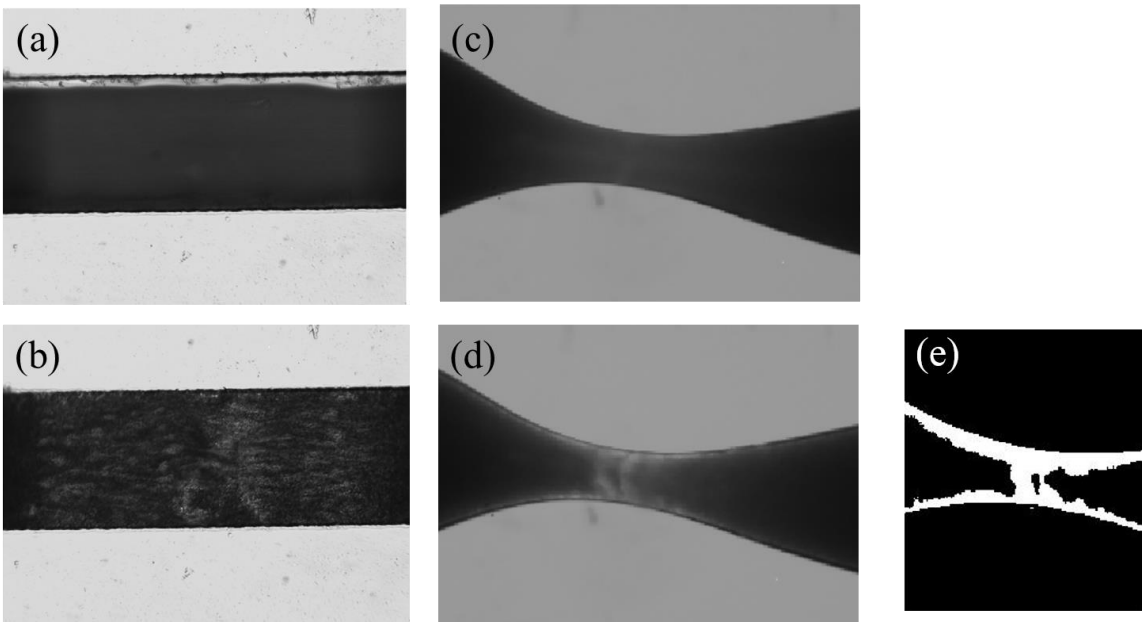

Figure 3-8: Experimental test sections, (a) and (b) non-thrombosed and occluded rectangular, microfluidic test section, (c) and (d) non-thrombosed and occluded circular, true-sized test section. Panel (e) shows regions identified as thrombus in the true-sized test section.

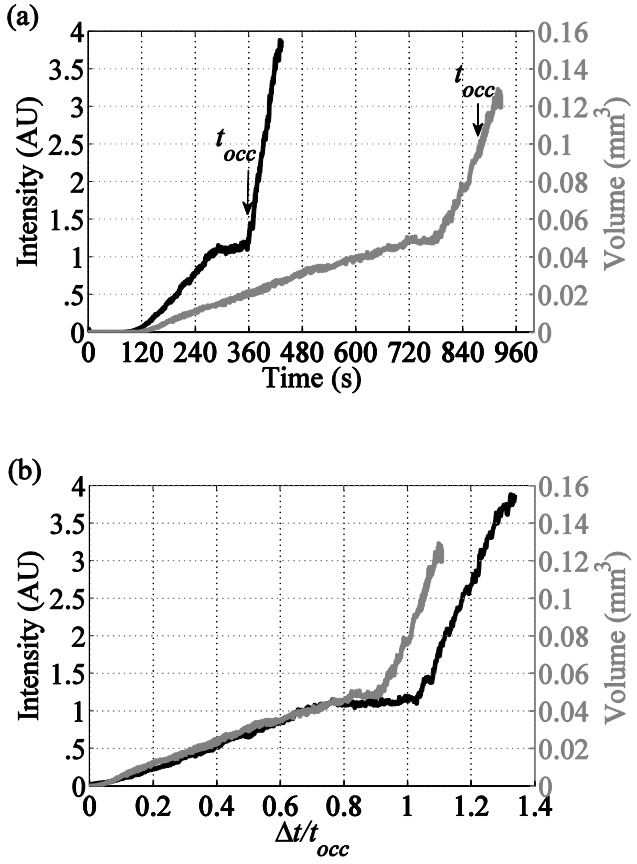

Figure 3-9: Intensity in 70 µm rectangular test section (black) and thrombus volume in true-sized circular test section (gray) versus (A) perfusion time and (B) non-dimensional time since t_{lag}, normalized by the occlusion time.

3.2.4 Discussion

Platelet thrombosis leading to arterial occlusion proceeds by platelet-surface interactions followed by platelet-platelet interactions, which are modulated by different adhesion receptors. To create these interactions *in vitro*, test section size is important. Based on the present analysis, the geometric dimensions of microfluidic assays can be used to create situations that are dominated by either type of interaction. The dominant interaction type was quantified by the ratio, *R*, of platelet-platelet to platelet-surface interactions and the percentage, *P*, of platelet-platelet interactions to total number of platelets. Analysis of

platelet shape showed that the spheres may be used as a reasonable approximation for discoid platelets. Platelet size also affects adhesion, but physiologic distributions of platelet populations do not result in large errors.

Test sections with circular geometry should be designed with $D \geq 90$ μm to create an assay dominated by platelet-platelet interactions ($R > 10$). For rectangular test sections, large aspect ratio channels with $h \geq 50$ μm or low aspect ratio channels with $h \geq 90$ μm should be used for predominately platelet-platelet interactions. Specifically, the applicability of a sufficiently large ($R > 10$) microfluidic test section for the study of occlusive arterial thrombosis in a coronary-sized vessel was demonstrated. Furthermore, experimental results may be extrapolated to conclude that in smaller test sections, thrombus formation would not progress past the lag time portion of the curve, and the distinct modes of large-scale, occlusive thrombus formation, particularly rapid platelet accumulation, would not be observed.

For predominately platelet-surface interactions ($P < 50\%$), a circular test section should be designed with $D \leq 20$ μm. For experiments that do not proceed to full occlusion, a rectangular test section with only the one surface functionalized may yield predominately platelet-surface interactions provided that the analysis is limited such that the thrombus thickness is less than 10 μm.

Table 3-4 lists the results of the present analysis applied to test section geometries from previous studies. In all experiments of this type, the dominant type of platelet interaction is determined by three factors: 1) test section geometry, 2) final thrombus volume determined either by occlusion or experimental time, and 3) the type of measurement endpoint. Several studies (Houdijk et al., 1986; Neeves et al., 2008;

Sakariassen et al., 1983; Sixma et al., 1998), address platelet-surface adhesion by measurement of surface coverage only as the experimental measurement endpoint. The results of the study by Gutierrez et al. (2008) were not conducive to the present analysis, and the study was classified as a platelet-surface study due to the short test time of one minute. For these studies, R and P were calculated for thrombosis of the full test section volume. In all cases, the use of additional measurement endpoints combined with sufficiently long test times for large thrombus volumes would allow these test sections to be used for platelet-platelet interaction studies as well as platelet-surface interaction. For the remaining studies listed, either thrombus volume or full test section occlusion was measured, and the present analysis was applied to distinguish between studies measuring platelet-surface and platelet-platelet interactions. Except in the study by Savage et al. (1998), these studies had $R >> 10$ and $P > 95\%$, indicating that the results of these experiments are dominated by platelet-platelet interactions and not platelet-surface interactions. In Savage et al. (1998) thrombus volume was constrained by short experiments times, thus isolating the analysis platelet-surface interactions.

Table 3-4: Application of Analysis to Previous High Shear Platelet Adhesion and Aggregation Assays

Test Section Geometry	*R*	*P*	Type of Adhesion	Determining Factor	Ref.
Cylindrical (stenosed)					
D = 2 mm D = 1.3 mm D = 0.9 mm D = 4 mm	174.9 213.4 78.2 73.8	99.4% 99.5% 98.7% 98.7%	Platelet-Platelet	Thrombus volume	(Badimon et al., 1986; Badimon & Badimon, 1989; Mailhac et al., 1994)
D = 300 um	41.4	97.6%	Platelet-Platelet	Test section geometry	(Bark et al., 2012; Ku & Flannery, 2007; Para et al., 2011)
Parallel Plate					
h = 1 mm, w = 10 mm α = 10	564.6	99.8%	Platelet-Surface†	Measurement endpoint	(Houdijk et al., 1986; Sakariassen et al., 1983)
h = 254 μm, w = 0.22 cm α = 8.7	2.4 0.4 -0.3	0.04% 0.02% -0.03%	Platelet-Surface	Thrombus volume	(Savage et al., 1996; 1998; 1999; Usami et al., 1993)
h = 0.1 mm, w = 5 mm α = 50	55.6	98.2%	Platelet-Surface†	Measurement endpoint	(Sixma et al., 1998)
h = 60 μm, w = 250 μm α = 4.2	32.9	97.1%	Platelet-Platelet	Test section geometry	(Colace et al., 2012; Maloney et al., 2010)
h = 80 μm, w = 100 μm α = 1.25	44.2	97.8%	Platelet-Surface†	Measurement endpoint	(Neeves et al., 2008)
h = 24 μm, w = 200 μm α = 8.3	12.6	92.6%	Platelet-Surface†	Thrombus volume	(Gutierrez et al., 2008)
h = 80 μm, w = 300 μm α = 3.75	44.2	97.8%	Platelet-Platelet	Test section geometry	(Hosokawa et al., 2011)
h = w = 40 μm α = 1	21.6	95.6%	Platelet-Platelet	Test section geometry	(Hosokawa et al., 2012)

Table 3-4: Application of Analysis to Previous High Shear Platelet Adhesion and Aggregation Assays

Test Section Geometry	*R*	*P*	Type of Adhesion	Determining Factor	Ref.
Parallel Plate (stenosed)					
w = 5 mm h = 0.7 mm, α = 7.1	394.9	99.8%	Platelet-Platelet	Thrombus volume	(Barstad et al., 1994; 1995; 1995; Bossavy et al., 1999; Sakariassen et al., 1990)
h = 0.28 mm, α = 17.9	157.4	99.4%			
h = 0.14 mm, α = 35.7	78.2	98.7%			
h = 0.08 mm, α = 62.5	44.2	97.8%			
h = 250 μm, w = 750 μm α = 3	140.4	99.3%	Platelet-Platelet	Test section geometry	(Li et al., 2012)

† - For studies that measured surface coverage, and therefore only platelet-surface interactions, the maximum possible *R* and *P* for the given geometry were calculated

In occlusive thrombus formation, which can lead to heart attack and stroke, many more platelet-platelet interactions occur compared to platelet-surface interactions, and thus it would be advantageous to design a test section dominated by platelet-platelet interactions while minimizing the flow rate required for pathological shear rates. The present analysis yields the minimum test section dimensions that result in more platelet-platelet interactions, providing an optimum test section size for both reducing blood volume and ensuring the observation of relevant adhesion events. For clinical application of high shear platelet testing, it is necessary to reduce the required blood volume to less than 10 mL, amounts obtainable by routine phlebotomy.

The present analysis may also be applied to the adhesion and accumulation of other cells in microfluidic assays. For example, leukocyte accumulation may occur simultaneously with platelet aggregation (Hu et al., 2003; Khreiss, Jozsef, Potempa, &

Filep, 2004), or in response to platelet microparticle release (Forlow, McEver, & Nollert, 2000) or ischemic stroke (Ritter, Orozco, Coull, McDonagh, & Rosenblum, 2000). Design of microfluidic channels to isolate leukocyte-leukocyte or leukocyte-platelet adhesion by laying down a layer of platelets within a microfluidic channel may improve understanding of leukocyte accumulation in thrombus formation. Another area of application may be three-dimensional cell culture, particularly of tumor cells (Kim, Yeon, & Park, 2007; Wu, Di Carlo, & Lee, 2008). The present analysis may be used to provide geometric constraints for the culture of tumor spheroids for cancer and metastasis research.

Finally, particulate-particulate and particulate-surface interactions are of critical importance to the transport of colloids in which the suspended particles may adhere to channel walls resulting in fouling and blockage. Colloidal fouling is observed in many processes, ranging from biological applications as described here to industrial processes and devices like filtration, papermaking, heat exchangers, and oil pipelines (Adamczyk, Siwek, & Szyk, 1995). Indeed, the mitigation of colloidal fouling is of perhaps greater importance in microfluidic systems where relatively small volumes of particle deposits may result in channel blockage (Mustin & Stoeber, 2010). The analysis described in the present work may be applied to design microfluidic channels to investigate a multitude of fouling processes by separating the mechanisms of particulate-surface and particulate-particulate deposition and adhesion. For a relevant application, the algebraic equations presented may be applied by specifying the correct particle characteristics, namely a and v, proper deposition composition described by p, and applicable channel geometry V and A.

The present analysis of platelet accumulation has several limitations. For a given analysis condition, all platelets were assumed to have the same shape and adhere in the same orientation though in physical experiments, platelet shape and adhesion orientation may vary. Additionally, only the extremes of platelet adhesion orientation were analyzed. Cell and clot deformability and mechanics were not modeled. Coagulation and fibrin formation was not considered in the present analysis, nor were the possible effects of other clotting proteins, such as von Willebrand factor, considered. Incorporation of erythrocytes in the thrombus was not modeled nor was the adhesion of leukocytes considered. The presence of other clot constituents were accounted for by including the percent of the thrombus composed of platelets, p, in the analysis. Additionally, the present analysis does not account for the effects of hemodynamics environment, platelet activation, coagulation, biomolecular interactions, or time dependence. Rather, the present study characterizes microfluidic channels based on the type of platelet interactions, regardless of the underlying mechanisms. This type of characterization may aid in classifying previous experimental results based on platelet interaction type and may be used in the design of future microfluidic flow assays to isolate the interaction of interest.

3.2.5 Conclusion

Geometric analysis of thrombus formation in microfluidic test sections showed that test section size and thrombus volume strongly affect the proportion of platelet-platelet and platelet-surface interactions in platelet adhesion and aggregation assays. Though platelet size and shape affect platelet-platelet to platelet-surface interaction ratio and percent platelet-platelet interaction, comparison of likely platelet adhesion orientations and Monte

Carlo simulation of normal human platelet size distribution suggests that quantitative algebraic relationships and a spherical platelet shape assumption are sufficient to classify platelet aggregations studies as either dominated by platelet-platelet or platelet surface interactions. The relationships obtained from the present analysis may be used to design microfluidic test sections to separately investigate platelet-surface adhesion and platelet-platelet accumulation. In square (low aspect ratio) and round test sections, a height or diameter 90 μm is necessary for channel occlusion to be dominated by platelet-platelet interactions ($R > 10$). The required height for $R > 10$ may be decreased to 50 μm for rectangular aspect ratios ≥ 10. Analytical results were supported by experiments comparing two test sections of different sizes and shapes, but both with $R > 10$. The derived equations may be extended to microfluidic and nanofluidic test section design for other types of cell adhesion and aggregation, three-dimensional cell culture, and colloidal fouling applications.

3.3 Fluid Mechanic Design

The most physiologically relevant cross sectional shape for assessing arterial thrombus formation is circular. Circular cross sections also have the advantage of uniform shear around their full circumference. However, circular microfluidic test sections present several challenges and limitations, in particular manufacturing complications and optical distortions when imaging. Since experimental evidence suggests that platelet accumulation is strongly dependent on shear rate, analyses were performed to define a rectangular test section such that 90% of the collagen-coated long boundary was within the wall shear range of interest, 3500-6000 s^{-1}. Considering Poiseuille flow in a rectangular duct

(Papanastasiou, Georgiou, & Alexandrou, 1999) (see Figure 3-10 for geometry and boundary conditions), and solving for shear rate gives

$$\left.\frac{\partial u_x}{dz}\right|_{z=-b} = -\frac{1}{2\mu}\frac{\partial P}{\partial x}b^2\left[\frac{2}{b} - 4\sum_{k=1}^{\infty}\frac{(-1)^k}{\alpha_k^3}\frac{\cosh(\alpha_k y/b)}{\cosh(\alpha_k c/b)}\frac{\alpha_k}{c}\sin(-\alpha_k)\right] \quad (3\text{-}25)$$

$$\alpha_k = (2k-1)\frac{\pi}{2}, \quad k = 1, 2, \ldots$$

where μ is the fluid viscosity, $\partial P/\partial x$ is the pressure gradient, and *b* and *c* are the channel half-width and half-height, respectively. For a known flow rate, *Q*, the pressure gradient is

$$\frac{\partial P}{\partial x} = \frac{-3\mu Q}{bc^3}\left[1 - \frac{6c}{b}\sum_{k=1}^{\infty}\frac{\tanh(\alpha_k b/c)}{\alpha_k^5}\right]^{-1} \quad (3\text{-}26)$$

A parameter sweep of eq. (3-26) over *h, w,* and *Q* was performed for *k* = 1-5 using Matlab to isolate combinations that met the shear criteria above. The minimum *w* and *Q* meeting the shear requirement for each *h* investigated are shown in Table 3-5.

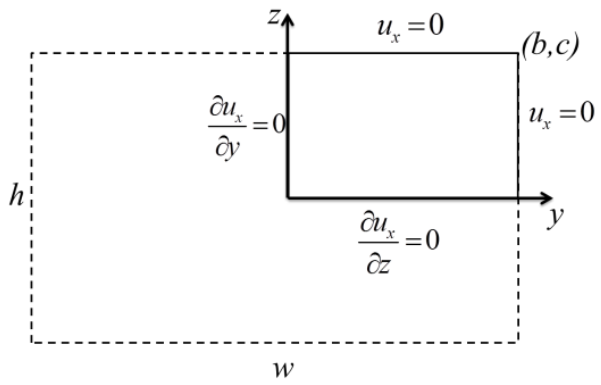

Figure 3-10: Geometry and boundary conditions for Poiseuille flow in a rectangular duct

Table 3-5: Results of parameter sweep for Poiseuille flow in rectangular duct

h (μm)	w (μm)	Q (μm^3/s, mL/min)	
50	400	7.35e8,	0.041
65	450	1.41e9,	0.085
70	475	1.72e9,	0.103
75	500	2.10e9,	0.126
80	500	2.10e9,	0.126
90	500	3.20e9,	0.192
100	600	4.86e9,	0.292

Given the small dimensions of the proposed test section, the Fahraeus-Lindqvist effect may result in altered apparent viscosity of the blood. The Fahraeus-Lindqvist effect is the observation that blood flowing in small capillary tubes has a lower apparent viscosity (Fåhræus & Lindqvist, 1931). This is the result of the formation of a cell-free plasma skimming layer close to the wall with a lower viscosity than whole blood. In very small tubes, the apparent viscosity increases as red blood cells must squeeze through the tube. In the present design, the apparent viscosity affects the pressure-driven flow rate through the test section. The flow rate, Q, scales according to

$$Q \propto \frac{\Delta p}{R} \tag{3-27}$$

where Δp is the pressure drop across the test section and R is the hydraulic resistance of the test section. R scales as $1/\mu$, where μ is the apparent viscosity, and the wall shear rate, γ, is directly proportional to Q. Using the empirical correlations of Pries, Secomb, and Gaehtegens (1996), the apparent viscosity for the dimensions used in the present device is expected to range from 2.5-3.5 $\times$ 10^{-3} Pa-s. Propagating this viscosity variation through the scaling above for a device designed to yield a maximum shear rate of 6000 s^{-1} for a constant blood viscosity of 3.5 $\times$ 10^{-3} Pa-s, as was used here, shows that the corrected shear rate due to the Fahraeus-Lindqvist viscosity reduction (worst-case) is expected to be

8400 s^{-1}. Previous studies have shown that thrombus growth rate and lag time are about equal at these shear rates (Bark et al., 2012; Mehrabadi, 2014), so no correction in was applied.

3.4 Thrombus Growth Considerations

For a thrombosis device to be clinically useful, it should require a low blood volume (<10 mL) and provide results quickly. The projected occlusion time (test time) and required blood volume were calculated for each geometry under consideration. Previous results for rate of thrombus growth under different shear rates were used (Bark et al., 2012). In particular, the time for the thrombus to reach a thickness of 10 μm, the "lag time," t_{lag}, depends on initial wall shear rate, $\dot{\gamma}_i$ and was calculated in seconds as

$$t_{lag} = 718\dot{\gamma}_i^{-0.2} \tag{3-28}$$

Since the wall shear rate varies across the rectangular channel, the mean shear rate was used in eq. (3-28). For thrombus growth after the lag time, thrombus deposition was simulated in 0.1 s time steps. At each time step, the shear rate, $\dot{\gamma}$, was computed from eq. (3-25) for the shrinking lumen. Then the thrombus deposition rate, J, in $\mu m^3/\mu m^2$-min was calculated as (Bark et al., 2012)

$$J = \begin{cases} 186\dot{\gamma}^{0.0382} - 229, & \dot{\gamma} < 6000 s^{-1} \\ 506 - 434\dot{\gamma}^{0.0124}, & \dot{\gamma} > 6000 s^{-1} \end{cases}. \tag{3-29}$$

The simulation was continued until the residual lumen had decreased to 0.1% of the initial height to yield the estimated occlusion time. The total occlusion time was obtained by adding the lag time, and the estimated blood volume was calculated by multiplying the flow rate by the total occlusion time. This method assumes that flow rate

is constant and the thrombus grows uniformly. Table 3-6 summarizes the results for estimated occlusion time and blood volume for the geometries under consideration. It was specified that the estimated blood volume should be less than 1 mL to allow for multiple tests from a single 10 mL blood draw, and the total occlusion time should be greater than 5-7 minutes to permit observation of rapid platelet accumulation described previously (Para et al., 2011). The selected channel geometry is highlighted.

Table 3-6: Estimated occlusion times and blood volumes for considered rectangular geometries

h (μm)	*w* (μm)	*Q* ($\mu m^3/s$, mL/min)	*Total Occlusion Time* (min)	*Total Blood Volume* (mL)
50	400	7.35e8, 0.041	6.5	0.286
70	475	1.72e9, 0.103	8.4	0.867
80	500	2.10e9, 0.126	9.1	1.146
90	500	3.20e9, 0.192	10.4	1.998
100	600	4.86e9, 0.292	11.4	3.325

The height of the non-stenosed regions of the test section were selected so that at least 85% of the long boundary had wall shear rates from 500-1000 s^{-1}, healthy arterial shear rates, with the same flow rate. Using eq. (3-25) and the same methods described above, the non-stenosed channel height was selected to be 170 μm. In summary, the test section was specified as 475 μm wide, 70 μm high in the stenotic section, 170 μm high at the non-stenotic section.

3.4.1 Validation of Thrombosis Model

After the microfluidic device was fabricated (see Section 3.5), test sections were measured to have a mean stenotic height of 83 μm. Test sections were incubated for 24 hours prior

to experimentation with 0.1% equine collagen Type 1 (Chronopar; Chronolog, Inc.; Havertown, PA). Collagen has been shown to adsorb much more readily onto glass than PDMS (Li, 2013), resulting in a thrombogenic surface only on the glass bottom of the channels.

Whole blood was collected from 7 health volunteers under a protocol approved by the Georgia Institute of Technology IRB. Blood was anticoagulated at 15.8 USP unit/mL. The whole blood was filtered at 60 μm to remove any debris and microaggregates and was then perfused through the microfluidic test section under a constant pressure of 684 Pa. The discharge mass was measured using an electronic balance, and occlusion time was defined as when the discharge mass ceased to increase.

The computational model described above predicted an occlusion time of 5.4 min in the microfluidic set up, which compares favorably to the mean occlusion time of 5.7 ± 2.3 min obtained from experiments (Figure 3-11), which shows excellent agreement between the computational and experimental results.

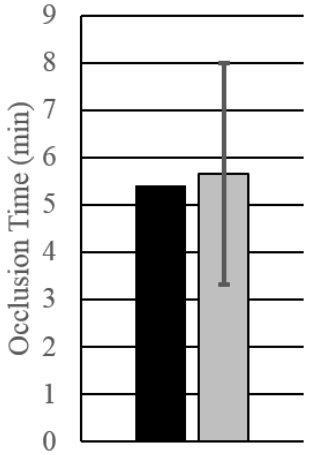

Figure 3-11: Predicted (black) and experimental (gray) occlusion times for thrombus formation in a microfluidic test section

3.5 Test Section Fabrication and Design for Manufacturing

Since the test section was design to be fully disposable, both laboratory fabrication and large-scale manufacturability were considered. Polydimethylsiloxane (PDMS) is widely used for the fabrication of microfluidic devices in the laboratory (Sackmann, Fulton, & Beebe, 2014), owing to its quick curing and ability to mold microscale features. The cured PDMS test section supplies three sides of the microfluidic test section, with the fourth side provided by glass plasma-bonded to the PDMS. The glass provides a substrate for collagen functionalization in the test section. See APPENDIX C for detailed fabrication protocol. However PDMS is not suitable for injection molding, a widely used and cost-effective large-scale manufacturing method (Mayor, J. R., personal communication, 2012). Injection molding is also not ideal for the laboratory setting due to the large equipment required. Thus, we aimed to develop a microfluidic mold which could be used in the laboratory to cast PDMS and which would serve as a template for future injection molding designs. Given the length scales identified in the preceding sections, micromachining, rather than soft lithography (applicable for length scales <50 μm), was selected as the mold fabrication technique, similar to Li et al. (2012).

The remaining specification in the test section was the transition from the physiological to pathological shear regions. A simple step was excluded from consideration due to the extremely high and low wall shear rates induced at the outside and inside corners, respectively. A sloped transition was considered, with the option of adding fillets at the outside corners. The maximum allowable shear rate at the corners was specified at 10 000 s^{-1}. The effects of the transition from the non-stenotic region to the stenotic region

on shear rate was investigated using numerical modeling (COMSOL 4.2; COMSOL, Inc.; Burlington, MA). Two-dimensional simulations were performed for slopes, α, of 15°, 30°, and 45° with fillet radii, *r*, at the corners of 0, 25, 50, and 100 μm (see Figure 3-12). Simulations were performed on approximately 400 000-element meshes (element size ~2.2 μm) with a velocity inlet boundary condition corresponding to the average velocity calculated from the flow rate in Table 3-5 and a zero-pressure outlet condition. Of critical importance was the estimated wall shear rate at the outside corners of the test section, where shear concentrations are expected.

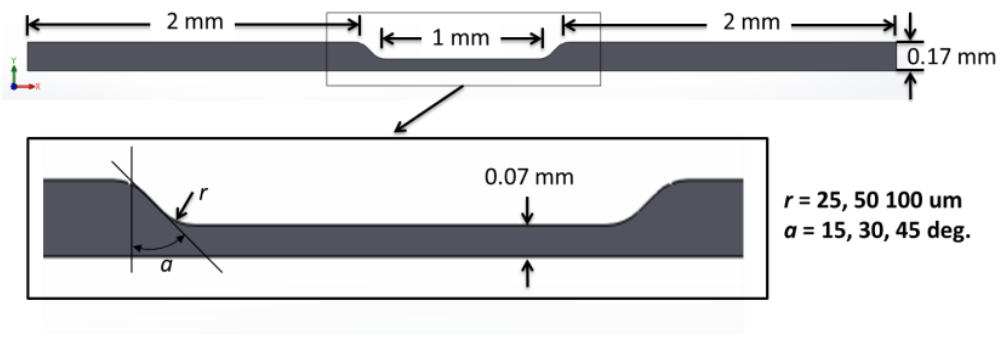

Figure 3-12: CFD geometry and variables

The shear rate along the upper wall was plotted versus arc length along the boundary to identify regions of shear concentrations, and the maximum wall shear rate for each condition was isolated (Figure 3-13). The results show a wall shear rate within the stenotic region of approximately 4400 s^{-1}, which meets the design criteria of shear rate between 3500 and 6000 s^{-1}. At the corners, peak shear rates reached as high as 16 000 s^{-1} in the case of α = 45° and *r* = 0. It was decided that for the peak shear rate should not exceed 10 000 s^{-1} to maintain the test conditions within the range of interest. For α = 15°,

the shear rate did no exceed 8000 s^{-1} for any value of *r*, so a test section with that geometry will be manufactured to eliminate the need for an additional machining operation to add fillets in the mold.

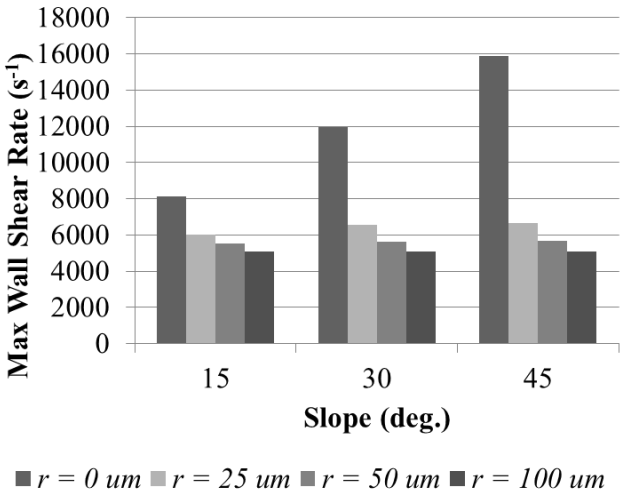

Figure 3-13: Maximum wall shear rate results obtained by CFD modeling

Following mold fabrication, the channel molds were measured used scanning white-light interferometry (Zygo OMP 0365E) (measurements performed by M. McMeekin). The eight channels in the mold have a mean stenotic height of 82.4 µm, a width of 480 µm, and a non-stenotic height of 182 µm (Mayor J. R. and McMeekin M., personal communication, 2012).

3.6 Image Processing

A non-contact, non-additive method of thrombus detection is advantageous in the point-of-care setting to allow for easy cleaning and minimal sample handling. A previous study

demonstrated that transmitted light through a growing thrombus increased in intensity over the course of the experiment and was useful for detecting occlusion (Li et al., 2012). However, this method did not provide an estimate of the physical volume of thrombus in the test section and was unable to provide real-time thrombus volume data. In the present work, confocal microscopy was used in conjunction with transmitted light microscopy to determine a relation between the thrombus height at a location and the light transmitted at that location.

3.6.1 Methods

Whole human blood was collected under a protocol approved by the Georgia Institute of Technology Institutional Review Board. Blood was anticoagulated with 3.5 USP units/mL. The blood was mixed with mepacrine at 10 μM final concentration to fluorescently label platelets (Savage et al., 1998). The blood was then perfused through the test section designed and fabricated as described in the preceding sections and incubated with 0.1% equine collagen Type 1 (Chronopar; Chronolog, Inc.; Havertown, PA). During the experiment, confocal microscopy stacks were collected (LSM 700; Carl Zeiss Microscopy; Jena, Germany) under 488 nm laser illumination. Transmitted light images (no confocal pinhole) were acquired simultaneously. The confocal image stacks spanned the full height of the channel, with slices 0.89 μm apart. Each stack took 1-2 minutes to acquire.

Confocal image stacks were processed with an in-house program (R2012a; The Mathworks, Inc.; Natick, MA) to determine the height of thrombus at each *x-y* pixel location. For each time point, the confocal image stack was read into the program. A Gaussian blur was applied, and every voxel identified as either thrombus or not thrombus

based on an intensity threshold of 5% of the maximum intensity for detecting the mepacrine labeled platelets. Outlying positive voxels were exclude by requiring that identified thrombus must occupy at least 4 voxels within a 5 voxel radius. From the binary matrix of thrombus location, the height of each thrombus was calculated from the number of slices with detected thrombus and the slice thickness. Next, the thrombus height was correlated to the change in transmitted intensity (subtracting the intensity in the first time point) in the most in-focus slice in the transmitted light stack using a logarithmic fit. Subsequently, three additional confocal experiments were performed to validate the interpolation method. The goodness of the interpolation was evaluated using an ANOVA analysis between the volume in each stack calculated from the confocal images and the volume interpolated from the fit.

3.6.2 Results

Figure 3-14 shows the growing thrombus using confocal microscopy and transmitted light. As the thrombus volume increases (top row, green), the transmitted light (bottom row, white) also increases. It should also be noted that the thrombus grows from the bottom, collagen coated glass surface and not from the PDMS channel sides or top.

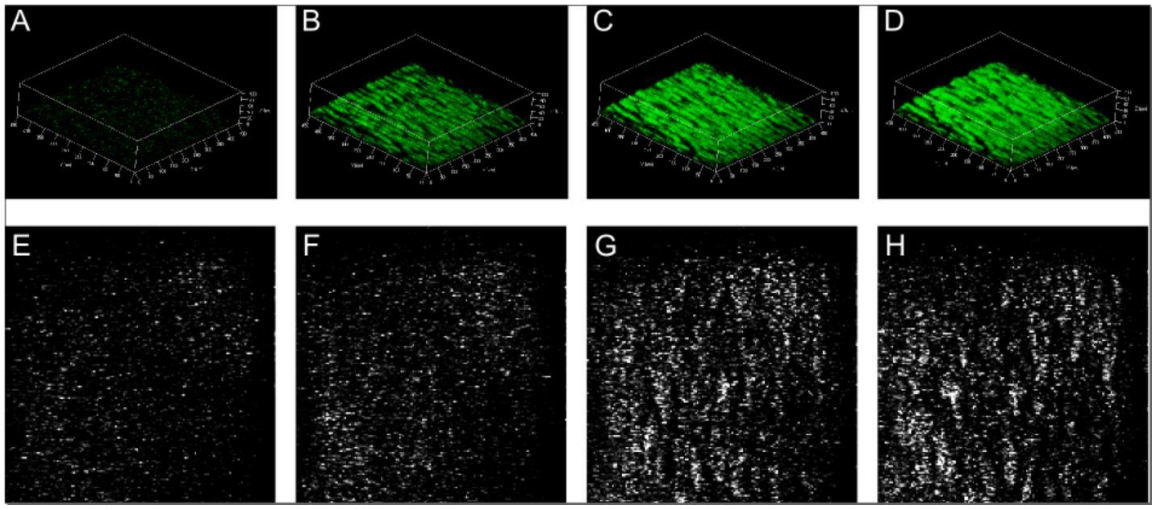

Figure 3-14: Thrombus formation visualized using confocal microscopy. Top row: 3D renderings of platelet accumulation. Bottom row: Corresponding transmitted light images showing an increase in transmittance as thrombus grows. Time points are at initiation of flow (A, E), 7.7 min (B, F), 15 min (C, G), and 21 min (D, H)

680 000 data points were obtained from the confocal experiment. The average transmitted intensity for each thrombus height is shown in Figure 3-15. There is a clear increase in transmittance with thrombus height, but large standard deviation. A logarithmic fit was perform (Figure 3-16) to interpolate the thrombus height from the change in transmitted intensity. The R^2 value was 0.90. For transmitted intensity changes less than 0.019, the corresponding height showed high variability, so all transmitted intensity changes less than 0.019 are assigned the mean thrombus height for those values of 3.115 µm. Converting the equation shown in Figure 3-16 to micrometers and applying the low-intensity threshold yields

$$h = \begin{cases} 3.115, & \Delta I < 0.07 \\ 21.1\ln(\Delta I) + 94.1, & \Delta I > 0.07 \end{cases} \quad \mu\text{m} \qquad (3\text{-}30)$$

where h is the interpolated thrombus height in μm and ΔI is the change in transmitted intensity. Applying eq. (3-30) to three subsequent data sets obtained as the first yielded the interpolated total volumes in the region of interest shown in Figure 3-17, plotted versus the volume obtained from confocal microscopy, treated here at the gold standard. ANOVA of the correlation between the confocal and interpolated volumes gives an adjusted R^2 of 0.79 and an f-value of 1.2×10^{-11}. The coefficient is 1.11, very close to unity, and the standard error is less than 20% for all but the earliest time points (before significant thrombus formation).

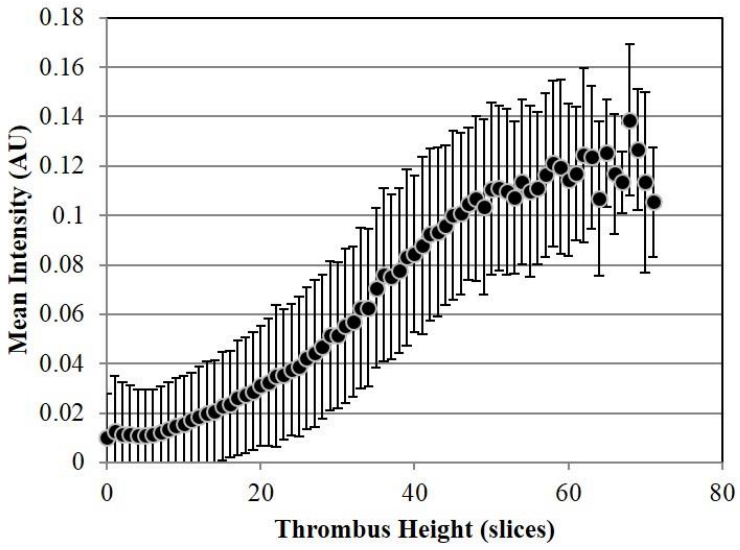

Figure 3-15: Mean change in intensity for each thrombus height. Error bars are standard deviation.

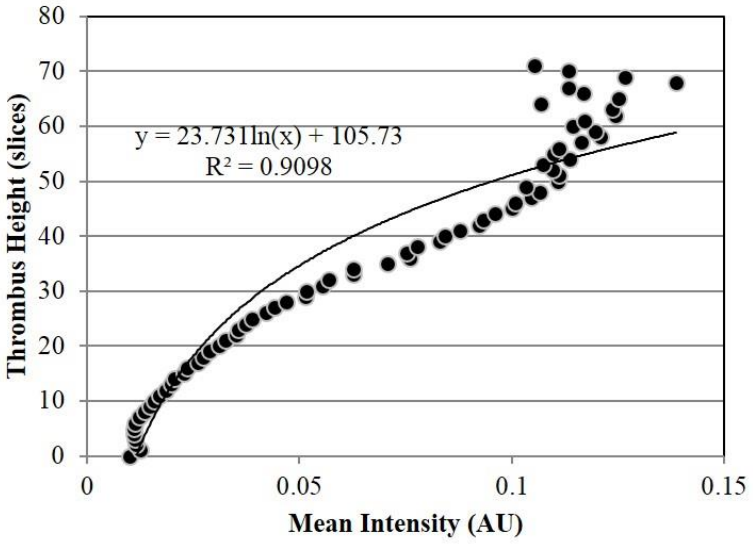

Figure 3-16: Logarithmic fit correlating thrombus height to mean change in intensity

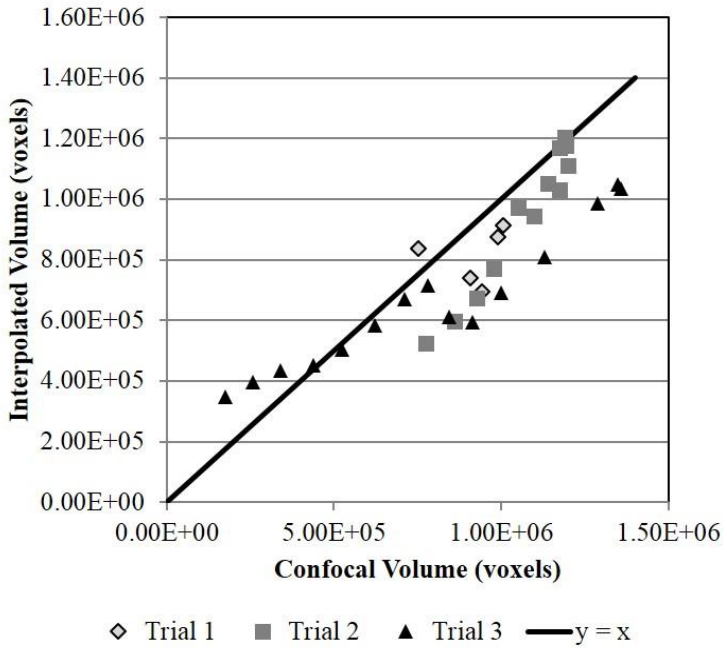

Figure 3-17: Validation of volume interpolation

3.6.3 Discussion

The volume interpolation correlating transmitted intensity to confocal thrombus volume yielded acceptably adequate results within 20% for most time points. The interpolation may be applied to standard light microscopy (see APPENDIX B for MATLAB code) by filtering the incident light at a similar wavelength as used in the confocal experiments (488 nm). When applied to light microscopy, the accuracy of the interpolation is limited by the increased light scattering caused by the non-coherent light source. Processing over 2000 images using the present method takes less than 30 minutes, opening the possibility of rapid image processing following thrombus formation in a similar device.

3.7 Characterization of Thrombus Formation in the Test Section

3.7.1 Methods

Whole blood was collected from 15 normal volunteers under a protocol approved by the Georgia Institute of Technology IRB. Subjects had no history of bleeding or thrombotic disorders and had not taken aspirin in the previous 10 days. Blood was collected in standard 10 mL green-top blood collection tubes (BD Vacutainer^{TM}; Becton, Dickinson, and Company; Franklin Lakes, NJ) and anti-coagulated at 15.8 USP units/mL heparin. Test sections were fabricated as described in Section 3.5 and incubated for 24 hours with 0.1% collagen (Chronopar; Chronolog, Inc.; Havertown, PA).

The collagen-coated microfluidic chips were installed in the experimental set up shown in Figure 3-18. The microfluidic channels were connected to an upstream reservoir at a height of 65 mm using 260 mm Tygon lab tubing (1/16 in.; Saint-Gobain North America; Valley Forge, PA) using connectors cut from rigid PTFE tubing (1.35 mm; Cole-

Parmer; Vernon Hills, IL). Downstream tubing and connectors led to a discharge reservoir placed on a precision balance (EP213C, Ohaus Corp.; Parsippany, NJ) to measure discharge mass. Up to 5 mL of blood was allowed to flow under a constant pressure head through the channel. Images of thrombus formation were acquired ever 500 ms using a microscope (DM6000 B; Leica Microsystems; Wetzlar, Germany) fitted with a high-resolution CCD camera (Pixelfly; PCO; Kelheim, Germany). Image acquisition was facilitated by the μManager open-source microscopy software (Edelstein, Amodaj, Hoover, Vale, & Stuurman, 2010). Occlusion time, t_{occ}, was measured as the time from first blood contact with the stenosis to the time when the balance mass stopped increasing for at least 1 minute. The experiment was repeated a total of 3 times for each subject.

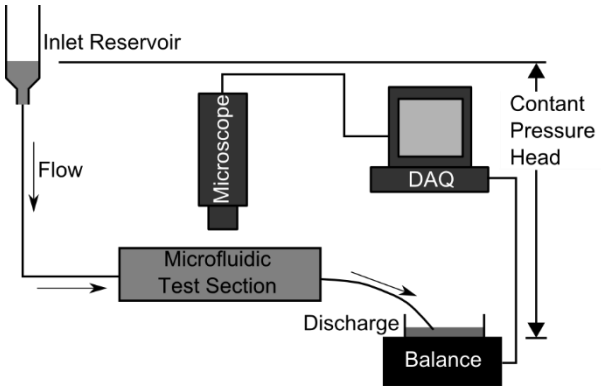

Figure 3-18: Experimental set-up from microfludic tests

Microscopy images were analyzed using MATLAB (R2013b; The Mathworks, Inc.; Natick, MA). First images were converted from 16-bit black-and-white to 8-bit color using the algorithm provided by the camera manufacturer ("Pixelfly, Pixelfly qe Operating Instructions,"). For analysis, the total intensity of the three color channels was used. A rectangular region of interest comprising the stenotic region was manually selected, and

the total intensity (arbitrary units, AU) increase since the reference images was computed for each time point. The reference images was selected as the image 30 sec after blood first contacted the channel. The lag time, t_{lag}, was defined as when the mean intensity over the region of interest increased by 100 AU. Alternatively, the image analysis method developed in Section 3.6 was used to estimate lag time. In this case, t_{lag} was defined as when the mean thrombus volume exceeded 3.14 $\mu m^3/\mu m^2$. The time between t_{lag} and t_{occ}, Δt, was also calculated. The thrombus growth rate, dV/dt, was computed as the slope of the linear regression of mean thrombus volume versus time from t_{occ} to t_{lag}.

3.7.2 **Results**

Figure 3-19 show typical thrombus growth profiles for both the volume interpolation method described in Section 3.6 and for change in transmitted intensity. In both cases, there is a period of relatively slow thrombus growth corresponding to the lag time, followed by rapid thrombus growth leading to occlusion. The rapid increase in intensity in the period after occlusion at 11. 5 min is likely due to an increase in the transmissivity of the thrombus caused by thrombus compaction.

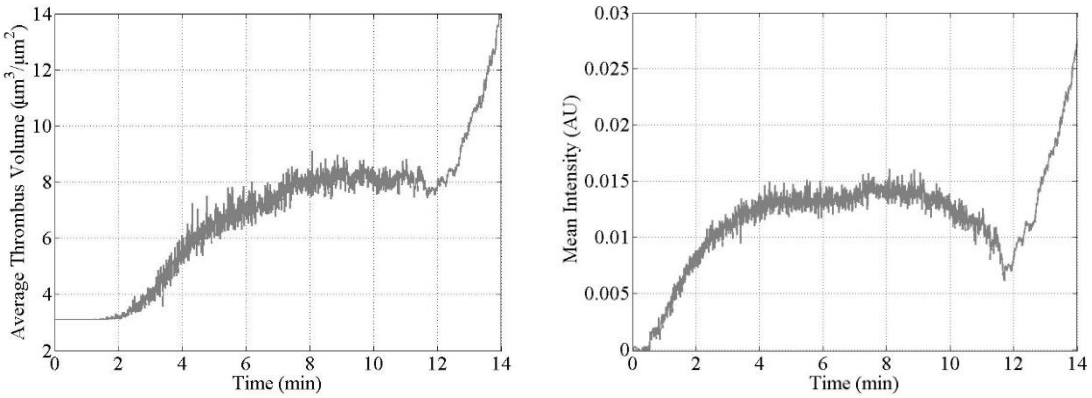

Figure 3-19: Characteristic Thrombus Growth: Left - interpolated average volume, Right - mean transmitted intensity change, t_{occ} = 11.5 min

The occlusion time was measured for each subject in 3 different experimental runs in separate microchannels (Figure 3-20). The average intrasubject variability was 28%, ranging from 3% to 61%. Intrasubject variability for PFA-100® has been reported as 28% (Poulsen et al., 2007). Intrasubject variability may be improved for the present device by compensating for small variations in channel dimensions.

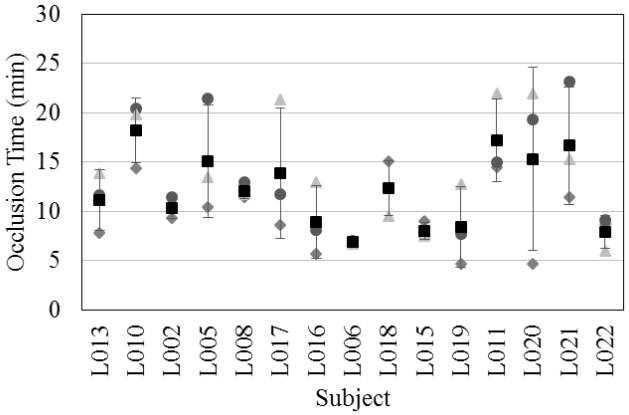

Figure 3-20: Occlusion times for n = 15 subjects, repeated 3x (circles, diamonds, and triangles); black squares represent the means of three trials and the error bars show standard deviation.

Thrombus growth rate determined by the volume interpolation method for the 15 subjects tested is shown in Figure 3-22. Intrasubject variability ranges from 8% to 102%, with a mean of 43%. Figure 3-23 show the lag times and time between lag time and occlusion time using both the volume interpolation method (top row) and transmitted light method (bottom row). Using the volume interpolation method, the intrasubject variability for lag time was between 2% and 95% with a mean of 46%. Using the transmitted light method, the variability was between 1% and 68% with a mean of 18%. For the volume interpolation method, Δt had an intrasubject variability of between 6% and 64% with a mean of 28%. For the volume interpolation method, Δt had an intrasubject variability of between 3% and 76% with a mean of 31%.

Taking all normal experimental occlusion times (45 total from 15 subjects) together gives a mean occlusion time of 12.2 min with a standard deviation of 5.1 min. The experimental distribution and the simulated normal distribution based on the mean and standard deviation are shown in Figure 3-21. All but one test falls within two standard deviations of the mean.

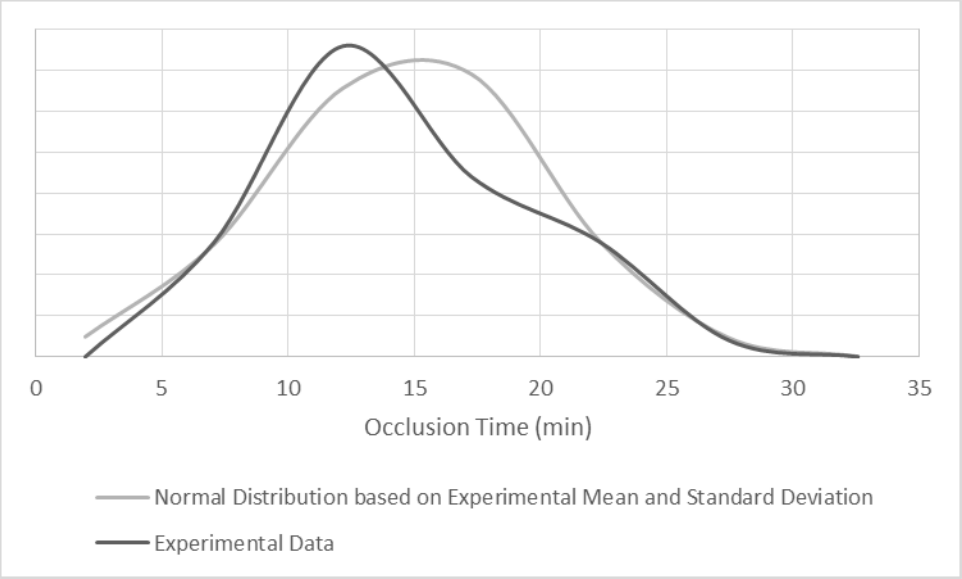

Figure 3-21: Distribution of all normal experimental results (n = 15, in triplicate, 45 total) and simulated normal distribution based on experimental mean and standard deviation.

Intrasubject variability may be due to variations in channel dimensions. Due to inherent variations in machining processes, the height of the stenosis varied from 76.5 μm to 85 μm between the 8 independent test channels. Based on the simple thrombosis model outlined in Sections 3.3 and 3.4 , the shear rate may be expected to vary by 8.8% between the channels, leading to an expected variation in the occlusion time of 12.6%, approximately half the variation observed in experiments. Additional variation is likely due to experimental variability between runs. The variation between test channels may be reduced by either improving machining techniques, which is quite difficult given the small scale and already tight tolerances, or by accounting for channel variations with a correction factor. The implementation of the volume interpolation method described in Section 3.6 also introduces possible error into the determination of the lag times and growth times.

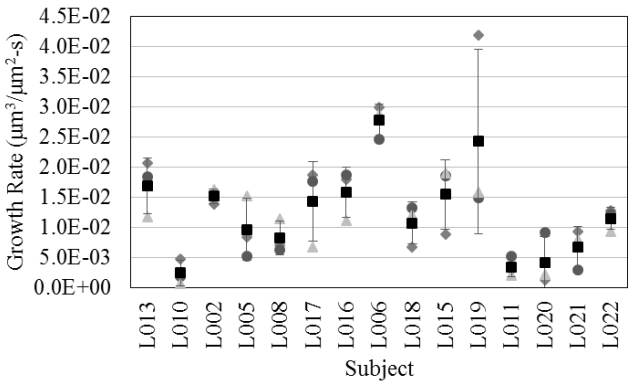

Figure 3-22: Thrombus growth rate using volume interpolation method for n = 15 subjects, repeated 3x (circles, diamonds, and triangles); black squares represent the means of three trials and the error bars show standard deviation.

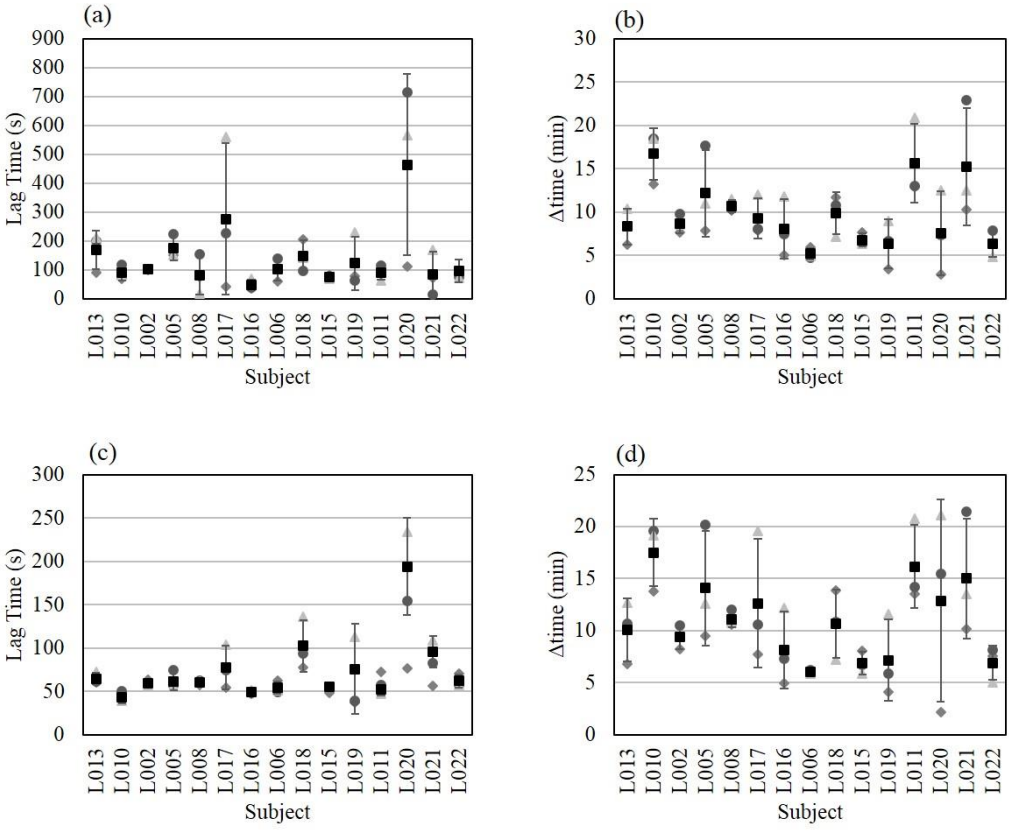

Figure 3-23: Lag time (left) and time from lag time to occlusion time (right): (a-b) using volume interpolation method, (c-d) using trnsmitted intensity method; repeated 3x per subject (circles, diamonds, and triangles); black squares represent the means of three trials and the error bars show standard deviation.

3.8 Summary

In the present work, a novel microfluidic assay for high shear thrombosis was developed. Special consideration was given to the fluid dynamic conditions and geometric constraints to ensure large-scale thrombus growth. An image processing approach was developed to obtain volumetric thrombus growth from transmitted light images. Thrombus formation in the test section was characterized for 15 subjects with 3 test cases each. The current design may be improved by accounting for variation in channel dimensions. For clinical use, the test section should be incorporated into an automated fluid handling system to interface with a blood collection tube. The developed test section was utilized in the following chapter to accommodate many high shear test conditions with a limited blood volume.

3.9 References

Adamczyk, Z., Siwek, B., & Szyk, L. (1995). Flow-Induced Surface Blocking Effects in Adsorption of Colloid Particles. *Journal of Colloid and Interface Science, 174*, 130-141.

Badimon, J. J., Badimon, L., Galvez, A., Chesebro, J., & Fuster, V. (1986). Influence of arterial damage and wall shear rate on platelet deposition: Ex vivo study in a swine model. *Arteriosclerosis, Thrombosis, and Vascular Biology, 6*, 312-320.

Badimon, L., & Badimon, J. J. (1989). Mechanisms of arterial thrombosis in nonparallel streamlines: Platelet thrombi grow on the apex of stenotic severely injured vessel wall, experimental study in a pig model. *Journal of Clinical Investigation, 84*, 1134-1144.

Bark, D. L., Para, A. N., & Ku, D. N. (2012). Correlation of thrombosis growth rate to pathological wall shear rate during platelet accumulation. *Biotechnology and Bioengineering, 109*(10), 2642-2650.

Barstad, R. M., Roald, H., Cui, Y., Turitto, V., & Sakariassen, K. (1994). A perfusion chamber developed to investigate thombus formation and shear profiles in flowing native human blood at the apex of a well-defined stenosis. *Arteriosclerosis, Thrombosis, and Vascular Biology, 14*, 1984-1991.

Barstad, R. M., Hamers, M. J. A. G., Stephens, R. W., & Sakariassen, K. (1995). Retinoic Acid Reduces Induction of Monocyte Tissue Factor and Tissue Factor/Factor VIIa-Dependent Arterial Thrombus Formation. *Blood, 86*(1), 212-218.

Barstad, R. M., Roald, H., Petersen, L. B., Stokke, K., Kierulf, P., & Sakariassen, K. (1995). Dietary supplement of omega-3 fatty acids has no effect on acute collagen-induced thrombus formation in flowing native blood. *Blood Coagulation and Fibrinolysis, 6*, 372-381.

Bossavy, J. P., Sakariassen, K. S., Thalamas, C., Boneu, B., & Cadroy, Y. (1999). Antithrombotic efficacy of the vitamin K antagonist fluindione in a human ex vivo model of arterial thrombosis - Effect of anticoagulation level and combination therapy with aspirin. *Arteriosclerosis Thrombosis and Vascular Biology, 19*(9), 2269-2275.

Cadroy, Y., Horbett, T. A., & Hanson, S. (1989). Discrimination between platelet-mediated and coagulation-mediated mechanisms in a model of complex thrombus formation in vivo. *Journal of Laboratory and Clinical Medicine, 113*, 436-448.

Colace, T., Jobson, J., & Diamond, S. L. (2011). Relipidated tissue factor linked to collagen surfaces potentiates platelet adhesion and fibrin formation in a microfluidic model of vessel injury. *Bioconjugate Chemistry, 22*, 2104-2109. doi: 10.1021/bc200326v

Colace, T., Muthard, R., & Diamond, S. L. (2012). Thrombus growth and embolism on tissue factor-bearing collagen surfaces under flow: Role of thrombin with and without fibrin. *Arteriosclerosis, Thrombosis, and Vascular Biology, 32*, 1466-1476. doi: 10.1161/ATVBAHA.112.249789/-/DC1

Davies, M. J., & Thomas, A. (1984). Thrombosis and acute coronary-artery lesions in sudden cardiac ischemic death. *New England Journal of Medicine, 310*(18), 1137-1140.

Edelstein, A., Amodaj, N., Hoover, K., Vale, R., & Stuurman, N. (2010). *Computer Control of Microscopes Using μManager*: John Wiley & Sons, Inc.

Fåhræus, R., & Lindqvist, T. (1931). *The viscosity of the blood in narrow capillary tubes* (Vol. 96).

Falk, E. (1983). Plaque rupture with severe pre-existing stenosis precipitating coronary thrombosis: Characteristics of coronary atherosclerotic plaques underlying fatal occlusive thrombi. *British Heart Journal, 50*, 127-134.

Forlow, S., McEver, R. P., & Nollert, M. (2000). Leukocyte-leukocyte interactions mediated by platelet microparticles under flow. *Blood, 95*, 1317-1323.

Frojmovic, M., & Panjwani, R. (1976). Geometry of normal mammalian platelets by quantitative microscopic studies. *Biophysical Journal, 16*, 1071-1089.

Frojmovic, M., & Milton, J. (1982). Human platelet size, shape, and related function in health and disease. *Physiological Reviews, 62*(1), 185-261.

Gutierrez, E., Petrich, B. G., Shattil, S. J., Ginsberg, M. H., Groisman, A., & Kasirer-Friede, A. (2008). Microfluidic devices for studies of shear-dependent platelet adhesion. *Lab on a Chip, 8*(9), 1486-1495. doi: 10.1039/b804795b

Hosokawa, K., Ohnishi, T., Kondo, T., Fukasawa, M., Koide, T., Maruyama, I., & Tanaka, K. A. (2011). A novel automated microchip flow-chamber system to quantitatively evaluate thrombus formation and antithrombotic agents under blood flow conditions. *J Thromb Haemost, 9*(10), 2029-2037. doi: 10.1111/j.1538-7836.2011.04464.x

Hosokawa, K., Ohnishi, T., Fukasawa, M., Kondo, T., Sameshima, H., Koide, T., . . . Maruyama, I. (2012). A microchip flow-chamber system for quantitative assessment of the platelet thrombus formation process. *Microvascular Research, 83*(2), 154-161. doi: 10.1016/j.mvr.2011.11.007

Houdijk, W. P., de Groot, P. G., Nievelstein, P. F., Sakariassen, K. S., & Sixma, J. J. (1986). Subendothelial proteins and platelet adhesion: von Willebrand factor and fibronectin, not thrombospondin, are involved in platelet adhesion to extracellular matrix of human vascular endothelial cells. *Arteriosclerosis, Thrombosis, and Vascular Biology, 6*(1), 24-33. doi: 10.1161/01.atv.6.1.24

Hu, H., Varon, D., Hjemdahl, P., Savion, N., Schulman, S., & Li, N. (2003). Platelet-leukocyte aggregation under shear stress: Differential involvement of selectins and integrins. *Thrombosis and Haemostasis, 90*, 679-687. doi: 10.1160/th03-05-0274

Khreiss, T., Jozsef, L., Potempa, L. A., & Filep, J. G. (2004). Opposing effects of C-reactive protein isoforms on shear-induced neutrophil-platelet adhesion and neutrophil aggregation in whole blood. *Circulation, 110*(17), 2713-2720. doi: 10.1161/01.CIR.0000146846.00816.DD

Kim, M. S., Yeon, J. H., & Park, J. K. (2007). A microfluidic platform for 3-dimensional cell culture and cell-based assays. *Biomed Microdevices, 9*(1), 25-34. doi: 10.1007/s10544-006-9016-4

Ku, D. N., & Flannery, C. J. (2007). Development of a flow-through system to create occluding thrombus. *Biorheology, 44*, 273-284.

Li, M., Ku, D., & Forest, C. (2012). Microfluidic system for simultaneous optical measurement of platelet aggregation at multiple shear rates in whole blood. *Lab on a Chip, 12*, 1355-1362.

Li, M. (2013). *Microfluidic System for Thrombosis Under Multiple Shear Rates and Platelet Therapies.* (PhD), Georgia Institute of Technology, Atlanta, GA.

Mailhac, A., Badimon, J., Fallon, J., Fernandez-Ortiz, A., Meyer, B., Chesebro, J., . . . Badimon, L. (1994). Effect of an eccentric severe stenosis on fibrin(ogen) deposition on severely damaged vessel wall in arterial thrombosis: Relative contribution of fibrin(ogen) and platelets. *Circulation, 90*, 988-996. doi: 10.1161/01.CIR.90.2.988

Maloney, S. F., Brass, L., & Diamond, S. L. (2010). P2Y12 or P2Y1 inhibitors reduce platelet deposition in a microfluidic model of thrombosis while apyrase lacks efficacy under flow conditions. *Integrative Biology, 2*(4), 153-220. doi: 10.1039/b919728a
10.1039/B919728A

Maxwell, M. J., Dopheide, S. M., Turner, S. J., & Jackson, S. P. (2006). Shear induces a unique series of morphological changes in translocating platelets: Effects of morphology on translocation dynamics. *Arteriosclerosis, Thrombosis, and Vascular Biology, 26*(3), 663-669. doi: 10.1161/01.ATV.0000201931.16535.e1

Maxwell, M. J., Westein, E., Nesbitt, W. S., Giuliano, S., Dopheide, S. M., & Jackson, S. P. (2007). Identification of a 2-stage platelet aggregation process mediating shear-dependent thrombus formation. *Blood, 109*(2), 566-576. doi: 10.1182/blood-2006-07-028282

Mehrabadi, M. (2014). *Effects of Red Blood Cells and Shear Rate on Thrombus Growth.* (PhD), Georgia Institute of Technology, Atlanta, GA.

Mustin, B., & Stoeber, B. (2010). Deposition of particles from polydisperse suspensions in microfluidic systems. *Microfluidics and Nanofluidics, 9*(4-5), 905-913. doi: 10.1007/s10404-010-0613-4

Neeves, K. B., Maloney, S. F., Fong, K. P., Schmaier, A. A., Kahn, M. L., Brass, L. F., & Diamond, S. L. (2008). Microfluidic focal thrombosis model for measuring murine platelet deposition and stability: PAR4 signaling enhances shear-resistance of platelet aggregates. *Journal of Thrombosis and Haemostasis, 6*, 2193-2201. doi: 10.1111/j.1538-7836.2008.03188.x

Papanastasiou, T. C., Georgiou, G. C., & Alexandrou, A. N. (1999). Unidirectional flows *Viscous Fluid Flow*. Boca Raton, FL: CRC Press.

Para, A. N., Bark, D. L., Lin, A., & Ku, D. N. (2011). Rapid platelet accumulation leading to thrombotic occlusion. *Annals of Biomedical Engineering, 39*(7), 1961-1971. doi: 10.1007/s10439-011-0296-3

Paulus, J. (1975). Platelet Size in Man. *Blood, 46*, 321-336.

Pixelfly, Pixelfly qe Operating Instructions. PCO.

Poulsen, T. S., Mickley, H., Korsholm, L., Licht, P. B., Haghfelt, T., & Jørgensen, B. (2007). Using the Platelet Function Analyzer-100 for monitoring aspirin therapy. *Thrombosis Research, 120*(2), 161-172. doi: http://dx.doi.org/10.1016/j.thromres.2006.08.010

Pries, A. R., Secomb, T. W., & Gaehtgens, P. (1996). Biophysical aspects of blood flow in the microvasculatur. *Cardiovascular Research, 32*, 654-667.

Ritter, L. S., Orozco, J. A., Coull, B. M., McDonagh, P. F., & Rosenblum, W. I. (2000). Leukocyte Accumulation and Hemodynamic Changes in the Cerebral Microcirculation During Early Reperfusion After Stroke Editorial Comment. *Stroke, 31*(5), 1153-1161. doi: 10.1161/01.str.31.5.1153

Ruggeri, Z. M., & Mendolicchio, G. L. (2007). Adhesion Mechanisms in Platelet Function. *Circulation Research, 100*(12), 1673-1685. doi: 10.1161/01.RES.0000267878.97021.ab

Sackmann, E. K., Fulton, A. L., & Beebe, D. J. (2014). The present and future role of microfluidics in biomedical research. *Nature, 507*(7491), 181-189. doi: 10.1038/nature13118

Sakariassen, K. S., Aarts, P., & de Groot, P. G. (1983). A perfusion chamber developed to investigate platelet interaction in flowing blood with human vessel wall cells, their extracellular matrix, and purified components. *Journal of Laboratory and Clinical Medicine, 102*(4), 522-535.

Sakariassen, K. S., Joss, R., Muggli, R., Kuhn, H., Tschopp, T. B., Sage, H., & Baumgartner, H. R. (1990). Collagen type III induced ex vivo thrombogenesis in humans. Role of platelets and leukocytes in deposition of fibrin. *Arteriosclerosis, Thrombosis, and Vascular Biology, 10*(2), 276-284. doi: 10.1161/01.atv.10.2.276

Savage, B., Saldivar, E., & Ruggeri, Z. M. (1996). Initiation of platelet adhesion by arrest onto fibrinogen or translocation on von Willebrand factor. *Cell, 84*, 289-297.

Savage, B., Almus-Jacobs, F., & Ruggeri, Z. M. (1998). Specific synergy of multiple substrate–receptor interactions in platelet thrombus formation under flow. *Cell, 94*, 657-666.

Savage, B., Ginsberg, D., & Ruggeri, Z. M. (1999). Influence of Fibrillar Collagen Structure on the Mechanisms of Platelet Thrombus Formation Under Flow. *Blood, 94*, 2704-2715.

Sixma, J., de Groot, P. G., van Zanten, H., & Ijsseldijk, M. (1998). A new perfusion chamber to detect platelet adhesion using a small volume of blood. *Thrombosis Research, 92*, S43-S46.

Usami, S., Chen, H.-H., Zhao, Y., Chien, S., & Skalak, R. (1993). Design and construction of a linear shear stress flow chamber. *Annals of Biomedical Engineering, 21*, 77-83.

Wu, L. Y., Di Carlo, D., & Lee, L. P. (2008). Microfluidic self-assembly of tumor spheroids for anticancer drug discovery. *Biomed Microdevices, 10*(2), 197-202. doi: 10.1007/s10544-007-9125-8

CHAPTER 4: CONTRIBUTION OF PLASMA AND PLATELET VON WILLEBRAND FACTOR TO OCCLUSIVE HIGH SHEAR THROMBOSIS

4.1 Introduction

Myocardial infarction (MI) and ischemic stroke result from rapid, occlusive thrombus formation at the site of atherosclerotic plaque rupture (Lilly, 2007). Thrombus formation at atherosclerotic lesions occurs at high shear rates (Bark & Ku, 2010; Bark, Para, & Ku, 2012) and follows distinct pathways (Jackson, 2007). Briefly, collagen exposed by plaque cap rupture acts as a thrombogenic surface. At high shear rates, plasma von Willebrand factor (vWF) is adsorbed onto the surface. Platelets then bind to vWF at the A1 domain via platelet receptor GPIb. Bound platelets are activated by shear and/or soluble agonists and irreversibly bind via integrin $\alpha_{IIb}\beta_3$. Activated platelet release prothrombotic and proinflammatory factors, including vWF, initiating a feed-forward amplification of thrombus growth. Clinical investigations have indicated that increased vWF levels are associated with increased risk of recurrent MI (Jansson, Kilsson, & Johnson, 1991), MI in patients with angina pectoris (Thompson, Kienast, Pyke, Haverkate, & van de Loo, 1995), and stroke (Wieberdink et al., 2010). On the other hand, low levels of vWF are characteristic of von Willebrand Disease (VWD), a bleeding disorder with symptoms including nose bleeding, skin bruises and hematomas, prolonged bleeding from trivial wounds, oral cavity bleeding, and excessive menstrual bleeding (Sadler et al., 2000).

It is well-accepted that platelets are a key constituent of arterial thrombi and vWF is critical for platelet adhesion at high shear rates, but few studies have investigated the independent role of vWF in large-scale thrombus accumulation, particularly at high shear

rates (>3000 s^{-1}) relevant to MI and ischemic stroke. The objective of the present study is to determine the relative roles and minimum concentrations of plasma vWF and platelets in large-scale occlusive thrombus formation at high shear rates (>3000 s^{-1}). Previously, we have theoretically shown that the number of exposed A1 domains on elongated, netlike vWF is likely to be the limiting factor in capturing circulating platelets (Wellings & Ku, 2012). We thus hypothesize that the contribution of vWF to high shear thrombus formation is equal to or greater than that of platelets. Further, we theoretically predicted that the high concentration of vWF released from alpha-granules is important to the continued capture of platelets as the thrombus narrowed the lumen and shear increased to > 100 000 s^{-1}. Thus, we hypothesize that vWF from platelets is important of occlusive high shear thrombus formation. To achieve high shear rates with reasonable blood volumes, we employ a microfluidic device in conjunction with human-derived blood analogs containing controlled vWF concentrations and platelet counts and normal (40%) hematocrit. We also consider *in vitro* thrombus formation in blood from patients with known VWD to study the relative contributions of platelet and plasma vWF. The results of this study lead to a better understanding of the roles of plasma vWF, platelet vWF, and platelet count in high shear thrombosis.

4.2 Methods

4.2.1 Blood Collection and Preparation

Blood from normal volunteers was collected under a protocol approved by the Georgia Institute of Technology IRB. Volunteers has no history of bleeding or thrombotic disorders and had not taken aspirin in the last 10 days. Blood for dilution experiments was collected

in 60 mL syringes and anti-coagulated with heparin at 15.8 USP units/mL to match standard green-top blood collection tubes (BD Vacutainer™; Becton, Dickinson, and Company; Franklin Lakes, NJ). Blood was also collected in 60 mL syringes and anti-coagulated with acid-citrate-dextrose solution at a 6:1 ratio for platelet isolation. Blood for comparison to VWD patient results was collected in standard 10 mL green-top (heparin, 15.8 USP units/mL) blood collection tubes (BD Vacutainer™; Becton, Dickinson, and Company; Franklin Lakes, NJ). Additional blood was collected from all subjects for a complete blood count and from select subjects for ristocetin cofactor (VWF:RCo) assays. VWF:RCo quantifies the ability of vWF to aggregate platelets.

Blood from VWD patients was collected under a protocol approved by the Emory University IRB and the Georgia Institute of Technology IRB. Subjects had been previously diagnosed with any type of VWD and no platelet defects and were returning to clinic for routine follow-up. Blood was collected in standard 10 mL green-top (heparin, 15.8 USP units/mL) blood collection tubes (BD Vacutainer™; Becton, Dickinson, and Company; Franklin Lakes, NJ).

Blood analogs were produced by diluting whole blood from normal volunteers with normal saline at 90% and 99% dilutions. Red blood cells (RBC) were isolated by centrifugation and washed twice with normal saline (see APPENDIX D). RBCs were filtered under gravity at 38 μm using nylon mesh and added to the dilutions to 40% hematocrit, yielding a blood analog with normal RBC count and 10% or 1% of normal platelet count and plasma protein concentrations. To test the contributions of vWF to high shear thrombosis, vWF (Humate-P®; CLS Behring, King of Prussia; PA) was added at 50, 100, and 200 IU/dL plasma, corresponding to the normal range of plasma vWF levels

(Sadler, 2003). To test the contribution of platelets, platelets were isolated from whole blood using a double centrifugation procedure (Cazenave et al., 2004) (see APPENDIX E). Humate-P® has been shown to have the same vWF multimer distribution as human plasma (Fukui et al., 1988). Platelets were resuspended in Tyrode's albumin buffer, and platelet count was obtained using a hemocytometer. On the hemocytometer, platelets appeared discoid and non-aggregated, indicating limited platelet activation before experimentation. Platelets were added to the blood analog at 120 000 platelets/μL. Platelets were added to the blood analog at 120 000 platelets/μL. Additional experiments were conducted adding recombinant human ADAMTS13 (R&D Systems, Inc.; Minneapolis, MN), which cleaves vWF (Springer, 2011), at normal concentration (0.75 mg/mL) (Soejima et al., 2006) to 90% dilutions with restored vWF. One experiment was conducted with ADAMTS13 added at six times normal concentration. All blood analogs were filtered under gravity at 50 μm using nylon mesh (McMaster-Carr Supply Company; Elmhurst, IL) immediately before experimentation. Table 4-1 summarizes the blood analogs considered.

Table 4-1: Blood analogs produced by hemodilution

	Dilution	**vWF Added (IU/dL saline)**	**Platelets Added (10^3/μL)**
Normal Whole Blood Control	0%	0	0
Negative Control	90%	0	0
Normal vWF and Normal Platelet	90%	100	120
Normal Platelet Only	90%	0	120
Normal vWF Only	90%	100	0
Low Normal vWF Only	90%	50	0
High Normal vWF Only	90%	200	0
Normal vWF and Normal Platelet (99% dilution)	99%	100	120
Normal Platelet Only (99% dilution)	99%	0	120
Normal vWF Only (99% dilution)	99%	100	0

4.2.2 Microfluidic Test Platform

To obtain high fluid shear rates with small blood volumes, a stenotic microfluidic test section was designed. The test section was designed to mimic the shear conditions experienced by a platelet as it travels from a health artery into a stenotic region and returning to health artery. The eight fabricated rectangular test sections are 480 μm and 77-85 μm (82 μm mean) deep at the stenosis. The stenotic length is 1 mm. Outside the stenosis the channel depth is 182 μm. Perfusion under a constant 65 mm pressure head yields wall shear rates across 90% of the width of 3500-6000 s^{-1} in the stenotic region and 500-1000 s^{-1} in the non-stenotic region, corresponding to normal arterial wall shear rates (Jackson, 2007). Additionally, the stenotic region was designed to favor large-scale platelet accumulation as opposed to surface adhesion by ensuring a sufficiently large volume-to-surface ratio (test section height >50 μm) (see Section 0).

The designed test section was fabricated from polydimethylsiloxane (PDMS) (Li, Ku, & Forest, 2012). A brass mold was micro-machined according to the design. PDMS was poured into the mold, degassed, and heat cured. Inlet and outlet ports were manually punched in each channel, and the PMDS chip was mounted on a glass microscope slide using plasma bonding. The completed microfluidic chip was allowed to cure at 70-75°C for 1 hour and then at room temperature overnight. After full cure, the microfluidic channels were filled with 0.1% collagen Type I solution (Chronopar; Chronolog, Inc.; Havertown, PA) and incubated for 24 hours (Bernardo et al., 2004). Collagen Type I was selected to mimic extracellular matrix exposed by atherosclerotic plaque rupture. De Witt et al. (2014) showed that collagen Type I is among the most potent platelet-adhesive surfaces under flow, initiating relatively large aggregates of activated platelets.

4.2.3 Data Acquisition and Analysis

The collagen-coated microfluidic chips were installed in the experimental set up shown in Figure 4-1. The microfluidic channels were connected to an upstream reservoir at a height of 65 mm using 260 mm Tygon lab tubing (1/16 in.; Saint-Gobain North America; Valley Forge, PA) using connectors cut from rigid PTFE tubing (1.35 mm; Cole-Parmer; Vernon Hills, IL). Downstream tubing and connectors led to a discharge reservoir placed on a precision balance (EP213C, Ohaus Corp.; Parsippany, NJ) to measure discharge mass. Up to 5 mL of blood or blood analog was allowed to flow under a constant pressure head through the channel. Images of thrombus formation were acquired every 0.5 second using a microscope (DM6000 B; Leica Microsystems; Wetzlar, Germany) fitted with a high-resolution (1392 × 1020 pixels) CCD camera (Pixelfly; PCO; Kelheim, Germany). Image acquisition was facilitated by the μManager open-source microscopy software (Edelstein, Amodaj, Hoover, Vale, & Stuurman, 2010). Occlusion time, t_{occ}, was measured as the time from first blood contact with the stenosis to the time when the balance mass stopped increasing for at least 1 minute. Blood from normal subjects collected in blood collection tubes was tested three times to characterize the experimental platform.

Microscopy images were analyzed using MATLAB (R2013b; The Mathworks, Inc.; Natick, MA). First images were converted from 16-bit black-and-white to 8-bit color using the algorithm provided by the camera manufacturer. For analysis, the total average intensity (grayscale) of the three color channels was used. A rectangular region of interest comprising the stenotic region was manually selected, and the total intensity (arbitrary units, AU) increase since the initial reference image (when blood first contacted the

channel) was averaged over the area was computed for each time point. To assess the phases of thrombus formation, lag time, t_{lag}, was determined as the time at which the total intensity increased by 100 AU within the region of interest, starting 30 s after first blood contact with the stenosis. Rapid growth time, t_g, was calculated as the occlusion time minus the lag time.

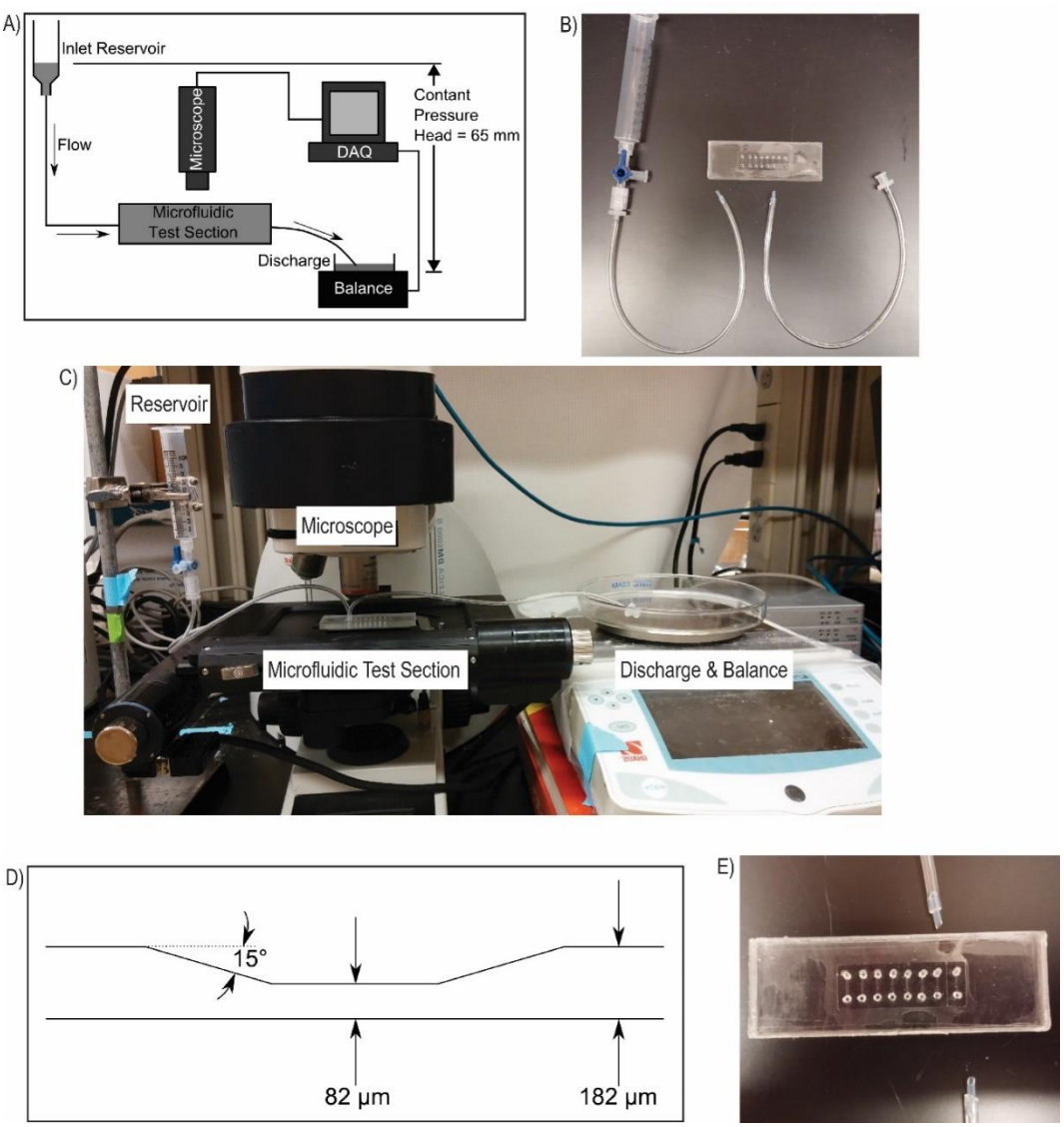

Figure 4-1: Microfluidic experimental set-up. A) diagram overall set-up, B) components of experimental set up, C) photograph of experimental set-up, D) diagram of microfluidic test section (width is 480 µm into page), E) photograph of microfluidic chip

4.2.4 Statistical Analysis

Data is shown as mean ± standard deviation throughout. Statistical significance was evaluated at the 0.05 level, and data analyses were performed using SAS 9.3 (Cary, NC) and R Project (Vienna, Austria). Rates of occlusion and thrombus were calculated using frequencies and percents within control and successive blood dilation samples. Rate comparisons for occlusion and thrombus (yes vs. no) were made using an exact form of the Chi-square goodness of fit test. Time to occlusion was gauged across control and blood dilution groups using Kaplan-Meier curves and log-rank tests. Log-rank p-values were calculated overall and for each pairwise comparison using the Holm-Bonferroni method (Holm, 1979). Samples that did not occlude were censored after 35 minutes of follow-up. Univariate and multivariable logistic regression was employed to identity significant risk factors associated with occlusion. Potential predictors included platelet counts and vWF at baseline and after dilution. Model fit was guided by backward elimination techniques and non-significant variables were systematically removed, provided the model fit did not substantially change. Adjustments were made for within-sample, correlated data using Generalized Estimating Equations (GEEs). Model fits were assessed via receiver operating characteristic curve (ROC) and Quasi-Akaike Information Criterion (QIC) statistics (Pan, 2001).

4.3 Results

Characteristic normal thrombus growth in the microfluidic test section is shown in Figure 4-2. Under grayscale imaging, the test section initially appears black as no thrombus has formed (Figure 4-2A). Thrombus begins to appear as patchy bright regions

(Figure 4-2B and C). At occlusion, large thrombus deposits are clearly visible throughout the stenotic portion of test section (Figure 4-2D). The change in total transmitted intensity (average of three color channels) across the test section is shown in Figure 4-2E. Initial slow deposition followed by rapid thrombus accumulation is apparent. The final sharp increase in intensity may be due to clot contraction as the channel nears occlusion. The timescale of the intensity increase is in good agreement with previous results of the timescale of clot and platelet contraction of 8-12 min (Jen & McIntire, 1982; Lam et al., 2011).

All syringe-collected control cases led to channel occlusion measured by mass flow (n = 12, p < 0.001, Figure 4-3A) with a mean occlusion time of 6.1 ± 2.2 min (intersubject variability of 36%). Normal subjects had platelets counts of 245 ± 66 × 10^3 /μL (n = 12) and VWF:RCo of 75 ± 69 IU/dL (n = 6). Conversely, none of the 90% dilution cases led to channel occlusion (n = 7, p = 0.016), indicating that dilution reduces the necessary components of high shear thrombosis to the point of eliminating thrombotic occlusion. 90% dilutions with restored platelets and vWF (100 IU/dL) occluded the channel in all cases (t_{occ} = 13.7 ± 2.5 min). Restoring platelets in 90% dilutions led to occlusion in 2/5 subjects (p = 1) with the remainder showing visible thrombus (t_{occ} = 27.2 ± 1.8 min). However, restoring vWF to 100 IU/dL in 90% dilutions restored occlusion in 6/7 subjects (p = 0.125), with a mean occlusion time of 16.6 ± 1.4 min. Experiments with added ADAMTS13 at normal concentration occluded in 4/5 subjects, and occlusion time was not reduced. Adding ADAMTS13 at six times normal concentration also did not prevent occlusion (n = 1). Thus, vWF is capable of forming occlusive thrombus, even with very low platelet counts (10% of normal). Restoring vWF

alone also restored occlusion in more subjects and yielded a more rapid occlusion time than restoring platelets alone.

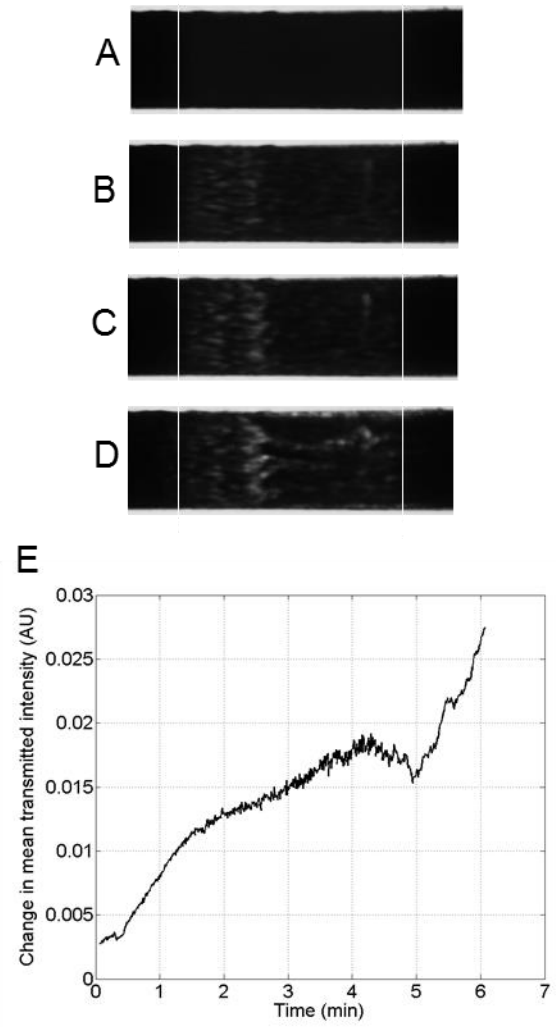

Figure 4-2: Normal thrombus formation in microfluidic test section. The test section appears black before thrombus formation and thrombus appears white within the test section. The stenotic region is bound by the white lines. Flow is from left to right top to bottom. A) at initiation of blood flow, B) at 50% occlusion time, C) at 75% occlusion time, D) at full occlusion. The test section appears black before thrombus formation and thrombus appears white within the test section. Flow is from top to bottom. E) Change in mean transmitted intensity during experiment. Note initial slow-growth phase followed by rapid thrombus growth beginning at approximately 30 seconds. Occlusion occurs at the end of the plot.

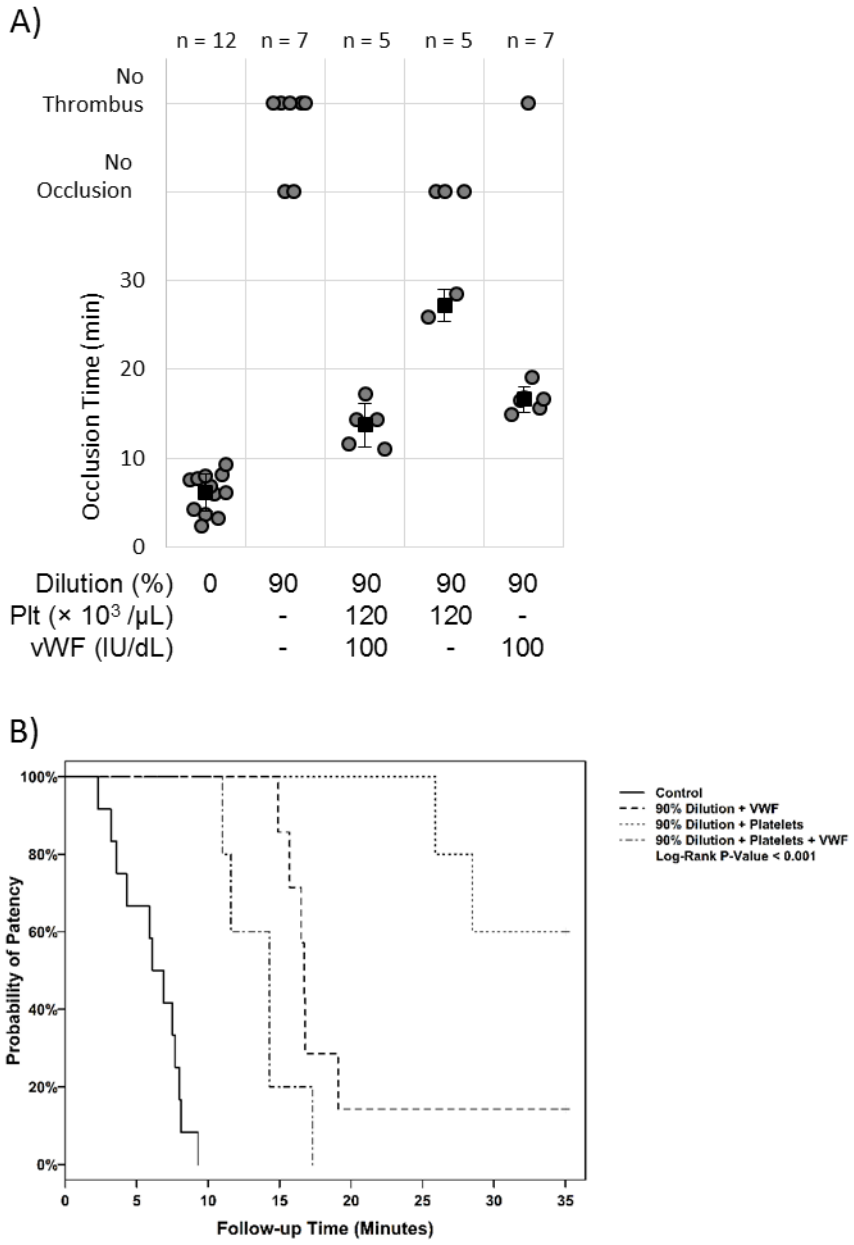

Figure 4-3: Thrombotic occlusion in microfluidic test section for 90% dilutions of whole human blood with normal additions of vWF and platelets. A) Occlusion times, "No Occlusion" indicates that test section did not occlude within 5 mL of blood analog but thrombus was visible during test; "No Thrombus" indicates that no thrombus was detected during the experiment; B) Kaplan-Meier analysis of patency probability.

Kaplan-Meier analysis (Figure 4-3) showed significantly lower probability of occlusion in the cases of 90% dilution comparted to control ($p < 0.001$, adjusted pairwise comparison). Qualitative comparison of 90% dilution with restored vWF (100 IU/dL) to 90% dilution with restored platelets indicate lower probability of occlusion in conditions with decreased platelet count compared to conditions with decreased vWF concentration ($p = 0.054$). The addition of platelets to 90% dilution with normal vWF cases did not have a significant effect on occlusion probability ($p = 0.073$). However, the addition of vWF to 90% dilution with normal platelet cases significantly increases the probability of occlusion ($p = 0.006$). Multivariable logistic regression for occlusion indicated that the resultant platelet count and resultant vWF concentration after dilution are significant predictors of occlusion (Table 4-2). The odds ratio (OR) for a 100,000 platelet/μL increase was 4.43 (95% confidence interval 2.96-6.65), and the OR for a 10 IU/dL increase in vWF is 1.26 (95% confidence interval 1.10-1.45). A QIC model evaluates the ability of particular variables to account fully for the outcome, where a lower number indicates a better fit. The QIC model fit statistics were 82.25 for platelet count after dilution and 39.36 for vWF concentration after dilution, indicating that vWF concentration after dilution is a stronger predictor of occlusion. Not only is vWF capable of forming occlusive thrombus with very low platelet count, it is more predictive of thrombotic occlusion.

Table 4-2: Multivariable logistic regression for occlusion (yes vs. no)

Characteristic	OR (95% CI)	P-Value	QIC Model Fit[3]
Platelet count (after dilution)	4.43 (2.96 – 6.65)[1]	<0.001	82.25
vWF (after dilution)	1.26 (1.10 – 1.45)[2]	0.001	39.36

[1]OR are based upon 100,000 unit increase in platelet characteristics
[2]OR are based upon 10 unit increases in VWF characteristics
[3]Smaller values indicate better model fit

In 90% dilutions, added vWF was varied from 50 IU/dL to 200 IU/dL (Figure 4-4). At low-normal levels of vWF (50 IU/dL), 2/6 subjects occluded (p = 0.688). When 100 IU/dL vWF was added to 90% dilution, 6/7 subjects occluded (p = 0.125). At high-normal levels of vWF (200 IU/dL), 6/6 subjects occluded (p = 0.031). Though additional vWF resulted in more subjects occluding at each subsequent experimental condition, the occlusion times were not affected.

Surprisingly, 99% dilutions with restored platelets and vWF (100 IU/dL) did not lead to thrombotic occlusion (Figure 4-5A). Rather, large-scale thrombus formed, but embolized repeatedly without fully occluding the vessel. Figure 4-5B shows the change in transmitted intensity for one such case, and rather than rapidly increasing as in Figure 4-2E, the curve shows over ten large peaks and valleys over a long experiment time, from thrombus growth and detachment rather than occluding. Note that the time scale is in tens of minutes to compress the time. Embolization occurs within 60 to 180s. 99% dilutions with either restored platelets or restored vWF (100 IU/dL) did not show thrombus formation in nearly all cases.

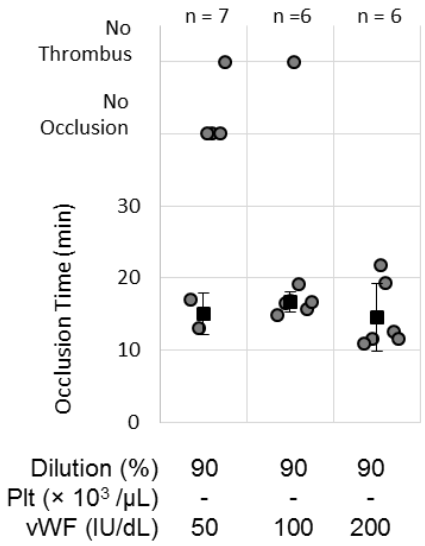

Figure 4-4: Occlusion times in microfluidic test section for 90% dilutions of whole human blood with vWF additions ranging from 50 to 200 IU/dL.

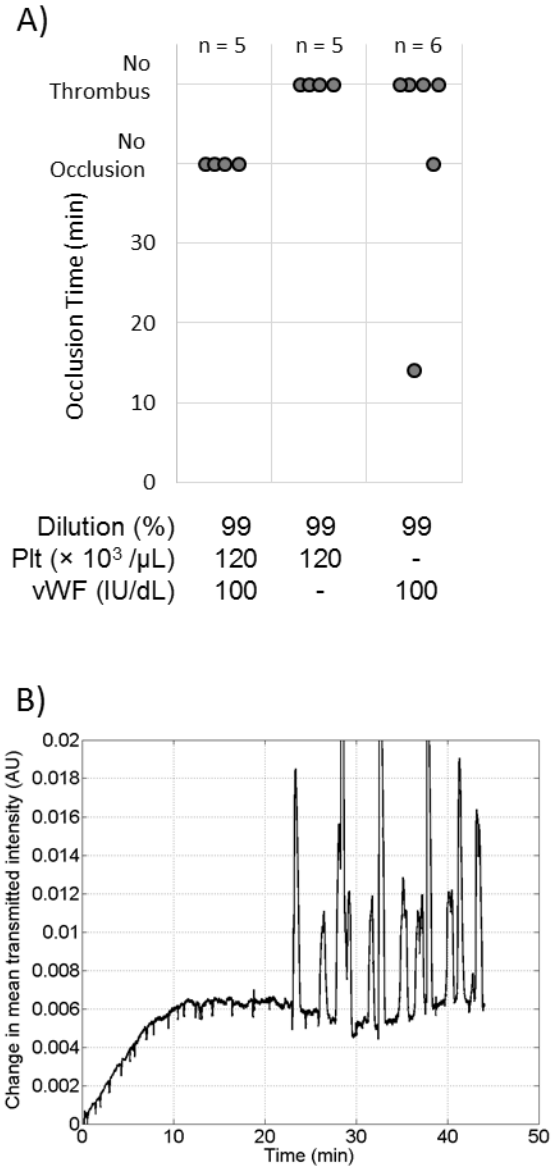

Figure 4-5: A) Occlusion times in microfluidics test sections for 99% dilutions of whole human blood with additions of normal levels of plasma vWF and platelets. "No Occlusion" indicates that test section did not occlude within 5 mL of blood analog but thrombus was visible during test; "No Thrombus" indicates that no thrombus was detected during the experiment; B) 99% dilution with 100 IU/dL vWF and 120 000 platelets/µL forms large thrombus but does not form stable occlusive thrombus. Spikes in transmitted intensity indicate growth and embolization of thrombus. Embolization is sudden within 60 to 180 s.

Blood from VWD patients showed decreased occlusion compared to normal controls (Figure 4-6A). All blood tube-collected control cases led to channel occlusion (n = 15) with a mean occlusion time of 9.5 ± 3.4 min. Normal subjects had a mean platelet count of 275 ± 69 × 10^3 /μL. VWD patients were separated *post hoc* into two groups for analysis. Severe VWD patients has VWF:RCo < 15, and mild VWD patients had 15 < VWF:RCo < 50 (Favaloro et al., 2009). VWD patients had a mean platelet count of 280 ± 109 × 10^3 /μL. Mild VWD blood occluded in 4/6 subjects tested. Severe VWD blood did not occlude in any of the five subjects tested. As a screening test for VWD using a threshold of t_{occ} = 11 minutes, the test platform yields a sensitivity of 1, a specificity of 0.67, a positive predictive value of 0.71, and a negative predictive value of 1. When vWF was added *in vitro* to mild VWD samples, occlusion was restored in the two non-occluding subjects, but the occlusion times for the occluding subjects were not shortened. The addition of vWF to severe VWD subjects restored occlusion in only one subject. Kaplan-Meier analysis shows that mild VWD samples and mild VWD samples treated with *in vitro* vWF have a lower probability of occlusion compared to normal subjects (p < 0.01, Figure 4-6B). The probability of occlusion between the *in vitro* treated and untreated groups was not statistically different (p = 0.815). Restoring plasma vWF in subjects with VWD, that is, in subjects deficient in platelet vWF, does not lead to occlusion. Thus, platelet vWF is important for thrombotic occlusion.

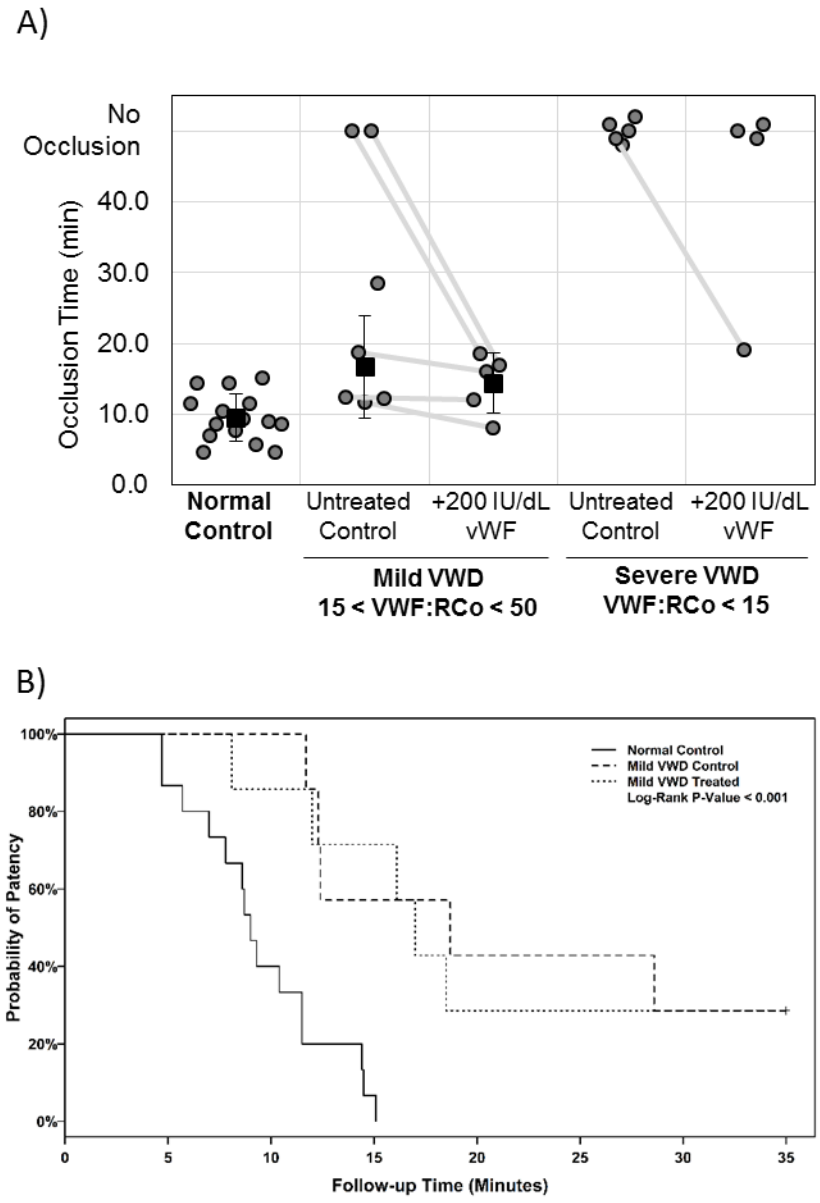

Figure 4-6: Thrombotic occlusion in microfluidic test section for normal subjects and VWD patients with and without in vitro added vWF. A) Occlusion times, B) Kaplan-Meier analysis of occlusion probability.

Lag times and rapid growth times (Figure 4-7) were calculated for all 90% dilutions conditions. Lag time was also calculated for 99% dilution with restored platelets and plasma vWF, and rapid growth time was calculated for that condition as the time from lag

time to the first intensity spike/embolization event. Lag time for 90% dilutions with both platelets and vWF restored were shorter than for dilutions with only platelets or only vWF restored but still significantly longer than for the whole blood control (Figure 4-7A). Restoring only vWF reduced both lag time and growth rate more than restoring only platelets. Rapid growth time and lag time were correlated (R = 0.81). However, restoring vWF and platelets did not change rapid growth time over restoring plasma vWF only (Figure 4-7B). Figure 4-7C combines the lag times and rapid growth times and shows that the portion of total occlusion time quantified by the lag time is greater when only vWF is restored compared to when both platelets and vWF are restored.

Figure 4-8 shows lag times and rapid growth times for VWD experiments for subjects that reached occlusion (tests forming no thrombus cannot be analyzed for lag time and non-occluding tests cannot be analyzed for rapid growth time). VWD samples showed increased lag time and rapid growth time. Restoring plasma vWF does not have a statistically significant effect on either lag time or growth time.

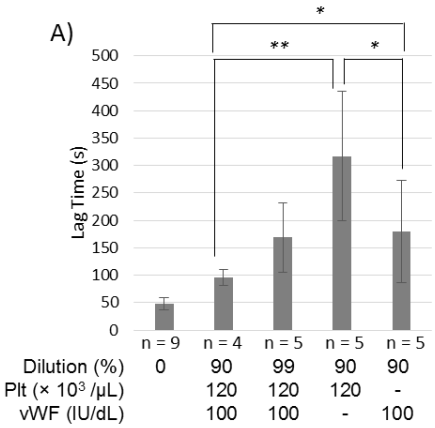

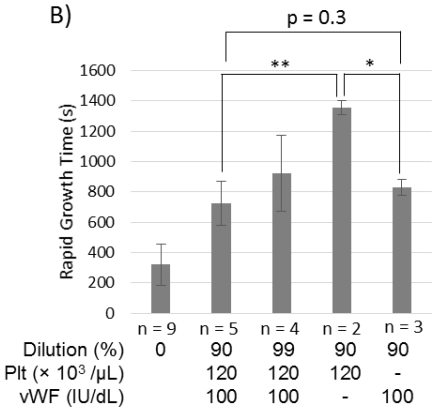

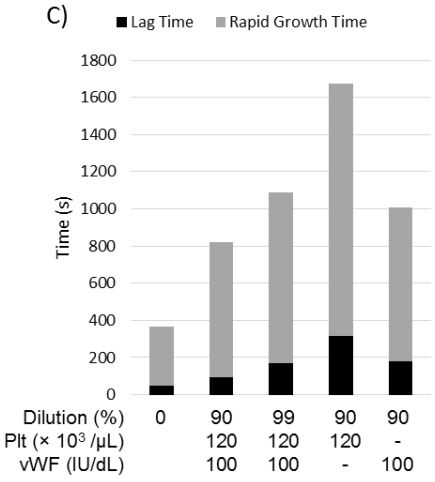

Figure 4-7: A) Lag time and B) rapid growth time for dilutions experiments, C) Combined lag and rapid growth times for occlusion experiments. * indicates $p < 0.l$, ** indicates $p < 0.05$ (Student's t-test). Lag times and rapid growth times were all significantly longer than control ($p < 0.001$).

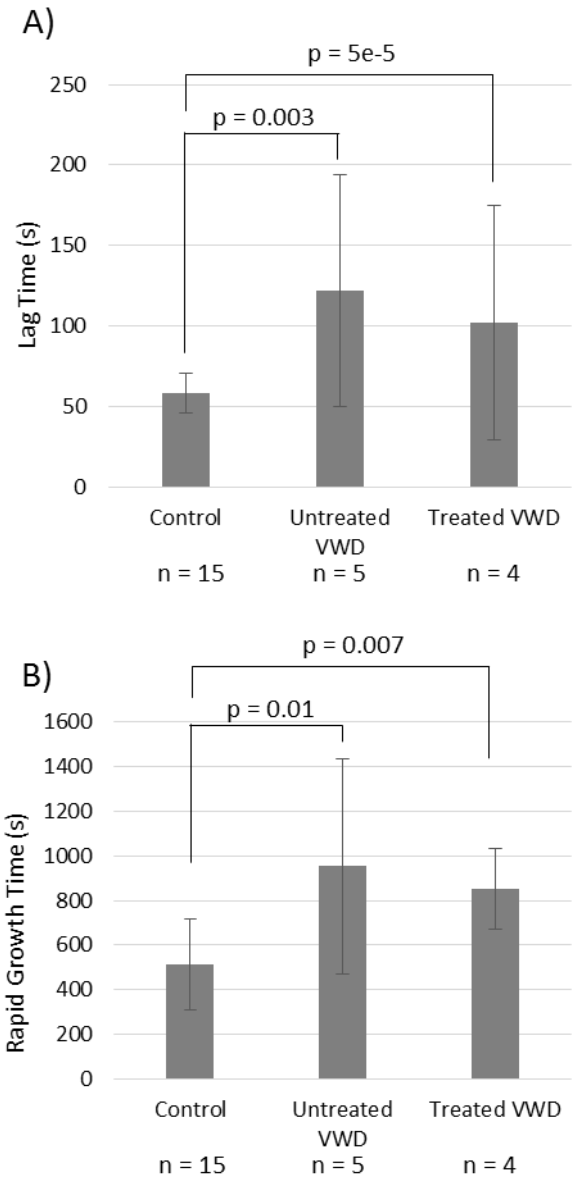

Figure 4-8: A) lag time and B) rapid growth time for VWD experiments

4.4 Discussion

Thrombus formation under high fluid shear rate is mediated by platelets and vWF. In the present study, we utilize dilutions of whole blood to demonstrate that large-scale occlusive

thrombus can form in microchannels with a normal concentration of vWF with very low platelet count. We show that VWF is the primary mediator of high shear thrombosis, and vWF concentration is a better predictor of occlusion than platelet count. We also utilize blood from patients diagnosed with VWD to show that platelet vWF is important for occlusive thrombus formation.

Human blood diluted to 90% with only normal concentrations of vWF added (100 IU/dL) led to thrombotic occlusion in most cases, despite having only 10% normal platelet count. Hence, vWF is capable of supporting high shear thrombosis even with very few platelets. However, 99% dilutions with added vWF did not result in occlusion in most cases, so there is a minimum concentration of platelets necessary for occlusive thrombus formation. In these cases, platelets may serve two roles: 1) as nodes for supporting vWF binding and 2) as carriers that release vWF stores upon activation. The occlusion times for 90% dilutions with added vWF were 2.7 times longer than for controls (6.1 ± 2.2 min versus 16.6 ± 1.4 min). The increase in occlusion time may be due to the time required for sufficient platelets to be transported to the growing thrombus or to a decrease in vWF release by platelets. It should be noted, however, that the increase in occlusion time does not indicate that an equal number of platelets must be incorporated into the growth thrombus as in the whole blood case. For instance, if the same number of platelets were required to form occlusive thrombus, one would expect the occlusion time with 10% of normal platelet count to be 10 times as long as the whole blood control. The decreased platelet requirement may be facilitated by vWF self-assembly (Dayananda, Singh, Mondal, & Neelamegham, 2010) and net formation (Colace & Diamond, 2013), both processes that are enhanced by high shear rates. VWF nets have been proposed as a mechanism for rapid

and efficient platelet capture at high shear rates (Wellings & Ku, 2012) and may facilitate thrombotic occlusion in blood analogs with very low platelet counts. 90% dilutions with only platelets restored occluded the microchannel in 2/5 cases with occlusion times >20 minutes, which closely recapitulates results for VWD samples. However, logistic regression showed vWF concentration after dilution was more predictive of occlusion than platelet count after dilution.

Our results are consistent with Ogawa et al. (2013), which showed that 40% hemodilution decreased thrombus onset and growth and that adding vWF accelerated thrombosis at shear rates of 1100 s^{-1}. However, their hemodilutions also reduced RBC count, which is known to reduce diffusive transport (Zydney & Colton, 1988) and slow thrombus formation (Mehrabadi, 2014). Additionally, the modest hemodilutions of 40% used in the previous study retain high residual concentrations of plasma proteins and platelet count. The present study employs higher shear rates more relevant to arterial thrombosis, fixed hematocrit (40%) to control for changes in shear enhanced diffusivity, and larger dilutions to isolate and analyze the individual contributions of vWF and platelets.

Blood samples from subjects with known VWD were utilized to investigate the contributions of plasma and platelet vWF. VWD samples have both low plasma vWF and low platelet vWF, whereas diluted samples have platelets with normal vWF content. While the *in vitro* addition of vWF restored occlusion in both non-occluding samples with mild VWD (15 < VWF:RCo < 50), vWF addition did not restore occlusion in 3/4 subjects with severe VWD (VWF:RCo < 15). Thus, in subjects with very low plasma and platelet vWF levels, plasma vWF alone is not sufficient in most cases to restore occlusion, and platelet

vWF is important for thrombotic occlusion at high shear rates. Subjects with higher platelet vWF levels may be capable of occlusive thrombus formation once plasma vWF levels were restored because plasma vWF facilitates the initial capture of platelets, allowing for the local release of platelet vWF stores. Though the patients with VWD had no evidence of platelet defects, it is possible that undetected defects may exist. One study showed that platelets from VWD subjects had a lower surface density of collagen receptors (Di Paolo et al., 1999), and other differences from normal platelets may be possible. Collagen receptor density is unlikely to have a strong effect on the results of the present study since platelet binding at high shear rate is modulated by vWF and the majority of thrombus growth here is not surface adhesion but volumetric accumulation. Another study showed that VWD blood perfused over rabbit subendothelium yielded normal platelet adhesion to the surface in some cases but reduced thrombus volume growth in the same cases (Turitto, Weiss, & Baumgartner, 1984). These results support the conclusion of the present study that a moderate concentration of plasma vWF is sufficient for surface-platelet adhesion, but vWF release from platelets is required for large-scale thrombus growth.

Our results support previous modeling that concluded that high vWF local concentration facilitated vWF release from platelets is necessary for platelet capture at high shear rates (Wellings & Ku, 2012). Our results are in agreement with those of Moake, et al. (1988), who used a cone-and-plate model to show that platelet aggregation under high shear stress (up to 60 dynes/cm^2 or a shear rate of approximately 1700 s^{-1}) is mediated by either plasma vWF or vWF released from platelets. Isolated platelets resuspended in buffer showed little aggregation, but vWF added to the suspension induced aggregation under shear. Severe VWD platelets in buffer showed no aggregation. The present study extends

these results to a single-pass system at higher shear rates that better mimics the shear conditions of a stenotic artery. Whereas the previous study investigated only small platelet aggregates, the present studied used large occlusive thrombus formation as the endpoint to better model thrombi responsible for MI and ischemic strokes. The major finding of the present study is that normal vWF can lead to thrombotic occlusion even with small platelet counts, showing the dominance of vWF in high shear thrombosis. This is even more surprising as many would guess that platelet bulk would be critical to creating the mass of the thrombus. Taking the results together, it can be concluded that a threshold of plasma vWF is necessary to initiate thrombosis at high shear rate and sufficient vWF release from platelets may be necessary for large, rapid occlusive thrombosis.

A previous study in mice showed that plasma vWF alone could support hemostasis based on tail bleeding time, and platelet vWF could reduce bleeding time in some vWF-deficient mice (Kanaji, Fahs, Shi, Haberichter, & Montgomery, 2012). Microfluidic experiments in the same study showed that either plasma- or platelet-derived vWF supported platelet adhesion to a collagen surface under shear rates of 2000 s^{-1}. The results of the present study show that while plasma vWF alone may be able to support surface adhesion of platelets in the formation of hemostatic platelet plugs, platelets containing vWF are necessary for large-scale occlusive thrombus at high shear rates. In particular, vWF release from platelets may be necessary to support the rapid thrombus growth that leads to thrombotic occlusion by increasing the local concentration of vWF. Platelet-derived vWF has also be shown to have a higher molecular weight distribution than plasma vWF, which are more hemostatically active (McGrath et al., 2013). The same study showed that vWF

released by platelets is resistant to cleavage by ADAMTS13, which may further contribute to rapid thrombus growth leading to occlusion.

Surprisingly, when all other plasma proteins are diluted to 1% of their normal concentrations and vWF and platelets are restored, stable occlusive thrombus does not form, though large thrombus forms and embolizes. These results suggest that an addition plasma protein(s) is necessary for thrombus stability and occlusion. Maxwell et al. (2007) noted that stable platelet aggregates do not form at shear rates of 1800 s^{-1} on a vWF-only matrix but do form on a vWF-fibrinogen matrix, indicating that fibrinogen may play a stabilizing role in thrombus formation. It is unclear if fibrinogen plays such a role at the higher shear rates employed in the present study. Alternatively, Ni et al. (2003) noted that stable occlusive thrombus in an arteriole injury model (shear rate ~1200 s^{-1}) did not form in most mice deficient in plasma fibronectin, suggesting another potential stabilizing factor. Thrombospondin-1 has also been proposed as an alternative high-shear thrombosis-mediating protein (Bergmeier et al., 2006). Future studies should utilize the present method with selective additions of these candidate proteins to determine the critical stabilizing factor(s).

Lag time and rapid growth time were analyzed for select cases to provide insight into the mechanisms of the three phases of thrombus growth. The correlation of lag time and rapid growth time may indicate that similar mechanisms are at work in each phase, namely plasma vWF adsorption, platelet binding, and vWF release from activated platelets. Results showed that restoring only plasma vWF reduces lag time more than restoring only platelets, which may reflect more rapid adsorption of vWF onto the thrombogenic surface due to higher plasma concentration. Restoring both vWF and platelets further reduces lag

time, which may indicate that lag time involves both plasma vWF adsorption and platelet capture and activation. In contrast, restoring plasma vWF and platelets was shown to have the same effect on rapid growth time as restoring only plasma vWF, indicating that once lag time is reached, rapid thrombus growth proceeds at the same rate with either low platelet count or restored platelet count. This may indicate that the necessary condition for the process to progress past the lag phase and into the rapid growth phase is the adsorption of plasma vWF and the subsequent capture and activation of a sufficient number of platelets. In the case with only plasma vWF restored, it takes longer for the threshold number of platelets to be captured and activated due to the lower platelet count. However, once the captured platelets activate, the feed-forward mechanism of platelet vWF release may sustain rapid thrombus growth. This may reflect a combination of vWF self-assembly and net formation and very efficient capture of platelets by the vWF network. This notion of the requirement of vWF release from platelets for progression past lag time is further supported by the lag time and rapid growth time results for VWD samples in which restoring plasma vWF does not affect lag time or rapid growth time. A reduction in vWF release from VWD platelets may act to both restrain the process to the lag phase and reduce the positive feedback of rapid growth. It is important to note that the most severe VWD samples did not progress out of lag time, even with restored plasma vWF. The transition from lag time to rapid growth time by vWF release from platelets is consistent with the timescales of platelet activation, with platelet integrin activation occurring in seconds (Frojmovic, Wong, & van de Ven, 1991; Shattil, Kashiwagi, & Pampori, 1998; Takagi & Springer, 2002), platelet alpha- and dense-granule release occurring in about 1 minute (Kaplan, Nossel, Drillings, & Lesznik, 1978), and platelet spreading beginning in

2-5 minutes (Kulkarni & Jackson, 2004). Note that lag time for normal subjects is 48 ± 11 s, on the same timescale as granule release.

The results of the present study have clinical implications for the prevention of arterial thrombosis. Presently, anti-platelet agents, primarily aspirin and $P2Y_{12}$ inhibitors (*e.g.* clopidogrel, prasugrel, and ticagrelor) are the treatments-of-choice for long-term therapy for their relatively low cost and oral administration. That thrombus may form with only 10% of normal platelet count may explain some of the documented aspirin and clopidogrel non-response (Gum, Kottke-Marchant, Welsh, White, & Topol, 2003; Mueller et al., 2003). The effectiveness of these therapies in many patients may be in part the result of decreased platelet activation leading to decreased vWF release from platelets. Non-responsiveness may also be due to platelet activation via alternative pathways, such as shear (Hellums, Peterson, Stathopoulos, Moake, & Giorgio, 1987; Ramstack, Zuckerman, & Mockros, 1979) or GPIb binding (Kroll, Harris, Moake, Handin, & Schafer, 1991). Alternative anti-thrombotic agents that target vWF are currently under development (Ulrichts et al., 2011) and may provide an additional or alternative treatment for patients who are non-responsive to anti-platelet drugs. The present results may also have important implications for bleeding in surgery or trauma. In case of severe bleeding with fluid replacement via saline, the blood undergoes hemodilution, which can lead to reduced hemostasis. Our results indicate that replacing only platelets may be insufficient for restoring hemostatic function as plasma vWF may be of greater importance at high shear rates.

The present study has several limitations. Blood was anticoagulated with heparin for transport, which reduces the contribution of fibrin formation in thrombus formation.

Sodium citrate with subsequent re-calcification instead of heparin could be used to retain fibrin formation. For some studies, blood was collected in blood collection tubes, which induce higher shear rates and may prematurely activate platelets. This was controlled for in the present study, but may lead to differences in thrombus growth and occlusion times compared to *in vivo* thrombosis. The present study did not determine the additional critical factors besides vWF and platelets that are necessary for high shear stable thrombus formation. Multiple platelet counts and normal platelets in VWD plasma/blood were not investigated. Calcium ion concentration was not controlled or restored in hemodilutions, which may impair platelet activation. The vWF concentrate (Humate-P®) also contained coagulation Factor VIII. The addition of Factor VIII is not expected to have a large effect on the results since the blood was anticoagulated with heparin.

In conclusion, vWF is more contributory to high shear thrombosis compared to platelets and other plasma proteins. VWF can support occlusive thrombus formation even with low platelet counts, and vWF release from platelets may be important for occlusive thrombosis. However, an additional plasma factor(s) may be necessary for stable thrombus formation. Greater understanding of the contribution of vWF and a third plasma factor to high shear thrombosis may lead to more effective prevention of high shear thrombosis.

4.5 References

Bark, D. L., & Ku, D. N. (2010). Wall shear over high degree stenoses pertinent to atherothrombosis. *Journal of Biomechanics, 43*(15), 2970-2977. doi: 10.1016/j.jbiomech.2010.07.011

Bark, D. L., Para, A. N., & Ku, D. N. (2012). Correlation of thrombosis growth rate to pathological wall shear rate during platelet accumulation. *Biotechnology and Bioengineering, 109*(10), 2642-2650.

Bergmeier, W., Piffath, C. L., Goerge, T., Cifuni, S. M., Ruggeri, Z. M., Ware, J., & Wagner, D. D. (2006). The role of platelet adhesion receptor GPIb far exceeds that of its main ligand, von Willebrand factor, in arterial thrombosis. *Proceedings of the National Academy of Sciences, 103*(45), 16900-16905. doi: 10.1073/pnas.0608207103

Bernardo, A., Bergeron, A. L., Sun, C. W., Guchhait, P., Cruz, M. A., López, J. A., & Dong, J.-F. (2004). Von Willebrand factor present in fibrillar collagen enhances platelet adhesion to collagen and collagen-induced platelet aggregation. *Journal of Thrombosis and Haemostasis, 2*(4), 660-669.

Cazenave, J. P., Ohlmann, P., Cassel, D., Eckly, A., Hechler, B., & Gachet, C. (2004). Preparation of washed platelet suspensions from human and rodent blood. *Methods in Molecular Biology, 272*, 13-28.

Colace, T., & Diamond, S. L. (2013). Direct observation of von Willebrand factor elongation and fiber formation on collagen during acute whole blood exposure to pathological flow. *Arteriosclerosis, Thrombosis, and Vascular Biology, 33*, 105-113. doi: 10.1161/ATVBAHA.112.300522/-/DC1
10.1161/ATVBAHA.112.300522>

Dayananda, K. M., Singh, I., Mondal, N., & Neelamegham, S. (2010). von Willebrand factor self-association on platelet GpIbα under hydrodynamic shear: effect on shear-induced platelet activation. *116*(19), 3990-3998. doi: 10.1182/blood-2010-02-269266

de Witt, S. M., Swieringa, F., Cavill, R., Lamers, M. M. E., van Kruchten, R., Mastenbroek, T., . . . Cosemans, J. M. E. M. (2014). Identification of platelet function defects by multi-parameter assessment of thrombus formation. *Nat Commun, 5*. doi: 10.1038/ncomms5257

Di Paolo, J., FEDERICI, A. B., Mannucci, P. M., Canciani, M. T., Kritzik, M., Kunicki, T. J., & Nugent, D. (1999). Low Platelet alpah-2 beta-1 Levels in Type I von Willebrand Disease Correlate With Impaired Platelet Function in a High Shear Stress System. *Blood, 93*(11), 3578-3582.

Edelstein, A., Amodaj, N., Hoover, K., Vale, R., & Stuurman, N. (2010). *Computer Control of Microscopes Using μManager*: John Wiley & Sons, Inc.

Favaloro, E. J., Thom, J., Patterson, D., Just, S., Dixon, T., Koutts, J., . . . Baker, R. (2009). Desmopressin therapy to assist the functional identification and characterisation of von Willebrand disease: Differential utility from combining two (VWF:CB and VWF:RCo) von Willebrand factor activity assays? *Thrombosis Research, 123*(6), 862-868. doi: http://dx.doi.org/10.1016/j.thromres.2008.10.008

Frojmovic, M., Wong, T., & van de Ven, T. (1991). Dynamic measurements of the platelets membrane glycoprotein IIb-IIIa receptor for fibrinogen by flow cytometry. *Biophysical Journal, 59*, 828-837.

Fukui, H., Nishino, M., Terada, S., Nishikubo, T., Yoshioka, A., Kinoshita, S., . . . Yoshioka, K. (1988). Hemostatic effect of a heat-treated factor VIII concentrate (Haemate P) in von Willebrand's disease. *Blut, 56*(4), 171-178. doi: 10.1007/BF00320748

Gum, P. A., Kottke-Marchant, K., Welsh, P. A., White, J., & Topol, E. J. (2003). A prospective, blinded determination of the natural history of aspirin resistance among stable patients with cardiovascular disease. *Journal of the American College of Cardiology, 41*(6), 961-965. doi: 10.1016/s0735-1097(02)03014-0

Hellums, J. D., Peterson, D. M., Stathopoulos, N. A., Moake, J. L., & Giorgio, T. D. (1987). Studies on the mechanisms of shear-induced platelet activation. In A. Hartmann & W. Kuschinsky (Eds.), *Cerebral Ischemisa and Hemorheology* (pp. 80-89). Berlin: Springer.

Holm, S. (1979). A simple sequentially rejective multiple test procedure. *Scandinavian Journal of Statistics, 6*, 65-70.

Jackson, S. P. (2007). The growing complexity of platelet aggregation. *Blood, 109*(12), 5087-5095. doi: 10.1182/blood-2006-12-027698

Jansson, J., Kilsson, T., & Johnson, O. (1991). von Willebrand factor in plasma: A novel risk factor for recurrent myocardial infarction and death. *British Heart Journal, 66*, 351-355.

Jen, C. J., & McIntire, L. V. (1982). The structural properties and contractile force of a clot. *Cell Motility, 2*, 445-455.

Kanaji, S., Fahs, S. A., Shi, Q., Haberichter, S. L., & Montgomery, R. R. (2012). Contribution of platelet vs. endothelial VWF to platelet adhesion and hemostasis. *J Thromb Haemost, 10*(8), 1646-1652. doi: 10.1111/j.1538-7836.2012.04797.x

Kaplan, K. L., Nossel, H. L., Drillings, M., & Lesznik, G. (1978). Radioimmunoassay of platelet factor 4 and beta-thromboglobulin: Development and application to studies of paltelets release in relation to fibrinopeptide A generation. *British Journal of Haematology, 39*, 129-146.

Kroll, M. H., Harris, T. S., Moake, J. L., Handin, R. I., & Schafer, A. I. (1991). von Willebrand factor binding to platelet GpIb initiates signals for platelet activation. *Journal of Clinical Investigation, 88*(5), 1568-1573.

Kulkarni, S., & Jackson, S. P. (2004). Platelet factor XIII and calpain negatively regulate integrin alphaIIbbeta3 adhesive function and thrombus growth. *Journal of Biological Chemistry, 279*(29), 30697-30706. doi: 10.1074/jbc.M403559200

Lam, W. A., Chaudhuri, O., Crow, A., Webster, K. D., Li, T. D., Kita, A., . . . Fletcher, D. A. (2011). Mechanics and contraction dynamics of single platelets and implications for clot stiffening. *Nat Mater, 10*(1), 61-66. doi: 10.1038/nmat2903

Li, M., Ku, D., & Forest, C. (2012). Microfluidic system for simultaneous optical measurement of platelet aggregation at multiple shear rates in whole blood. *Lab on a Chip, 12*, 1355-1362.

Lilly, L. (Ed.). (2007). *Pathophysiology of Heart Disease* (4th ed.). Philadelphia, PA: Lippincott Williams & Williams.

Maxwell, M. J., Westein, E., Nesbitt, W. S., Giuliano, S., Dopheide, S. M., & Jackson, S. P. (2007). Identification of a 2-stage platelet aggregation process mediating shear-dependent thrombus formation. *Blood, 109*(2), 566-576. doi: 10.1182/blood-2006-07-028282

McGrath, R. T., Biggelaar, M. v. d., Byrne, B., O'Sullivan, J. M., Rawley, O., O'Kennedy, R., . . . O'Donnell, J. S. (2013). Altered glycosylation of platelet-derived von Willebrand factor confers resistance to ADAMTS13 proteolysis. *Blood, 122*(25), 4107-4110. doi: 10.1182/blood-2013-04496851

Mehrabadi, M. (2014). *Effects of Red Blood Cells and Shear Rate on Thrombus Growth.* (PhD), Georgia Institute of Technology, Atlanta, GA.

Moake, J. L., Turner, N. A., Stathopoulos, N. A., Nolasco, L., & Hellums, J. D. (1988). Shear-induced platelet aggregation can be mediated by vWF released from platelets, as well as by exogenous large or unusually large vWF multimers, requires adenosine diphosphate, and is resistant to aspirin. *Blood, 71*, 1366-1374.

Mueller, I., Besta, F., Schulz, C., Massberg, S., Schoenig, A., & Gawaz, M. (2003). Prevalence of clopidogrel non-responders among patietns with stable angina pectoris schedule for eelctive coronary stent placement. *Thrombosis and Haemostasis, 89*, 783-787.

Ni, H., Yuen, P. S. T., Papalia, J. M., Trevithick, J. E., Sakai, T., Fässler, R., . . . Wagner, D. D. (2003). Plasma fibronectin promotes thrombus growth and stability in injured arterioles. *Proceedings of the National Academy of Sciences, 100*(5), 2415-2419. doi: 10.1073/pnas.2628067100

Ogawa, S., Ohnishi, T., Hosokawa, K., Szlam, F., Chen, E. P., & Tanaka, K. A. (2013). Haemodilution-induced changes in coagulation and effects of haemostatic components under flow conditions. *British Journal of Anaesthesia, 111*(6), 1013-1023. doi: 10.1093/bja/aet229

Pan, W. (2001). Akaike's Information Criterion in generalized estimating equations. *Biometrics, 57*(1), 120-125.

Ramstack, J., Zuckerman, L., & Mockros, L. (1979). Shear-induced activation of platelets. *Journal of Biomechanics, 12*, 113-125.

Sadler, J. E., Mannucci, P., Berntorp, E., Bochkov, N., Boulyjenkov, V., Ginsburg, D., . . . Srivastrava, A. (2000). Impact, Diagnosis and Treatment of von Willebrand Disease. *Thrombosis and Haemostasis, 84*, 160-174.

Sadler, J. E. (2003). Von Willebrand disease type 1: a diagnosis in search of a disease. *Blood, 101*(6), 2089-2093. doi: 10.1182/blood-2002-09-2892

Shattil, S. J., Kashiwagi, H., & Pampori, N. (1998). Integrin signaling: The platelet paradigm. *Blood, 91*(8), 2645-2657.

Soejima, K., Nakamura, H., Hirashima, M., Morikawa, W., Nozaki, C., & Nakagaki, T. (2006). Analysis on the Molecular Species and Concentration of Circulating ADAMTS13 in Blood. *Journal of Biochemistry, 139*(1), 147-154. doi: 10.1093/jb/mvj013

Springer, T. A. (2011). Biology and physics of von Willebrand factor concatamers. *J Thromb Haemost, 9 Suppl 1*, 130-143. doi: 10.1111/j.1538-7836.2011.04320.x

Takagi, J., & Springer, T. A. (2002). Integrin activation and structural rearrangement. *Immunological Reviews, 186*, 141-163.

Thompson, S. G., Kienast, J., Pyke, S. D. M., Haverkate, F., & van de Loo, J. C. W. (1995). Hemostatic Factors and the Risk of Myocardial Infarction or Sudden Death in Patients with Angina Pectoris. *New England Journal of Medicine, 332*(10), 635-641. doi: doi:10.1056/NEJM199503093321003

Turitto, V. T., Weiss, H. J., & Baumgartner, H. R. (1984). Platelet interaction with rabbit subendothelium in von Willebrand's disease: Altered thrombus formation distince of defective platelet adhesion. *Journal of Clinical Investigation, 74*, 1730-1741.

Ulrichts, H., Silence, K., Schoolmeester, A., Jaegere, P. d., Rossenu, S., Roodt, J., . . . Holz, J.-B. (2011). Antithrombotic drug candidate ALX-0081 shows superior preclinical efficacy and safety compared with currently marketed antiplatelet drugs. *Blood, 118*, 757-765. doi: 10.1182/blood-2010-11-317859

Wellings, P. J., & Ku, D. N. (2012). Mechanisms of platelet capture under very high shear. *Cardiovascular Engineering and Technology, 3*(2), 161-170. doi: 10.1007/s13239-012-0086-6

Wieberdink, R., van Schie, M., Koudstaal, P., Hofman, A., Witteman, J., De Maat, M., . . . Breteler, M. (2010). High von Willebrand factor levels increase the risk of stroke: the rotterdam study. *Stroke, 41*, 2151-2156. doi: 10.1161/STROKEAHA.110.586289

Zydney, A., & Colton, C. (1988). Augmented solute transport in the shear flow of a concentrated suspension. *Physiochemical Hydrodynamics, 10*(1), 77-96.

CHAPTER 5: CONCLUSIONS AND FUTURE WORK

This dissertation investigated the contribution of vWF and platelets to high shear thrombosis relevant to MI and stroke. To accomplish this, a high shear thrombosis assay was developed to meet low blood volume requirements and fluid shear conditions while allowing for the formation of large-scale occlusive thrombus. Microfluidic conditions were selected to mimic the shear environment of a stenotic coronary vessel to address the long-term objective of a clinical assay. Unlike currently available assays, the present test provides for a well-defined shear rate across the full test section and real-time thrombus and embolization monitoring in a clinically reasonable blood volume without the addition of soluble platelet agonists.

As part of the design of the microfluidic assay, the effect of flow pulsatility on high shear thrombus formation was investigated (CHAPTER 2). It was found that thrombus formation characteristics (occlusion time, lag time, and growth rate) under pulsatile flow were not statistically different from steady flow under the same mean wall shear rate. When the steady wall shear rate was matched to the peak shear rate under pulsatile flow, the lag time was significantly shorter than under either mean shear steady flow conditions or pulsatile flow conditions. The present results extend the work of van Breugel (1988) to higher shear rates relevant to arterial stenosis and indicated that mean wall shear rate is among the most important fluid dynamic parameters influencing thrombus growth. These results provided evidence to proceed with the design of a microfluidic thrombosis assay that utilized steady flow conditions with confidence that the results have applicability to arterial flow conditions.

Design requirements for a relevant microfluidic assay were specified, including low blood volume (<10 mL), wall shear rate that varied from 500-1000 s^{-1} in the non-stenotic region to 3500-6000 s^{-1} in the stenotic region, and many more (10x) platelet-to-platelet binding events than platelet-to-surface binding events (CHAPTER 3). The first requirement was necessitated both by the need to assess many experimental conditions in the subsequent study of vWF and platelet contributions to high shear thrombosis and by the long-term goal of developing a point-of-care assay for assessing thrombosis risk and treatment. Wall shear ranges and profiles and occlusive thrombus size were selected to mimic the fluid environment and thrombus growth of a diseased coronary artery. The minimum channel height (50 μm) and diameter (50 μm) were determined using a geometric analysis of platelet accumulation (Casa & Ku, 2014), providing a lower bound for microfluidic channel size for the study of volumetric thrombosis. Analytical solutions for flow in a rectangular channel were used to determine the minimum channel width and corresponding flow rate to ensure that 90% of the channel width had a wall shear rate in the range of 3500-6000 s^{-1}. An aspect ratio of ~5.5-6.5 satisfies this requirement. To check the reasonableness of assay test times and blood volumes, the time to occlusion was also estimated using a simple model of thrombosis (Bark, Para, & Ku, 2012), predicting test times of 8.4 min and blood volumes of 0.9 mL, both in good agreement with experimental observations. The designed microchannels were then fabricated using micromachining techniques to produce a mold used for pouring PDMS. An image processing algorithm was also developed using confocal microscopy to correlate transmitted light to thrombus volume, allowing for the estimation of thrombus deposition and growth rate. Finally, thrombus formation was characterized in the test section for 15 normal subjects with 3 tests

each. Occlusion time of the test section has a within-subject variability of 28%, which may be improved by accounting for variations in channel dimensions. Future work may also aim to integrate the design test section into an automated point-of-care test for assessing patient response to therapy and predicting thrombosis risk. It was also shown that blood collection via blood collection tube (10 mL Vacutainer®) increased occlusion time compared to blood collected in a 60 mL syringe, highlighting the importance of standardized blood collection procedures for any platelet function/high shear thrombosis assay.

The present microfluidic assay improves on previous assays by incorporating a stenotic test section with controlled shear rates across the length of the test section and pathological shear rates in a small blood volume (<5 mL per test). Unlike most previous microfluidic thrombosis assays (Gutierrez et al., 2008; Hosokawa et al., 2011; Maloney, Brass, & Diamond, 2010; Neeves et al., 2008; Sakariassen, Aarts, & de Groot, 1983; Sixma, de Groot, van Zanten, & Ijsseldijk, 1998; Usami, Chen, Zhao, Chien, & Skalak, 1993), the present device employs a stenotic test section that provides for controlled shear rates throughout the test section and mimics the shear history of platelets passing from a healthy artery to a diseased portion. Test sections without a stenosis subject platelets to high shear rate across the length of the test section, which may induce platelet activation before the stenosis, in opposition to the pathological case. Compared to previous stenotic microfluidic test section (Li, Ku, & Forest, 2012; Sakariassen et al., 1990), the present design considerably reduces both the width and height of the test section, allowing for high wall shear rates to be achieved with smaller blood volumes. The reduction in dimensions was carefully considered to reduce edge effects across the width of the channel and to

ensure that the channel was of sufficient size to allow for volumetric thrombus growth rather than primarily platelet adhesion to a surface. The present device was designed to operate at higher shear rates (>3500 s^{-1}) than most previous test sections, which have been typically used to investigate shear rates <1500 s^{-1}.

The designed test section was implemented to study the relative contributions of vWF and platelets in high shear thrombosis (CHAPTER 4). Most notably, it was found that blood analogs with normal hematocrit and normal vWF concentration but only 10% of native platelet count were capable of forming thrombus under pathological shear rates. However, the rate of thrombus formation was much slower than that of whole blood. This finding indicates that vWF dominates high shear thrombosis. Previous results have demonstrated that vWF self-associates (Dayananda, Singh, Mondal, & Neelamegham, 2010) and forms tangled nets (Colace & Diamond, 2013) at elevated shear rates. The results here are suggestive that this self-associating and self-adhesion may be capable of forming occlusive thrombi.

Blood samples from VWD patients with plasma vWF restored to normal levels were used to assess thrombus formation in blood with normal plasma vWF levels but no vWF release from platelets. In this manner, it was found that plasma vWF alone was not sufficient to support rapid occlusive thrombus formation, and vWF release from platelet is likely required to achieve very rapid thrombus growth. Previously, it was unclear what distinct roles were played by plasma and platelet vWF (Jackson, 2007). Though vWF release by platelets was hypothesized as critical for platelet capture under high shear (Wellings & Ku, 2012), the present investigation provides experimental evidence for the importance of vWF release from platelets in rapid, occlusive thrombosis. It was also

demonstrated that the developed assay was capable of detecting VWD. Regression analysis showed that vWF concentration and platelet count are predictive of thrombotic occlusion, with vWF as the stronger predictor. Finally, blood analogs with plasma proteins reduced to 1% of their normal concentrations resulted in large scale thrombus growth that was unstable and never fully occluded the vessel, indicating that another plasma protein, possibly fibrinogen (Maxwell et al., 2007; Savage, Almus-Jacobs, & Ruggeri, 1998) or fibronectin (Ni et al., 2003), is required at least at 10% normal concentration for stable thrombus formation. Future studies should be conducted to conclusively identify this stabilizing plasma protein and its required concentration for occlusive thrombus formation.

The findings on the relative roles of platelets, plasma vWF, and platelet vWF have important implications in anti-thrombotic treatment. First, it is clear that thrombus can form even with very small platelet contribution, which may explain why some patients are non-responsive to anti-platelet agents (Gum, Kottke-Marchant, Welsh, White, & Topol, 2003; Mueller et al., 2003) and still suffer arterial thrombosis even when treated with anti-platelet agents. The success of existing anti-platelet agents, which inhibit various pathways of platelet activation, may be in part due to their inhibition of vWF release by platelets, reducing the high shear positive-feedback loop. Potential pharmacological agents are currently under development that target vWF rather than platelets for the prevention of thrombosis (Ulrichts et al., 2011) and may prove effective additional or alternative treatments for patients who are non-responsive to existing anti-platelet therapies.

The phenomenon of high shear occlusive thrombosis studied here is distinct from mechanisms of platelet activation and aggregation and lower shear thrombus formation investigated elsewhere. Many previous studies have limited investigation to shear rates

<1500 s^{-1} (Colace, Muthard, & Diamond, 2012; Flamm et al., 2012; Maloney et al., 2010; Neeves et al., 2008; Neeves, Illing, & Diamond, 2010; Okorie, Denney, Chatterjee, Neeves, & Diamond, 2008), whereas shear rates in arterial stenoses exceed 5000 s^{-1} and extend to >100 000 s^{-1} (Bark & Ku, 2010). The dominance of different thrombotic mechanisms at elevated shear rates (Jackson, 2007) requires separate study. Other studies have focused primarily on the early thrombotic events related to individual or small numbers of platelets: platelet adhesion to a surface and platelet activation and effects of shear on platelets (Al-Tamimi et al., 2012; Cranmer et al., 2011; Lee, Sturgeon, Jackson, & Hamilton, 2011; Maxwell, Dopheide, Turner, & Jackson, 2006; Maxwell et al., 2007; Nesbitt, Harper, Schoenwaelder, Yuan, & Jackson, 2012; Schoenwaelder et al., 2011; Schoenwaelder & Jackson, 2012; White et al., 2012), and platelet binding to vWF (Chen et al., 2013; Ruggeri, Orje, Haberman, Federici, & Reininger, 2006). The present study chose to focus on the accumulation of millions or billions of platelets under pathological shear in order to investigate thrombosis relevant to occlusive arterial thrombosis that leads to MI. Studies of individual or small aggregates of platelets confine their analysis to Phase I (lag time) of thrombus formation and often do not investigate Phase II (rapid platelet accumulation).

This dissertation also highlights some key considerations in thrombosis assay development. First, appropriate fluid dynamics should be selected to study the phenomenon of interest (e.g. deep vein thrombosis, arterial thrombosis, etc.). These include shear rates, edge effects, shear history, and flow pulsatility. In the present study, shear rates were selected for relevance to thrombosis at the site of atherosclerotic disease, where very high shear rates exist over a short extent. The shear range selected represented the “worst case” for thrombotic occlusion, i.e., the shear range which had been previously shown to yield

the most rapid thrombus growth (Bark et al., 2012). Second, geometric effects should be accounted for. In the quest for ever-smaller lab-on-a-chip assays, there exists a minimum dimension below which only platelet adhesion to a surface and not platelet accumulation will be observed. Selecting relevant dimensions is key to isolating the phenomenon of interest (platelet adhesion versus aggregation).

Though not extensively investigated here, the surface thrombogenic properties should also be considered in flow assays for thrombosis. Here, collagen Type I was selected to mimic extracellular matrix exposed by atherosclerotic plaque rupture. However, many other surface coatings (vWF, fibrinogen, fibronectin, other collagen types, etc.) have been investigated to identify the contributions and synergistic effects of other platelet binding surfaces. De Witt et al. (2014) showed that collagen Type I is among the most potent platelet-adhesive surfaces under flow, with other biological substrates initiating relatively large aggregates of activated platelets. Other potent surfaces included combination coatings (*e.g.* fibrinogen + vWF) that engaged multiple platelet receptors (*e.g.* GPIb and GPVI). Other surfaces that interacted with single receptors produced smaller aggregates of less activated platelets. Thus, the present study's use of collagen Type I again signifies the "worst case" scenario for arterial thrombosis, as well as a likely thrombotic substrate given its presence in arterial walls. The use of an alternative substrate would be expected to reduce early thrombus formation and thus increase the lag time. Beyond the use of native thrombogenic surface, future studies should investigate the potential of artificial surface to induce thrombosis under flow. Implantable cardiovascular devices, including artificial heart valves, vascular grafts, and ventricular assist devices, have serious thrombotic risks. Investigating thrombus formation under flow on the materials used in these devices, such

as PTFE (Teflon®), PET (Dacron®), pyrolytic carbon, nitinol, and stainless steel, may help to identify the most appropriate materials for a design application, reduce thrombotic potential by alleviating adverse fluid mechanics, and lead to new material development and passivation to prevent thrombosis. The surface characteristics of various materials are most likely to affect the lag time (Phase I) of thrombus formation, since once a surface is covered in platelets, the positive feedback mechanisms of platelet activation will drive the process in to rapid thrombus growth (Phase II) and thrombotic occlusion (Phase III).

In the search for more effective pharmaceuticals for the prevention of MI and ischemic stroke, flow assays may prove useful for drug candidate screening under shear conditions relevant to the conditions they are intended to prevent. In the clinic, a flow assay for thrombosis may be useful to assessing potential drug therapies for a specific patient and determining the effectiveness of and titrating current treatment. This type of testing may help identify patients that are not responsive to aspirin or clopidogrel and better treat them before they suffer an ischemic event. Finally, it is virtually impossible to predict which individuals will suffer a MI or ischemic stroke using current clinical techniques. A flow assay for thrombosis may provide additional predictive capabilities by assessing a specific patient's blood clotting potential. With appropriate identification, higher risk patients may be treated and monitored more aggressively than lower risk patients. Ultimately, improvements in anti-thrombotic drugs and their use and in patient-specific risk assessment for arterial thrombosis will reduce treatment costs and improve patient care.

5.1 References

Al-Tamimi, M., Tan, C. W., Qiao, J., Pennings, G. J., Javadzadegan, A., Yong, A. S. C., . . . Gardiner, E. E. (2012). Pathologic shear triggers shedding of vascular receptors: a novel mechanism for down-regulation of platelet glycoprotein VI in stenosed coronary vessels *Blood, 119*, 4311-4320. doi: 10.1182/blood-2011-10-386607
10.1182/blood-201110-386607

Bark, D. L., & Ku, D. N. (2010). Wall shear over high degree stenoses pertinent to atherothrombosis. *Journal of Biomechanics, 43*(15), 2970-2977. doi: 10.1016/j.jbiomech.2010.07.011

Bark, D. L., Para, A. N., & Ku, D. N. (2012). Correlation of thrombosis growth rate to pathological wall shear rate during platelet accumulation. *Biotechnology and Bioengineering, 109*(10), 2642-2650.

Casa, L. D. C., & Ku, D. N. (2014). Geometric design of microfluidic chambers: Platelet adhesion versus accumulation. *Biomed Microdevices, 16*(1), 115-126.

Chen, H., Fallah, M. A., Huck, V., Angerer, J. I., Reininger, A. J., Schneider, S. W., . . . Alexander-Katz, A. (2013). Blood-clotting-inspired reversible polymer–colloid composite assembly in flow. *Nat Commun, 4*, 1333. doi: http://www.nature.com/ncomms/journal/v4/n1/suppinfo/ncomms2326-m2_S1.html

Colace, T., Muthard, R., & Diamond, S. L. (2012). Thrombus growth and embolism on tissue factor-bearing collagen surfaces under flow: Role of thrombin with and without fibrin. *Arteriosclerosis, Thrombosis, and Vascular Biology, 32*, 1466-1476. doi: 10.1161/ATVBAHA.112.249789/-/DC1

Colace, T., & Diamond, S. L. (2013). Direct observation of von Willebrand factor elongation and fiber formation on collagen during acute whole blood exposure to pathological flow. *Arteriosclerosis, Thrombosis, and Vascular Biology, 33*, 105-113. doi: 10.1161/ATVBAHA.112.300522/-/DC1
10.1161/ATVBAHA.112.300522>

Cranmer, L., Ashworth, K., Yao, Y., Berndt, M. C., Ruggeri, Z. M., Andrews, R. K., & Jackson, S. P. (2011). High shear-dependent loss of membrane integrity and defective platelet adhesion following disruption of GPIb a-filamin interaction. *Blood, 117*, 2718-2727. doi: 10.1182/blood-2010-07-296194
10.1182/blood2010-07-296194

Dayananda, K. M., Singh, I., Mondal, N., & Neelamegham, S. (2010). von Willebrand factor self-association on platelet GpIbα under hydrodynamic shear: effect on shear-induced platelet activation. *116*(19), 3990-3998. doi: 10.1182/blood-2010-02-269266

de Witt, S. M., Swieringa, F., Cavill, R., Lamers, M. M. E., van Kruchten, R., Mastenbroek, T., . . . Cosemans, J. M. E. M. (2014). Identification of platelet function defects by multi-parameter assessment of thrombus formation. *Nat Commun, 5*. doi: 10.1038/ncomms5257

Flamm, M. H., Colace, T. V., Chatterjee, M. S., Jing, H., Zhou, S., Jaeger, D., . . . Diamond, S. L. (2012). Multiscale prediction of patient-specific platelet function under flow. *Blood, 120*(1), 190-198. doi: 10.1182/blood-2011-10-388140

Gum, P. A., Kottke-Marchant, K., Welsh, P. A., White, J., & Topol, E. J. (2003). A prospective, blinded determination of the natural history of aspirin resistance among stable patients with cardiovascular disease. *Journal of the American College of Cardiology, 41*(6), 961-965. doi: 10.1016/s0735-1097(02)03014-0

Gutierrez, E., Petrich, B. G., Shattil, S. J., Ginsberg, M. H., Groisman, A., & Kasirer-Friede, A. (2008). Microfluidic devices for studies of shear-dependent platelet adhesion. *Lab on a Chip, 8*(9), 1486-1495. doi: 10.1039/b804795b

Hosokawa, K., Ohnishi, T., Kondo, T., Fukasawa, M., Koide, T., Maruyama, I., & Tanaka, K. A. (2011). A novel automated microchip flow-chamber system to quantitatively evaluate thrombus formation and antithrombotic agents under blood flow conditions. *J Thromb Haemost, 9*(10), 2029-2037. doi: 10.1111/j.1538-7836.2011.04464.x

Jackson, S. P. (2007). The growing complexity of platelet aggregation. *Blood, 109*(12), 5087-5095. doi: 10.1182/blood-2006-12-027698

Lee, H., Sturgeon, S. A., Jackson, S. P., & Hamilton, J. R. (2011). The contribution of thrombin-induced platelet activation to thrombus growth is diminished under pathological blood shear conditions. *Thrombosis and Haemostasis, 107*(2), 328-337. doi: 10.1160/th11-06-0418

Li, M., Ku, D., & Forest, C. (2012). Microfluidic system for simultaneous optical measurement of platelet aggregation at multiple shear rates in whole blood. *Lab on a Chip, 12*, 1355-1362.

Maloney, S. F., Brass, L., & Diamond, S. L. (2010). P2Y12 or P2Y1 inhibitors reduce platelet deposition in a microfluidic model of thrombosis while apyrase lacks efficacy under flow conditions. *Integrative Biology, 2*(4), 153-220. doi: 10.1039/b919728a
10.1039/B919728A

Maxwell, M. J., Dopheide, S. M., Turner, S. J., & Jackson, S. P. (2006). Shear induces a unique series of morphological changes in translocating platelets: Effects of morphology on translocation dynamics. *Arteriosclerosis, Thrombosis, and Vascular Biology, 26*(3), 663-669. doi: 10.1161/01.ATV.0000201931.16535.e1

Maxwell, M. J., Westein, E., Nesbitt, W. S., Giuliano, S., Dopheide, S. M., & Jackson, S. P. (2007). Identification of a 2-stage platelet aggregation process mediating shear-dependent thrombus formation. *Blood, 109*(2), 566-576. doi: 10.1182/blood-2006-07-028282

Mueller, I., Besta, F., Schulz, C., Massberg, S., Schoenig, A., & Gawaz, M. (2003). Prevalence of clopidogrel non-responders among patietns with stable angina pectoris schedule for eelctive coronary stent placement. *Thrombosis and Haemostasis, 89*, 783-787.

Neeves, K. B., Maloney, S. F., Fong, K. P., Schmaier, A. A., Kahn, M. L., Brass, L. F., & Diamond, S. L. (2008). Microfluidic focal thrombosis model for measuring murine platelet deposition and stability: PAR4 signaling enhances shear-resistance of platelet aggregates. *Journal of Thrombosis and Haemostasis, 6*, 2193-2201. doi: 10.1111/j.1538-7836.2008.03188.x

Neeves, K. B., Illing, D. A. R., & Diamond, S. L. (2010). Thrombin Flux and Wall Shear Rate Regulate Fibrin Fiber Deposition State during Polymerization under Flow. *Biophysical Journal, 98*(7), 1344-1352. doi: 10.1016/j.bpj.2009.12.4275

Nesbitt, W. S., Harper, I. S., Schoenwaelder, S. M., Yuan, Y., & Jackson, S. P. (2012). A Live Cell Micro-imaging Technique to Examine Platelet Calcium Signaling Dynamics Under Blood Flow. *788*, 73-89. doi: 10.1007/978-1-61779-307-3_6

Ni, H., Yuen, P. S. T., Papalia, J. M., Trevithick, J. E., Sakai, T., Fässler, R., . . . Wagner, D. D. (2003). Plasma fibronectin promotes thrombus growth and stability in injured arterioles. *Proceedings of the National Academy of Sciences, 100*(5), 2415-2419. doi: 10.1073/pnas.2628067100

Okorie, U. M., Denney, W. S., Chatterjee, M. S., Neeves, K. B., & Diamond, S. L. (2008). Determination of surface tissue factor thresholds that trigger coagulation at venous and arterial shear rates: amplification of 100 fM circulating tissue factor requires flow. *Blood, 111*(7), 3507-3513. doi: 10.1182/blood-2007-08-106229

Ruggeri, Z. M., Orje, J., Haberman, R., Federici, A., & Reininger, A. J. (2006). Activation-independent platelet adhesion and aggregation under elevated shear stress. *Blood, 108*(6), 1903-1910. doi: 10.1182/blood-2006-04-011551

Sakariassen, K. S., Aarts, P., & de Groot, P. G. (1983). A perfusion chamber developed to investigate platelet interaction in flowing blood with human vessel wall cells, their extracellular matrix, and purified components. *Journal of Laboratory and Clinical Medicine, 102*(4), 522-535.

Sakariassen, K. S., Joss, R., Muggli, R., Kuhn, H., Tschopp, T. B., Sage, H., & Baumgartner, H. R. (1990). Collagen type III induced ex vivo thrombogenesis in humans. Role of platelets and leukocytes in deposition of fibrin. *Arteriosclerosis, Thrombosis, and Vascular Biology, 10*(2), 276-284. doi: 10.1161/01.atv.10.2.276

Savage, B., Almus-Jacobs, F., & Ruggeri, Z. M. (1998). Specific synergy of multiple substrate–receptor interactions in platelet thrombus formation under flow. *Cell, 94*, 657-666.

Schoenwaelder, S. M., Jarman, K. E., Gardiner, E. E., Hua, M., Qiao, J., White, M. J., . . . Jackson, S. P. (2011). Bcl-xL-inhibitory BH3 mimetics can induce a transient thrombocytopathy that undermines the hemostatic function of platelets. *Blood, 118*(6), 1663-1674. doi: 10.1182/blood-2011-04-347849

Schoenwaelder, S. M., & Jackson, S. P. (2012). Bcl-xL-inhibitory BH3 mimetics (ABT-737 or ABT-263) and the modulation of cytosolic calcium flux and platelet function. *Blood, 119*(5), 1320-1321. doi: 10.1182/blood-2011-10-387399

Sixma, J., de Groot, P. G., van Zanten, H., & Ijsseldijk, M. (1998). A new perfusion chamber to detect platelet adhesion using a small volume of blood. *Thrombosis Research, 92*, S43-S46.

Ulrichts, H., Silence, K., Schoolmeester, A., Jaegere, P. d., Rossenu, S., Roodt, J., . . . Holz, J.-B. (2011). Antithrombotic drug candidate ALX-0081 shows superior preclinical efficacy and safety compared with currently marketed antiplatelet drugs. *Blood, 118*, 757-765. doi: 10.1182/blood-2010-11-317859

Usami, S., Chen, H.-H., Zhao, Y., Chien, S., & Skalak, R. (1993). Design and construction of a linear shear stress flow chamber. *Annals of Biomedical Engineering, 21*, 77-83.

van Breugel, H. H., Sixma, J. J., & Heethaar, R. M. (1988). Effects of flow pulsatility on platelet adhesion to subendothelium. *Arteriosclerosis, Thrombosis, and Vascular Biology, 8*(3), 332-335. doi: 10.1161/01.atv.8.3.332

Wellings, P. J., & Ku, D. N. (2012). Mechanisms of platelet capture under very high shear. *Cardiovascular Engineering and Technology, 3*(2), 161-170. doi: 10.1007/s13239-012-0086-6

White, M. J., Schoenwaelder, S. M., Josefsson, E. C., Jarman, K. E., Henley, K. J., James, C., . . . Kile, B. T. (2012). Caspase-9 mediates the apoptotic death of megakaryocytes and platelets, but is dispensable for their generation and function. *Blood, 119*(18), 4283-4290. doi: 10.1182/blood-2011-11-394858

APPENDIX A: MATLAB IMAGE PROCESSING CODE FOR STENOTIC CAPILLARIES

```
function
[]=imageSubtraction_main(ref,first,last,step,con,ROIwidth,thresh
Percent,folder,outputFile)

%imageSubtraction_main.m is the calling function for automated thrombus
%detection. The inputs are:
%   ref         reference image number (integer)
%   first       first image to be processed (integer, ref + 1)
%   last        last image (occlusion) to be processed (integer)
%   step        step btwn images (integer)
%   con         conversion factor in px/mm (number)
%   ROIwidth    width in mm of ROI (number, current working value: 3 mm)
%   threshPercent   percentage of max intensity difference to identify as
%                       thrombus (number <1, current working value: 0.2)
%   folder          root folder with images (string)
%   outputFile      name for .mat save file (string)

%get time data from metadata file
id=fopen(sprintf('%s\\metadata.txt',folder));
display('Reading metadata...')
string=fscanf(id,'%s');
metadata = parse_json(string);      %parse_json is available from The
                                     Mathworkds      File      Exchange
                                     http://www.mathworks.com/
                                     matlabcentral/fileexchange/
                                     23393--another--json-parser
fclose(id);

%Read reference image
I=readColorImage(ref,folder);

%User provide inital crop
[I1,rect]=imcrop(I);
close all

%Find capillary edges
[upperEdge lowerEdge]=findEdge(I1);

%Recrop to same height but with width centered at throat and extending
half %of ROI width left and right
[~,center]=min(lowerEdge(:,2)-upperEdge(:,2));
rect2=zeros(1,4);
rect2(2)=rect(2);
rect2(4)=rect(4);
rect2(3)=ROIwidth*con;
rect2(1)=rect(1)+center-ROIwidth/2*con;
I1=imcrop(I,rect2);
clear I rect
```

```
%Re-find upper and lower edges in new crop
[upperEdge lowerEdge]=findEdge(I1);
Isave=cell(1,last-first+2);
Isave{1}=I1;

%convert image to 8-bit
int1=uint8(sum(I1,3)/((2^8-1)*3)*(2^8-1));

%read occluded image and subtract to find threshold
I2=readColorImage(last,folder);
I2=imcrop(I2,rect2);


%brightness correction
int2=brightnessCorrection(I2,I1);

%Image subtraction
Ithresh=int2-int1;
threshold=threshPercent*max(max(Ithresh));  %detect  thrombus  if  pixel
value is
                                            at least XX% of max
clear Ithresh

%Pre-allocate arrays
I3=cell(numel(first:step:last),1);
thromb=cell(numel(first:step:last),1);
thrombEdgeLower=cell(numel(first:step:last),1);
thrombEdgeUpper=cell(numel(first:step:last),1);
A=zeros(size(thromb));
V=zeros(size(thromb));
time=zeros(size(thromb));

%Loop through image subtraction for all images
A(1)=0;
a=1;
b=2;
for i=first:step:last
    display(sprintf('Processing image %u',i))
    I2=readColorImage(i,folder);
    I2=imcrop(I2,rect2);
    Isave{b}=I2;

    int2=brightnessCorrection(I2,I1);

    %image subraction and thresholding
    I3{a,1}=int2-int1;
    thromb{a,1}=I3{a,1}>threshold;

    %Calculate thrombus area in plane
    A(a)=sum(sum(thromb{a,1}));

    %Find thrombus edges

[thrombEdgeLower{a},thrombEdgeUpper{a}]=findThrombusEdge(thromb{a},uppe
rEdge,lowerEdge);
```

```
%Volume calculation

V(a)=thrombusVolume(thrombEdgeLower{a},thrombEdgeUpper{a},upperEdge,low
erEdge,con);


eval(sprintf('time(%u)=metadata.FrameKey_%u_0_0.ElapsedTime_ms;',a,i));
%ms, read from metadata structure
    a=a+1;
    b=b+1;
end

display('Saving data...')
save(sprintf('%s\\%s',folder,outputFile), 'A', 'V', 'thrombEdgeLower',
'thrombEdgeUpper',    'I3',    'time',    'upperEdge',    'lowerEdge',
'thromb','first','last','step','con','threshPercent','threshold','ROIwi
dth','metadata','Isave')
```

```
function [I]=readColorImage(imNum,folder)

%Reads color image number imNum generated by colorImage.m from folder

if imNum<10
    I=imread(sprintf('%s\\colorImg_00000000%u.tif',folder,imNum));
elseif imNum<100
    I=imread(sprintf('%s\\colorImg_0000000%u.tif',folder,imNum));
elseif imNum<1000
    I=imread(sprintf('%s\\colorImg_000000%u.tif',folder,imNum));
else
    I=imread(sprintf('%s\\colorImg_00000%u.tif',folder,imNum));
end
```

```
function [upperEdge lowerEdge]=findEdge(I1)

%Finds edges of capillary tube in image I1 based on laplacian of gaussian
%filter

I2=uint8(sum(I1,3)/((2^8-1)*3)*(2^8-1));

filt1=fspecial('laplacian',0.5);
filt2=fspecial('gaussian',3,1);

I3=imfilter(imfilter(I2,filt1),filt2);
%imshow(imadjust(I3))

bin=I3>0.25*max(max(I3));
%figure
%imshow(bin);

ind=find(bin);
[I,J]=ind2sub(size(bin),ind);

clear bin
%sort into canditate top and bottom edge points
a=1;
b=1;
for i=1:size(J)
    if I(i)>size(I1,1)/2
        lowerI(a,1)=I(i);
        lowerJ(a,1)=J(i);
        a=a+1;
    else
        upperI(b,1)=I(i);
        upperJ(b,1)=J(i);
        b=b+1;
    end
end

%Loop through each x-coordinate and find inner most edge point candidate
for i=min(J):max(J)
    lowerJtrans=flipud(lowerJ);
    lowerItrans=flipud(lowerI);
    [~,loc]=ismember(i,lowerJtrans);
    if loc~=0
        lowerEdge(i,2)=lowerItrans(loc);
        lowerEdge(i,1)=lowerJtrans(loc);
    end

    [~,loc]=ismember(i,upperJ);
    if loc~=0
        upperEdge(i,2)=upperI(loc);
        upperEdge(i,1)=upperJ(loc);
    end

end

%while size(upperEdge,1)~=size(lowerEdge,1)
```

```
    if size(upperEdge,1)<size(lowerEdge,1)
        upperEdge(size(upperEdge,1)+1,:)=upperEdge(size(upperEdge,1)-
1,:);
    elseif size(upperEdge,1)>size(lowerEdge,1)
        lowerEdge(size(lowerEdge,1)+1,:)=lowerEdge(size(lowerEdge,1)-
1,:);
    end
%end

%Adjust 0 leading element and fix any other zero elements
upperEdge(1,2)=upperEdge(2,2);
lowerEdge(1,2)=lowerEdge(2,2);
for i=2:size(lowerEdge,1)
    if lowerEdge(i,2)==0
        lowerEdge(i,2)=lowerEdge(i-1,2);
        lowerEdge(i,1)=lowerEdge(i-1,1)+1;
    end
    if upperEdge(i,2)==0
        upperEdge(i,2)=upperEdge(i-1,2);
        upperEdge(i,1)=upperEdge(i-1,1)+1;
    end
end

%while size(upperEdge,1)~=size(lowerEdge,1)
    if size(upperEdge,1)<size(lowerEdge,1)
        upperEdge(size(upperEdge,1)+1,:)=upperEdge(size(upperEdge,1)-
1,:);
    elseif size(upperEdge,1)>size(lowerEdge,1)
        lowerEdge(size(lowerEdge,1)+1,:)=lowerEdge(size(lowerEdge,1)-
1,:);
    end
%end

%fix any outlying points
for j=1:5
for i=3:(size(upperEdge,1)-1)
    if    (upperEdge(i,2)-upperEdge(i+1,2))>3    ||    (upperEdge(i,2)-
upperEdge(i-1,2))>3
        upperEdge(i,2)=(upperEdge(i+1,2)+upperEdge(i-1,2))/2;
    end
    if    (lowerEdge(i,2)-lowerEdge(i+1,2))>3    ||    (lowerEdge(i,2)-
lowerEdge(i-1,2))>3
        lowerEdge(i,2)=(lowerEdge(i+1,2)+lowerEdge(i-1,2))/2;
    end
end
end
```

```
function [I2]=brightnessCorrection(I1,ref)

%brightnessCorrection.m returns the brightness-corrected intensity image
%of I1 based on the brightness of the reference image, ref.

%Calculate mean intensity of reference
refBright=mean(mean(uint8(sum(ref,3)/((2^8-1)*3)*(2^8-1))));

%Calculate mean intensity of image of interest
brightMean=mean(mean(uint8(sum(I1,3)/((2^8-1)*3)*(2^8-1))));

%Add the difference in brightness between the images to the image of
%interest
I2=uint8(sum(I1,3)/((2^8-1)*3)*(2^8-1))+(refBright-brightMean);
```

```
function [V]=thrombusVolume(lowerThrombEdge,upperThrombEdge,upperEdge,
lowerEdge,con)

%thrombusVolume.m computes the thrombus volume in mm^3 based on the method
%described in Para (2011) from the lower thrombus boundary, the upper
%thrombus boundary, upper and lower capillary  boundaries, and the
%conversion factor (con) in pixels per mm

%Calculated Di and Do
    Do=(lowerEdge(:,2)-upperEdge(:,2))/con;
    Di=(lowerThrombEdge-upperThrombEdge)/con;

%Estimated thrombus volume
Vsub=(Do.^2-Di.^2)/4*pi*1/con;
for j=1:size(Vsub)
    if Vsub(j)<0
        Vsub(j)=0;
    end
end
V=sum(Vsub);
```

```
function []=colorImage(first,last,step,folder)

%Converts images captured using micromanager stored in folder to color
%tifs starting with first image, stepping by step, and ending with last
%image. Images are saved to a subdirectory 'color'

%Check to see if color folder exists and creat if not

if exist(sprintf('%s\\color',folder),'dir')~=7
    mkdir(sprintf('%s\\color',folder))
end

for n=first:step:last
    clear I red green blue rgb
    %Read image
    if n<10
        I=imread(sprintf('%s\\img_00000000%u__000.tif',folder,n));
    elseif n<100
        I=imread(sprintf('%s\\img_0000000%u__000.tif',folder,n));
    elseif n<1000
        I=imread(sprintf('%s\\img_000000%u__000.tif',folder,n));
    else
        I=imread(sprintf('%s\\img_00000%u__000.tif',folder,n));
    end

    a=1;
    %Interpolate color to pixels based on pixelfly documentation
    for i=1:2:(size(I,1)-4)
        b=1;
        for j=1:2:(size(I,2)-4)
            red(a,b)=(9*I(i+2,j+2)+3*I(i,j+2)+3*I(i+2,j)+I(i,j))/16;
            green(a,b)=(I(i+1,j+2)+I(i+2,j+1))/2;

blue(a,b)=(9*I(i+1,j+1)+3*I(i+1,j+3)+3*I(i+3,j+1)+I(i+3,j+3))/16;
            b=b+1;
        end
        a=a+1;
    end

    %Convert to 8bit three-color
    rgb(:,:,1)=uint8(double(red)/4095*255);
    rgb(:,:,2)=uint8(double(green)/4095*255);
    rgb(:,:,3)=uint8(double(blue)/4095*255);

    %display figure and save as tif
    figure
    imshow(rgb)
    if n<10

saveas(gcf,sprintf('%s\\color\\colorImg_00000000%u.tif',folder,n));
    elseif n<100

saveas(gcf,sprintf('%s\\color\\colorImg_0000000%u.tif',folder,n))
    elseif n<1000
```

```
saveas(gcf,sprintf('%s\\color\\colorImg_000000%u.tif',folder,n))
    else
        saveas(gcf,sprintf('%s\\color\\colorImg_00000%u.tif',folder,n))
    end
    close all
end


%Repeat for last image (in case last ~= first + n*step)
clear I red green blue rgb
if last<10
    I=imread(sprintf('%s\\img_00000000%u__000.tif',folder,last));
elseif last<100
    I=imread(sprintf('%s\\img_0000000%u__000.tif',folder,last));
elseif last<1000
    I=imread(sprintf('%s\\img_000000%u__000.tif',folder,last));
else
    I=imread(sprintf('%s\\img_00000%u__000.tif',folder,last));
end
a=1;
for i=1:2:(size(I,1)-4)
    b=1;
    for j=1:2:(size(I,2)-4)
        red(a,b)=(9*I(i+2,j+2)+3*I(i,j+2)+3*I(i+2,j)+I(i,j))/16;
        green(a,b)=(I(i+1,j+2)+I(i+2,j+1))/2;

blue(a,b)=(9*I(i+1,j+1)+3*I(i+1,j+3)+3*I(i+3,j+1)+I(i+3,j+3))/16;
        b=b+1;
    end
    a=a+1;
end

rgb(:,:,1)=uint8(double(red)/4095*255);
rgb(:,:,2)=uint8(double(green)/4095*255);
rgb(:,:,3)=uint8(double(blue)/4095*255);

imshow(rgb)
if last<10

saveas(gcf,sprintf('%s\\color\\colorImg_00000000%u.tif',folder,last));
elseif last<100

saveas(gcf,sprintf('%s\\color\\colorImg_0000000%u.tif',folder,last))
elseif last<1000
    saveas(gcf,sprintf('%s\\color\\colorImg_000000%u.tif',folder,last))
else
    saveas(gcf,sprintf('%s\\color\\colorImg_00000%u.tif',folder,last))
end
close all

%copy metadata to color folder
copyfile(sprintf('%s\\metadata.txt',folder),sprintf('%s\\color\\metadat
a.txt',folder));
```

```
function [lagTime rate]=thrombusRate(folder,file,badIndex,lagThresh,
outputFile,plotOn)

%Calculates lagTime in sec and rate of thrombus formation in mm3/s from
%the .mat file generated by imageSubraction_main.m and specified by
%"folder" and "file." To exclude frames from analysis, include the indices
%of the bad frames in a vector "badIndex." The lag time threshold
%(lagThresh) is 0.01 mm3. The arguments are:
%
%   folder      folder containing the .mat file for analysis (string)
%   file        .mat file generated by imageSubtraction_main.m (string)
%   badIndex    vector containing indices of bad frames, if any (e.g.
                flicker frames, upstream debris, etc.)
%   lagThresh   threshold of thrombus volume in mm3 below which is
                considered "lag time" (current working value = 0.01
                mm3)
%   outputFile  name of .mat to save lagTime and rate (enter [] if no
                save is requested
%   plotOn       binary input for to plot volume vs. time, linear fit of
                thrombus growth after lag time, and lagThresh (1 = plot,
                0 = don't plot)

load(sprintf('%s\\%s',folder,file),'V','time')

time=(time-time(1))/1000;     %convert time from ms to sec

%Remove bad points (based on visual image inspection)
for i=1:numel(badIndex)
    V(badIndex(i)-(i-1))=[];
    time(badIndex(i)-(i-1))=[];
end

%Parse volume array into lag and growth regions
bin=V>lagThresh;
[~,ind]=max(bin);

growthV=V(ind:length(V));
growthTime=time(ind:length(V));

lagTime=time(ind);

p=polyfit(growthTime,growthV,1);   %mm3/s

rate=p(1);

if plotOn==1
    figure
    hold on
    plot(time,V,'b');
    plot(growthTime,polyval(p,growthTime),'r')
    plot(time,lagThresh*ones(size(time)),'--k')
    xlabel('Time (s)')
    ylabel('Thrombus Volume (mm^3/s)')
    if numel(outputFile)>0
        saveas(gca,sprintf('%s\\%s.fig',folder,outputFile));
```

```
    end
end

if numel(outputFile)>0
    save(sprintf('%s\\%s.mat',folder,outputFile),'lagTime','rate')
end
```

APPENDIX B: MATLAB CODE FOR MICROFLUIDIC IMAGE PROCESSING WITH VOLUME INTERPOLATION

```
%optional functional call:
%function []=microProcessing_main(first,last,step,con,threshPercent,
%folder,outputFile)

clear all
folder ='F:\LCexperiments\2014-11-18\
2014-11-18_L023blood+L012plate_control_2\color'; %directory containing
                                                  images to be processed
startImage=43; %image to start processing
ref=107;       %image to use as references
first=ref+1;   %first image to be processed
last=1506;     %last image to be processed
step=1;        %step between images processed
con=202/480;   %length conversion factor pixels per micron
outputFile='2014-11-18_L023blood+L012plate_control_laterRef'; %output
                                                               file name

%get time data from metadata file
id=fopen(sprintf('%s\\metadata.txt',folder));
display('Reading metadata...')
string=fscanf(id,'%s');
metadata = parse_json(string);
fclose(id);
eval(sprintf('t0=metadata.FrameKey_%u_0_0.ElapsedTime_ms;',startImage))
; %read t1 from metadata structure

%Read reference image
I=readColorImage(first,folder);
Icrop=readColorImage(last,folder);

%User provide ROI
[~,rect]=imcrop(Icrop);
I1=imcrop(I,rect);

int1=sum(I1,3)/(3*2^8-1);
s=fspecial('gaussian',5,1);
int1=imfilter(int1,s);

b=1;
%loop through all images
for i=first:step:last
    display(sprintf('Processing image %u',i))

    %read in, crop, and store raw image
    I2=readColorImage(i,folder);
    I=imcrop(I2,rect);
    Isave{b}=I;

    %convert image to intensity and subtract
```

```
    int{b}=sum(I,3)/(3*2^8-1);
    int{b}=imfilter(int{b},s);
    subtract=int{b}-int1;

    %calculate average thrombus volume using confocal correlation
    %(pixel-by-pixel)
    h{b}=(23.731*log(subtract) + 105.73);
    h{b}(isinf(h{b}))=0;
    h{b}=h{b}.*double(subtract>0.019)+3.5*double(subtract<=0.019);
%correlation is height in confocal slices, slice interval = 0.89

    h{b}=h{b}*0.89; %convert from height in "slices" to height in um

    V(b)=sum(sum(h{b}*con^2,1),2);       %volume in cubic um
    Vmean(b)=V(b)/(rect(3)*rect(4)*con^2); %average height over area
                                            (accounts for different ROI)

    %calculate average thrombus volume using confocoal correlation
    %(bulk intensity)
    VmeanBulk(b)=mean(mean(subtract))*436.83+3.098; %mean height in
                                                              slices
    VmeanBulk(b)=VmeanBulk(b)*0.89; %convert to mean height in microns


eval(sprintf('time(%u)=metadata.FrameKey_%u_0_0.ElapsedTime_ms;',b,i));
%ms, read from metadata structure
    time(b)=time(b)-t0;
    b=b+1;
end

save(sprintf('%s\\%s',folder,outputFile),'-v7.3','Isave','int','int1',
'time','h','V','Vmean','VmeanBulk','rect');
```

APPENDIX C: PROTOCOL FOR PDMS FABRICATION

A. PDMS Mixing and Pouring

1. Zero balance with weighing boat and plastic spoon.
2. Spoon 10-15 g Sylgard 184 base into weighing boat; note the exact mass
3. Zero balance and add 10% of above mass of curing agent (use disposable transfer pipette).
4. Fold components together until well mixed.
5. Spoon mixture into clean mold.

B. Degassing

1. Place filled mold in desiccator and cover with lid.
2. Open stopcock and turn on vacuum pump.
3. Tighten stopcock to seal chamber. Run vacuum pump until top of PDMS is bubbly. Tightly seal stopcock and turn off pump.
4. Let degas for 20 minutes.
5. Open stopcock to release vacuum and remove mold. Any remaining bubbles can be popped with toothpick or blown away.

C. Curing

1. Place degassed mold in oven at 120°C for 20 minutes. Be careful not to over-cure either by increasing the temperature or extending the time as the PDMS will become brittle and crack when inserting connectors.

2. Test doneness with toothpick away from channel area; should be solid/does not indent or form peak.
3. Let cool 20 minutes.
4. Use X-ACTO knife to separate the perimeter of the chip from the mold. Lift on corner up and carefully peel away the chip.

D. Punching

1. Sharpen a 16 gauge blunt needle using rotary tool; use grinding stone and speed stetting 5.

Green = 14 gauge, magenta = 16 gauge, pink = 18 gauge

1. With the feature side up, carefully use the needle tip to punch holes at each end of the test sections.
2. Use an 18 gauge blunt needle to pop out the punches.
3. Use Scotch tape to clean surfaces and seal both sides if stored.
4. *Note: If chip is to be bonded to cover glass, trim chip to size.

E. Bonding

1. Power on plasma cleaning; wait 1.5 minutes for warm up
2. Place chip and microscope slide/cover glass in chamber with bonding sides up.
3. Close valve on cover and place over opening; turn on vacuum pump and wait 1.5 minutes

4. Turn RF to high. Use needle valve to bleed in atmospheric air so color is bright magenta (between blue and violet).
5. Turn pump and RF off. Slowly bleed air back in and remove cover.
6. Quickly align and bond slide and chip; you have ~20 sec.
7. Turn off plasma cleaner.
8. Cure chip at 70°C for 1 hr. After cooling, cover with Scotch tape to keep clean and allow to rest overnight.

F. Collagen Coating (24 hrs before experiment)

1. Dilute stock Chronolog collagen 9:1 with saline. For 1 chip, make 50 μL solution (45 μL saline, 5 μL stock collagen).
2. Gently pipet 2.5 μL solution into each channel.
3. Seal in Tupperware with warm, moist paper towel.
4. Incubate for 24 hrs. Collagen is rinsed with PBS during device priming.

APPENDIX D: WASHED RED BLOOD CELL PREPARATION

Adapted from a protocol from the Emory Genetics Laboratory.

MATERIALS

Normal saline (0.9% w/v NaCl)

METHODS

1. Collect blood in anticoagulant of choice (heparin, citrate, etc.). Heparin (15.8 USP units/mL) was used in this dissertation.
2. Transfer 8 mL of blood into 15 mL centrifuge tubes.
3. Centrifuge for 5 minutes at 1800g (9 notches on Fisher Scientific Centrific™ Centrifuge). Make sure to balance the centrifuge.
4. Pipette off supernatant using either transfer pipet or micropipette.
5. Add normal saline to 8 mL. Mix saline and red blood cells by pipetting up and down.
6. Centrifuge for 5 minutes at 1200 g (6 notches on Fisher Scientific Centrific™ Centrifuge).
7. Repeat steps 4-6 once, or until supernatant is clear.

APPENDIX E: PLATELET ISOLATION PROTOCOL

Adapted from Cazenave et al. (2004) with input from the laboratory of Dr. Wilbur A. Lam.

MATERIALS

Stock:

Acid-Citrate-Dextose (ACD):

Molar Concentrations	Mass in 250 mL solution
39 mM citric acid	1.87 g citric acid
75 mM sodium citrate	4.84 g sodium citrate
135 mM dextrose	6.08 g dextrose

Sodium citrate is an anticoagulant that acts by chelating calcium ions, which are essential cofactors in the coagulation cascade. Calcium chelation also reduces platelet activation. Citric acid reduces the pH of the solution, which future inhibits platelet activation. Preventing platelet activation is critical for isolating platelets via centrifugation. Dextrose provides nourishment for the cells.

Tyrode's buffer:

Molar Concentrations	Mass in 250 mL solution
134 mM NaCl	1.96 g NaCl
12 mM $NaHCO_3$	0.25 g $NaHCO_3$
2.9 mM KCl	0.05 KCl
1 mM $MgCl_2$	0.03 $MgCl_2 + 6H_2O$ (check hydrate and adjust as needed)
10 mM HEPES	0.6 g HEPES

Bovine serum albumin (BSA) OR human serum albumin (HSA

Dextrose

For day of use:

Tyrode's albumin buffer: combine 10 mL Tyrode's buffer, 0.001 g glucose, and 1 mL BSA or HSA

METHODS

1. Collect blood in 6:1 ACD
2. Transfer 14 mL into 15 mL centrifuge tubes.
3. Centrifuge at 250g (2.7 notches on Fisher Scientific Centrific^{TM} Centrifuge) for 16 minutes. Make sure to balance the centrifuge.
4. Very gently pipette off the platelet-rich plasma (PRP) using micropipette and transfer into new centrifuge tubes.

5. Add 10% by volume ACD to PRP.
6. Centrifuge at 2200g (8 notches on Fisher Scientific Centrific™ Centrifuge) for 13 minutes.
7. Pipette off the supernatant.
8. Resuspend platelet pellet in Tyrode's albumin buffer by *gently* pipetting up and down. Volume of resuspending buffer depends on desired platelet count. As an estimate, platelet yield will be about 10% of total platelets in plasma sample.
9. Count platelets using hemocytometer. Adjust count by adding buffer to suspension.

REFERENCES

Cazenave, J. P., Ohlmann, P., Cassel, D., Eckly, A., Hechler, B., & Gachet, C. (2004). Preparation of washed platelet suspensions from human and rodent blood. *Methods in Molecular Biology, 272*, 13-28.